

2015-11-18

# Catalysts Evaluation for Catalytic Steam Cracking of De-asphalted Oil in a Fixed Bed Reactor

Garcia Hubner, Eduardo Antonio

---

Garcia Hubner, E. A. (2015). Catalysts Evaluation for Catalytic Steam Cracking of De-asphalted Oil in a Fixed Bed Reactor (Master's thesis, University of Calgary, Calgary, Canada). Retrieved from <https://prism.ucalgary.ca>. doi:10.11575/PRISM/25223

<http://hdl.handle.net/11023/2641>

*Downloaded from PRISM Repository, University of Calgary*

UNIVERSITY OF CALGARY

Catalysts Evaluation for Catalytic Steam Cracking of De-asphalted Oil in a Fixed Bed Reactor

by

Eduardo Antonio Garcia-Hubner

A THESIS

SUBMITTED TO THE FACULTY OF GRADUATE STUDIES  
IN PARTIAL FULFILLMENT OF THE REQUIREMENTS FOR THE  
DEGREE OF MASTER OF SCIENCE

GRADUATE PROGRAM IN CHEMICAL ENGINEERING

CALGARY, ALBERTA

NOVEMBER, 2015

©Eduardo Antonio Garcia-Hubner 2015

## **Abstract**

The present study aims to show performance of a catalytic steam cracking unit when processing de-asphalted oil, as part of a proposed upgrading scheme. Improve in the properties of the oil regarding viscosity and API gravity is intended, in order to make it pipeline transportable.

All the experiments were performed in a continuous bench scale plant fitted with a fixed bed reactor, working at 150-400 psi and temperatures between 350 °C and 400 °C. The results from the evaluation of the catalysts, shows capability for catalytic water dissociation, hydrogen production, hydrocarbon cracking and hydrogenation, especially one catalyst containing  $\text{Mo}_2\text{C}$ . This catalyst, working at 370°C and 400 psi, generated a product able to meet viscosity specification at 14°C. The Syncrude produced required 16% less diluent to be pumped and improvement in sulphur content and Total Acid Number (TAN) was also observed.

## **Acknowledgements**

I place on record, my sincerest gratitude to Dr. Pedro Pereira-Almao. I have been honored to receive the opportunity to work among such a talented and supportive staff like the one you lead. I am sure this excellent experience left an essential mark in my professional and personal growth. I would like also to thank you for all the guidance, wisdom and encouragement provided at any time during the materialization of this research project.

I also want to take this opportunity to thank Dr. Josefina Scott and Dr. Gerardo Vitale for their endless support and particularly, for their availability whenever doubts arose. To Azfar Hassan, Josune Carbognani, Laura Sosa and Dr. Argenis Agüero for their constant help in all the activities related to the laboratory. To Mr. Lante Carbognani and Dr. Scott for sharing their wisdom.

Thanks to Natural Science and Engineering Research Council of Canada (NSERC), Nexen Inc, Alberta Innovates Energy and Environmental Solutions; and The Chemical and Petroleum Engineering Department from University of Calgary, for providing the financial support to carry out this research.

In general, I want to thank all the members of the Catalysts for Bitumen Upgrading Group (CBUG). In one way or another, all of them were involved in the successful accomplishment of this research project.

Last but not least, I have special gratitude to my family. My parents, Eduardo Garcia and Maria Elena Hubner, have always given 100% of themselves to support me in achieving each one of my goals, no matter how hard they might seem. To my siblings, Adrian Garcia and Eira Garcia, and my grandma Clemencia Liscano. Finally, I wanted to thank to my beloved Lorena Bernal for being my life partner and encouraging me during the hardest moments.

*To: The eternal cotton lover*

*My dear friend mom*

*My amazing siblings*

*My love*

*This is for and thanks to you...*

## Table of Contents

<b>Abstract.....</b>	<b>ii</b>
<b>Acknowledgements .....</b>	<b>iii</b>
<b>Table of Contents .....</b>	<b>v</b>
<b>List of Tables .....</b>	<b>viii</b>
<b>List of Figures.....</b>	<b>ix</b>
<b>List of Symbols .....</b>	<b>xiii</b>
<b>Chapter One: Introduction .....</b>	<b>1</b>
1.1 Background .....	1
1.2 Objectives .....	5
<b>Chapter Two: Literature Review .....</b>	<b>7</b>
2.1 Petroleum .....	7
2.1.1 Classification .....	8
2.1.2 Chemical and fractional composition .....	9
2.2 Upgrading .....	14
2.2.1 Carbon rejection processes .....	16
2.2.2 Hydrogen addition processes .....	20
2.3 Catalytic Steam Cracking (CSC) .....	24
2.3.1 Thermodynamics and mechanism .....	26
2.3.2 Technologies .....	30
2.4 Catalyst Development .....	34
2.4.1 Cat 1: CsBaNi-Metakaolin.....	36
2.4.2 Cat 2: NiCe-Calcined Hydrotalcite.....	37
2.4.3 Cat 3: NiCe-Aegirine .....	39
2.4.4 Cat 4: NiCe-Faujasite.....	40

2.4.5 Cat 5: NiCe-Calcined Hydrotalcite+Molybdenum Carbide .....	42
<b>Chapter Three: Experimental Section .....</b>	<b>44</b>
3.1 Catalyst Preparation .....	44
3.1.1 Cat 1: CsBaNi-Metakaolin.....	44
3.1.2 Cat 2: NiCe-Calcined Hydrotalcite.....	45
3.1.3 Cat 3: NiCe-Aegirine .....	46
3.1.4 Cat 4: NiCe-Faujasite.....	47
3.1.5 Cat 5: NiCe-Calcined Hydrotalcite+Molybdenum Carbide .....	47
3.2 Catalyst Characterization .....	48
3.2.1 Textural properties .....	48
3.2.1 Temperature Programmed Techniques .....	49
3.2.1 Thermogravimetric Analysis (TGA) .....	50
3.2.1 X-Ray Diffraction (XRD).....	50
3.2.2 X-Ray Photoelectron Spectroscopy (XPS) .....	51
3.1 Carborundum cleaning.....	52
3.2 Feedstock .....	52
3.3 Plant description.....	54
3.3.1 Operating procedure .....	59
3.4 Characterization of Samples .....	62
3.4.1 High Temperature Simulated Distillation (HTSD).....	62
3.4.2 Water content .....	64
3.4.3 Oil density .....	64
3.4.4 Microcarbon residue .....	65
3.4.5 Gases .....	66
3.4.6 Viscosity .....	68
3.4.7 Microdeasphalting .....	68
3.4.8 Elemental analysis (Sulphur and Nitrogen).....	69
3.4.9 P-value .....	69
3.4.10 Bromine number .....	70
3.4.11 Total Acid Number (TAN) .....	70

<b>Chapter Four: Catalyst Characterization Results.....</b>	<b>72</b>
4.1 Nominal metal composition for each catalyst.....	72
4.2 Textural properties .....	73
4.3 Temperature Programmed Reduction (TPR) .....	74
4.4 Temperature Programmed Desorption of Ammonia (TPD) .....	78
4.5 Powder X-Ray Diffraction (XRD).....	83
4.1 X-Ray Photoelectron Spectroscopy (XPS) .....	89
4.1.1 Decomposition of Ni 2p <sub>3/2</sub> .....	91
4.1.2 Decomposition of Ce 3d <sub>5/2</sub> .....	94
<b>Chapter Five: Pilot Plant Operations .....</b>	<b>97</b>
5.1 Thermal steam cracking.....	98
5.2 Catalytic steam cracking .....	103
5.2.1 Preliminary catalyst screening .....	103
5.2.2 Catalyst stability and product comparison.....	108
5.2.3 Experimental demonstration of catalytic water splitting .....	114
5.2.4 Operational and catalyst improvements.....	118
5.3 Upgrading scheme evaluation.....	129
<b>Chapter Six: Summary and Recommended Future Work .....</b>	<b>132</b>
<b>References .....</b>	<b>137</b>
<b>Appendix A: STANDARD OPERATING PROCEDURE OF CATALYST TESTING UNIT (CTU-1) .....</b>	<b>142</b>
<b>Appendix B: Catalyst Characterization Data .....</b>	<b>174</b>



## List of Tables

Table 2.1. Properties of crude oils in comparison with residue (modified from Ancheyta, et al., 2009) .....	8
Table 2.2. Typical hydroprocessing reactions (Robinson & Dolbear, 2006) .....	22
Table 3.1. Bitumen and feedstock (DAO) properties .....	53
Table 3.2. Errors in the determination of distillations cuts.....	63
Table 3.3. Relative errors associated with the determination of gases by GC.....	67
Table 4.1. Nominal weight percentage of active metals in prepared catalysts. ....	73
Table 4.2. Textural properties of catalysts* .....	74
Table 4.3. Hydrogen uptake per gram of catalyst.....	78
Table 4.4. Ammonia desorption quantities for catalysts evaluated .....	83
Table 4.5. Experimental surface atomic composition of metals on the catalysts .....	91
Table 4.6. Binding energy for Ni 2p <sub>3/2</sub> in all the catalysts evaluated.....	92
Table 4.7. Binding energies for Ce 3d <sub>5/2</sub> signals.....	95
Table 5.1. Average mass balances obtained along all the performed runs .....	98
Table 5.2. Catalyst properties after reaction .....	111
Table 5.3. Product properties for similar conversions for Cat 1, Cat 2 and Cat 3 (400 °C and WHSV=1 h <sup>-1</sup> ). .....	113
Table 5.4. P-Value of products (400 °C and WHSV=1 h <sup>-1</sup> ). ....	114
Table 5.5. Recalculated signal ratios for CO <sub>2</sub> .....	117
Table 5.6. Process simulation for different scenarios and using WHSV=0.5 h <sup>-1</sup> .....	121
Table 5.7. Properties of products (Thermal and Catalytic) evaluated at 150 psi.....	125
Table 5.8. Product properties evaluated at 150 psi and 400 psi with Cat 5. ....	127
Table 5.9. Properties of the streams in the proposed upgrading scheme .....	131

## List of Figures

Figure 1.1. Upgrading scheme based on solvent de-asphalting and steam catalytic cracking unit. ....	5
Figure 2.1. Examples of different hydrocarbon groups for C <sub>6</sub> .....	10
Figure 2.2. Paraffinic, naphthenic and aromatic hydrocarbon composition in oil for different boiling points (Speight, 1999).....	11
Figure 2.3. Model molecules for asphaltenes type archipelago (a) and continental (b) (Ancheyta, et al., 2009) .....	14
Figure 2.4. Typical upgrading scheme (Speight, 2013).....	15
Figure 2.5. Upgrading pathways (Banerjee, 2012) .....	16
Figure 2.6. Schematic of the ROSE process (Gary & Handwerk, 2001).....	20
Figure 2.7. Possible dissociation reactions of adsorbed water (Thiel & Madey, 1987) .....	28
Figure 2.8. Thermodynamics of water dissociation on a metal surface (Thiel & Madey, 1987) .	29
Figure 2.9. Schematic of the transition state of water molecules on Cu (1 0 0) promoted with Li (Henderson, 2002). ....	30
Figure 2.10. Scheme for catalytic steam processing of asphaltenes-free hydrocarbons (Pereira-Almao, et al., 2013).....	34
Figure 2.11. Kaolinite structure (King, 2009).....	36
Figure 2.12. Hydrotalcite structure (Cantrell, et al., 2005).....	38
Figure 2.13. Pyroxene structure showing tetrahedral (yellow) and octahedral (green) layers. M2 cations are represented as purple atoms, M1 cations are grouped in the green octahedral (Vitale, 2013). ....	40
Figure 2.14. Structure of Zeolite Y (Lutz, 2014).....	41
Figure 2.15. Molybdenum Carbide crystallographic phases: a) cubic ( $\delta$ -MoC), b) hexagonal ( $\alpha$ -MoC) and c) orthorhombic ( $\beta$ -Mo <sub>2</sub> C). Turquoise and magenta spheres correspond to C and Mo atoms, respectively (dos Santos Politi, et al., 2013) .....	43
Figure 3.1. Simulated Distillation for the feedstock and products of the SDA Unit (Da Silva De Andrade, 2014).....	54
Figure 3.2. P&ID of the Catalyst Testing Unit (CTU-1) .....	56

Figure 3.3. Reactor assemblies .....	58
Figure 4.1. Catalysts after preparation .....	72
Figure 4.2. H <sub>2</sub> -TPR for Cat 1 .....	75
Figure 4.3. H <sub>2</sub> -TPR for Cat 2 .....	76
Figure 4.4. H <sub>2</sub> -TPR for Cat 3 .....	76
Figure 4.5. H <sub>2</sub> -TPR for Cat 4 .....	77
Figure 4.6. H <sub>2</sub> -TPR for Cat 5 .....	77
Figure 4.7. NH <sub>3</sub> -TPD for Cat 2 .....	79
Figure 4.8. NH <sub>3</sub> -TPD for Cat 3 .....	80
Figure 4.9. NH <sub>3</sub> -TPD for Cat 4 .....	81
Figure 4.10. NH <sub>3</sub> -TPD for Cat 5 .....	82
Figure 4.11. XRD diffractogram for Cat 1 .....	84
Figure 4.12. XRD diffractogram for Cat 2 .....	85
Figure 4.13. XRD diffractogram for Cat 3 .....	86
Figure 4.14. XRD diffractogram for as provided FAU. ....	87
Figure 4.15. XRD diffractogram for Cat 4. ....	87
Figure 4.16. XRD for Molybdenum Carbide.....	88
Figure 4.17. XRD diffractogram for Cat 5 fresh and treated in hydrogen at 500°C .....	89
Figure 4.18. Survey scan for Cat 1 .....	91
Figure 4.19. Decomposition of Ni 2p <sub>3/2</sub> for all catalysts.....	93
Figure 4.20. Decomposition of Ce 3d .....	95
Figure 5.1. Effect of temperature and residence time over the residue conversion in thermal cracking.....	100
Figure 5.2. API variation with residue conversion .....	101
Figure 5.3. Log of viscosity variation with residue conversion.....	102

Figure 5.4. Asphaltenes content vs. residue conversion .....	102
Figure 5.5. Microcarbon vs. residue conversion.....	103
Figure 5.6. Effect of temperature and catalyst type on residue conversion. Blue symbols correspond to runs at 380 °C and patterned red symbols at 400°C. The respective thermal conversions are also shown at 380 °C (dotted line) and 400 °C (continuous line). .....	105
Figure 5.7. Components gas flowrate reached at the end of each temperature for the catalytic runs, in comparison with the thermal runs.....	107
Figure 5.8. Deactivation profile of the catalyst tested at 400 °C and WHSV=1 h <sup>-1</sup> .....	108
Figure 5.9. Gas production at stabilization (400 °C and WHSV=1 h <sup>-1</sup> ). .....	109
Figure 5.10. Hydrogen and methane production evolution with time (400 °C and WHSV=1 h <sup>-1</sup> ). .....	110
Figure 5.11. Product Distribution at similar conversion for Cat 1, Cat 2 and Cat 3 (400 °C and WHSV=1 h <sup>-1</sup> ). .....	112
Figure 5.12. m/z-xx / m/z-44 ratios for experiments at 360, 380 and 400 °C .....	116
Figure 5.13. Results for Cat 4 evaluation at 380°C and WHSV=1 h <sup>-1</sup> . .....	119
Figure 5.14. Product distribution for Cat 4 in comparison with Cat 1, 2 and 3.....	120
Figure 5.15. Experimental results for water content/parameter variations .....	123
Figure 5.16. Evaluation of Cat 4 and Cat 5 at 150 psi. Blue symbols refer to runs at 350°C and patterned red symbols at 370°C. Lines correspond to the thermal runs.....	125
Figure 5.17. Pressure effect on residue conversion for Cat 5 evaluated at 350°C (blue symbols) and 370 °C (red symbols). Straight lines correspond to their respective thermal runs. Light blue for thermal at 150 psi and dark blue for thermal at 400 psi. ....	127
Figure 5.18. Gas analysis for Cat 5 evaluation at 150 and 400 psi.....	129
Figure 5.19. Upgrading Scheme with only gas and syncrude as products .....	131
Figure B.1. Isotherm and pore distribution charts for Cat 1 .....	174
Figure B.2. Isotherm and pore distribution charts for Cat 1 .....	174
Figure B.3. Isotherm and pore distribution charts for Cat 3 .....	175

Figure B.4. Isotherm and pore distribution charts for Cat 4 .....	175
Figure B.5. Isotherm and pore distribution charts for Cat 5 .....	176
Figure B.6. Survey scan for Cat 2.....	176
Figure B.7. Survey scan for Cat 3.....	177
Figure B.8. Survey scan for Cat 4.....	177
Figure B.9. Survey scan for Cat 5.....	178

### List of Symbols

BET	Brunauer–Emmett–Teller
Cat 1	CsBaNi-Metakaolin
Cat 2	NiCe-Calcined Hydrotalcite
Cat 3	NiCe-Aegirine
Cat 4	NiCe-Faujasite
Cat 5	NiCe-Calcined Hydrotalcite+Molybdenum Carbide
CSC	Catalytic Steam Cracking
DAO	De-Asphalted Oil
HTSD	High Temperature Simulated Distillation
MMBD	Million Barrels per Day
m/z	Mass to charge ratio
SAGD	Steam Assisted Gravity Drainage
Simdist	Simulated Distillation
TAN	Total Acid Number
TBP	True Boiling Point
TGA	Thermogravimetric Analysis
TPD	Temperature Programmed Desorption
TPR	Temperature Programmed Reduction
WHSV	Weight Hourly Space Velocity, h <sup>-1</sup>
XPS	X-ray Photoelectron Spectroscopy
XRD	X-ray Diffraction

## **Chapter One: Introduction**

### **1.1 Background**

The continuous increase in energy demand is a clear evidence of the worldwide unceasing growth of the economies, especially of the developing countries. According to the U.S Energy Information Administration (U.S. Energy Information Administration, 2014), an increase of 30.5% in the global petroleum consumption ending up in 86.8 MMBD was experienced between 1990 and 2010, as a consequence of the progress of the countries to reach an overall growth of 86% in their Gross Domestic Product. Furthermore, the projections indicate that the world will require an extra 32.6 MMBD of petroleum in the market by 2040 in order to satisfy, specifically, the demand of the developing countries not belonging to the Organization for Economic Cooperation and Development. Those countries are expected to grow about 290% between 2010 and 2040 with an average of 4.6% increase per year.

In order to meet the upcoming oil demand, the industry will have to face a variety of challenges associated with the production of this material regardless of operation costs and investments, as long as some profit can be generated. Out of the 6.5 trillions of technically recoverable oil reserves in the world, at least 58% are categorized as unconventional oil due to the complexities involved in the production of it, mainly attributable to the low porosity and permeability of the matrix rock and/or by the extra heaviness and high carbon content of the material. As part of the unconventional oil reserves, bitumen and extra heavy oil represent about 29% of the total (Gordon, 2013), where Venezuela and Canada are the world leaders with around 513 and 177 billion of barrels of proven reserves, respectively (Banerjee, 2012). Therefore, the development of technologies to improve the production, the quality of the products and the efficiency and economy of the process is a key point in the exploitation of this raw material.

Venezuelan and Canadian heavy oil are characterized both by API gravities between 8 and 12, but with important difference in the viscosity of them under reservoir conditions. In the case of Venezuela where the reservoirs are between 350-1000 m depth with temperatures around 60°C, the oil is mobile with viscosity varying between 1,000 and 5,000 cP. Whereas, the heavy oil found in Alberta-Canada with average reservoir temperature between 10-12°C is characterized with viscosities greater than one million centipoise. Therefore, the production of Canadian deep reservoirs requires the utilization of technologies such as Steam-Assisted Gravity Drainage (SAGD) to decrease the viscosity of the material by increasing the temperature of the reservoir with steam. In the case of northern Alberta, where the oil is found mixed with sand on the surface, the production is also achieved through surface mining followed by hot water extraction (Banerjee, 2012).

The high viscosity of the heavy oil not only impacts the production, but also affects the way in which the final product is transported from the wells to the refineries or final users. Pipeline specifications of API gravity greater than 19° and viscosity below 350 centistokes at pumping temperature are not usually met by this kind of oil, forcing the companies to treat it before proceeding to transportation (Banerjee, 2012). Two main pathways are preferred to pre-treat the crude: Dilution and/or Upgrading. Dilution consists in preparing a mixture, called dilbit, of heavy oil and about 30 vol. % of diluent, low molecular weight hydrocarbons (usually between C<sub>5</sub>-C<sub>12</sub>), to reduce the density of the oil. Once the dilbit is pumped to the refinery, the diluent may be removed from the oil by distillation and sent back to the field. The main disadvantages of this method lies in the high monetary value of the diluent, the dependence of the oil production on the availability of this light hydrocarbons in the market and the stability of the mixture, especially in heavy oils with high content of asphaltenes (Pereira-Almao, et al., 2013).

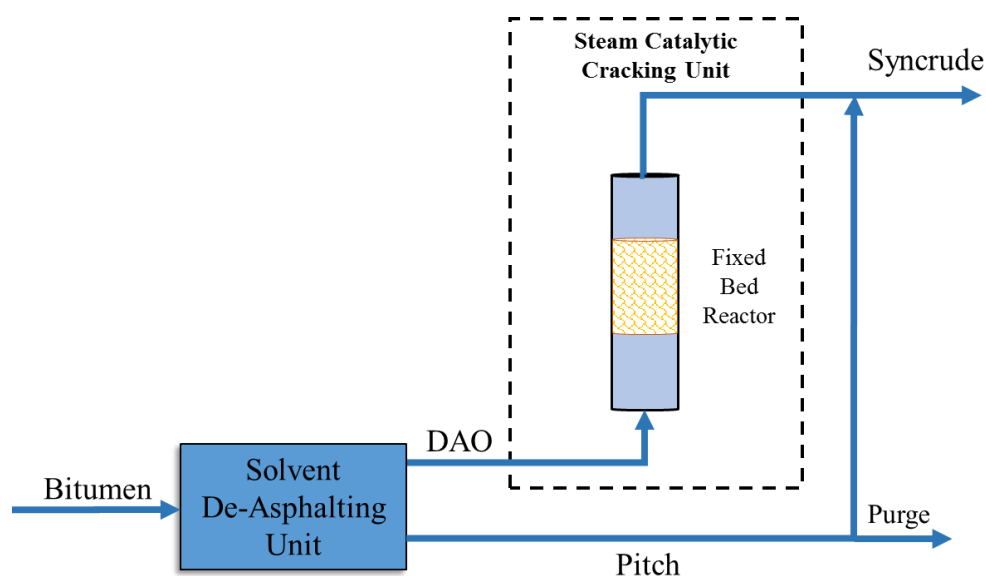


On the other hand, upgraders are large facilities consisting of a set of chemical and physical processes that aim to either separate the heavy fractions of the oil or to convert it into compounds of lower molecular weight (Griffiths & Dyer, 2008; Banerjee, 2012). Depending on the level of residue conversion, the final product is a synthetic crude (Syncrude), whose characteristics can be as good as a light conventional oil or one that just meets pipeline specifications. Most commercial upgraders consist of deep conversion refineries adaptation located in remote locations, which increase their high initial investment, complexity and the operational costs (Pereira-Almao, et al., 2013).

One technology proposed by Pereira-Almao, et al., 2013 (Patent US20130015100 A1) consists of a simple scheme for upgraders targeting mild improvement of the properties of the oil to reach pipeline specification, instead of reaching full conversion of the heavy fraction in it as done by other technologies such as coking. The idea is based on processing the heavy streams free of asphaltenes with steam in a tubular reactor, using nano catalysts in ultradispersed form. Water is dissociated by the catalyst to produce hydrogen and benefit the hydrogenation of the oil, which gives stability to the final product, reduces the production of olefins and polyaromatics and in general increases the H/C ratio. The streams are separated by distillation units and the asphaltenes are removed from the heavy cuts in the solvent de-asphalting unit. The final product, a synthetic crude oil, is a mixture of the lights and upgraded cuts with some of the original heavy material (Pereira-Almao, et al., 2013). One of the main advantages of this technology is the capability of having hydrogenation reactions during the upgrading without the need of using hydrogen, which is usually expensive to produce and transport.

Despite the high activity and low production cost involved in the use of ultradispersed catalysts during catalytic steam cracking, there are some drawbacks regarding the recovery of the catalytic

material and the costly separation process required (Pereira-Almao, et al., 2011). For that reason, the Catalyst for Bitumen Upgrading Group at the University of Calgary under the supervision of Dr. Pedro Pereira-Almao has put effort into developing supported catalysts able to perform steam catalytic cracking in a fixed bed reactor. This type of reactor has been around for a long time and used in different kinds of processes, which is the reason why its reliable operations are well known. Besides, the use of a catalytic bed allows the relatively easy replacement of it and even the in situ regeneration of the catalyst, if possible. However, supported catalysts in the presence of the whole bitumen rich in asphaltenes tend to plug and produce coke, leading to de-activation. Therefore, the upgrading scheme presented in the Figure 1.1 is proposed, where the oil is firstly deasphalted to split it into two streams: an asphaltenes rich stream called pitch and de-asphalted oil (DAO). The latter is processed in a steam catalytic cracking unit with a fixed bed reactor. Depending on the quality of the products in terms of viscosity and °API, they can be either mixed with the whole pitch or with a certain fraction of it until meeting pipeline specification. By means of this scheme, the complexity and investment cost of upgraders is considerably reduced, as well as, the important amount of energy required by distillation units at the beginning of most common processes.



**Figure 1.1. Upgrading scheme based on solvent de-asphalting and steam catalytic cracking unit.**

## 1.2 Objectives

In order to prove the viability of processing heavy oils via the scheme proposed above with steam catalytic cracking in a fixed bed reactor as conversion unit, a different kinds of supported catalysts were developed and tested in a bench scale plant. The catalysts consisted of solid extrudates containing combinations of transition metals, rare earth and alkali metals dispersed in selected oxide matrixes. Therefore, the general goal of the present research project is to evaluate those catalysts, and thus, determine whether the level of residue conversion and quality of the products obtained catalytically is suitable for implementing the proposed idea as a lower cost upgrader scheme.

To accomplish the previous general goal, the following specific objectives can be established:

- Design, procure and construct a bench scale plant able to operate with small amounts of the proposed catalysts, in order to avoid the preparation of a large amount of them.

- Prepare and characterize supported catalysts that promote the water splitting mechanism and thus, the targeted in-situ production of hydrogen.
- Evaluate the developed catalysts in the bench scale plant, using De-asphalted Oil (DAO) as feedstock in the presence of steam.
- Characterize the products obtained catalytically and compared them with the ones obtained via thermal steam cracking under the same conditions.
- Verify the water splitting mechanism by using labeled water and analyzing the gases in a quadrupole mass spectrometer.
- Incorporate into the catalyst hydrogen activating sites that could increase the global performance of the catalyst in the process.

## **Chapter Two: Literature Review**

The following chapter aims to generate the knowledge required to understand the background of the project and the different topics to be discussed during the development of it. Besides, it also highlights previous findings and their relationship with this subject. The literature review chapter is divided into four main sections, starting with a basic understanding of petroleum and its typical characteristics. Then, explanation about the concept of crude oil upgrading and different technologies currently applied is also presented. The third section introduces catalytic steam cracking and its basis, as an interesting and economical way to improve the properties of crude oils. Finally, a literature review and description of the metals and materials used for the elaboration of the supported catalyst used in this research, is also presented.

### **2.1 Petroleum**

The natural thermal evolution and transformation of sedimentary organic matter embedded in a specific rock, called source rock, is what it is known as Petroleum (Huc, 2011). Therefore, petroleum can be generally classified as the naturally occurring mixture of hydrocarbons, whether in liquid, gaseous or solid phase (Speight, 1999). Once petroleum is generated in the source rock, it migrates upwards through porous and fractured permeable rocks and along pervasive faults, until it is trapped by “defaults” of the draining system. This upward migration brings as a consequence a decrease in the temperature of the material, in some instances, the temperature values can be low enough to enable the development of bacterial activity that feeds on the petroleum and modifies its physical and chemical properties. As a result, an increase in the viscosity is experienced and heavy, extra heavy oil and bitumen are formed (Huc, 2011).

### 2.1.1 Classification

Even though there are considerable differences in chemical and fractional composition of the different kinds of crude oil, they are generally classified by physical properties like °API and viscosity. As shown in Table 2.1, light crude oils are considered as those with °API greater than 22, while heavy crude oils are in the range between 10 and 22 (Ancheyta, et al., 2009). Extra heavy crude oil and bitumen are in the same range of °API gravity (lower than 10), but with viscosity at reservoir conditions as the main difference between them. Extra heavy oil is characterized by having viscosities in the range 1,000-10,000 cP, while bitumen is denominated to be extra heavy oil with a viscosity greater than 10,000 cP (Banerjee, 2012). There is a significant increase in the complexity of handling and processing heavy and extra heavy oil in comparison with light oils. Heavy and extra heavy oils are characterized by a significant amount of contaminants, comparable to the amounts found in the heavier fractions of any crude oil. Besides, the composition of asphaltenes can reach up to 30%, which indicates that almost half of the heavy oil is composed by very large and heavy molecules. Therefore, converting the heavy fractions of heavy and extra heavy oils is as challenging as processing the residue from the distillation units.

**Table 2.1. Properties of crude oils in comparison with residue (modified from Ancheyta, et al., 2009)**

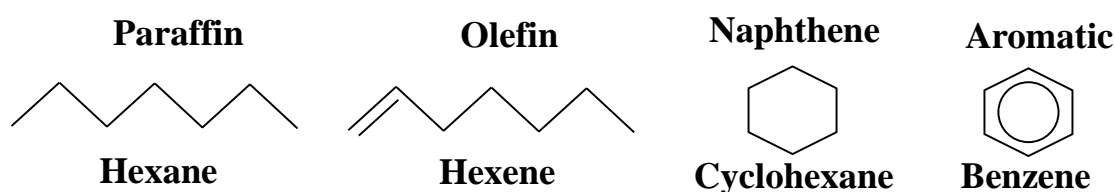
Classification	Hydrocarbons				Contaminants		
	API Gravity	Asphaltenes, wt. %	Resins, wt. %	Oils, wt. %	S, wt. %	N, wt. %	Metals (Ni+V), ppm
Extra Light	>50	0-<2	0.05-3	-	0.02-0.2	0.0-0.01	<10
Light Crude	22-32	<0.1-12	3-22	67-97	0.05-4.0	0.02-0.5	10-200
Heavy Crude	10-22	11-25	14-39	24-64	0.1-5.0	0.2-0.8	50-500
Extra Heavy	<10	15-40	-		0.8-6.0	0.1-1.3	200-600
Residue	-	15-30	25-40	<60	-	-	100>1000

Another definition well used in the oil industry to categorize crude oils is based on the type of recovery method used to produce the raw material. Conventional oil is the name assigned to those oils that can be produced by primary and even conventional secondary recovery methods. In general, the conditions of the reservoirs and the characteristic of the oil is such that no thermal methods are required to flow the material into the wellbore (Speight, 1999). Light oils and even heavy oils can be considered as conventional. However, extra heavy oils and bitumen require enhanced oil recovery methods to produce them, thus they are part of the so called unconventional oils (Banerjee, 2012). Even though shale oils are mostly light hydrocarbons, they are also classified within unconventionally produced oils. It is important to highlight that primary production is the one obtained at initial stages of the production, when the displacement of the oil is driven by the natural existing energy in the reservoir such as gas drive, gas-cap drive, water drive, fluid and rock expansion and gravity drainage. Secondary recovery methods require the injection of fluids such as water or gas to maintain the reservoir pressure and displace hydrocarbons. In tertiary recovery methods, or commonly named enhanced oil recovery methods (EOR), gases (hydrocarbons or CO<sub>2</sub>) or chemicals (polymers, surfactants etc.) are injected into the reservoir to favor the displacement of the oil. Thermal processes, either steam injection or in situ thermal generation by oil combustion, are also considered as EOR methods (Green & Willhite, 1998).

### ***2.1.2 Chemical and fractional composition***

The composition of the petroleum is influenced by several factors such as the location and the depth of the reservoirs and the age of the oil. Nevertheless, in general, it consists of a complex mixture of different kinds of hydrocarbons, including small amounts of organic compounds containing heteroatoms (nitrogen, sulphur and oxygen) and metals (vanadium, nickel, iron and copper) (Speight, 1999).

Due to the complexity of the hydrocarbon mixture in petroleum, it becomes very challenging to qualify and quantify all of them. However, it has been well established that olefinic groups are not present in the oil and acetylenic hydrocarbons are rarely found, while the hydrocarbon fraction of petroleum consists mainly of paraffins, naphthenes and aromatics (shown in Figure 2.1). The relationship between these three families lies in hydrogen addition or hydrogen loss type of interaction, which occur during the formation and maturation of the oil (Speight, 1999).



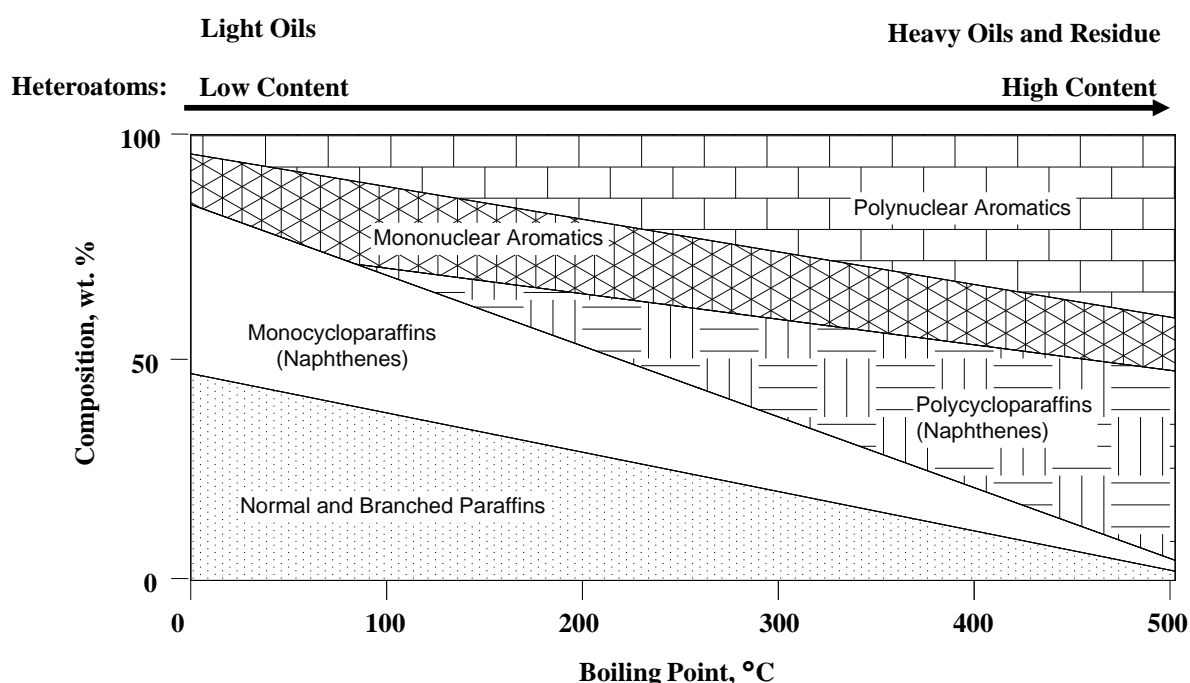
**Figure 2.1. Examples of different hydrocarbon groups for C<sub>6</sub>**

Going back to the basic concepts, paraffins are defined as saturated hydrocarbons with straight or branched chains, but without any ring structure. Naphthenes, conversely, are saturated hydrocarbons allocated in one or more ring structures. The naphthene hydrocarbons, containing side chains, are called alicyclic hydrocarbons. On the other hand, aromatics are hydrocarbons containing one or more ring systems such as benzene and naphthalene, which can also be linked up with naphthenic rings and paraffinic side chains (Speight, 1999).

As shown in Figure 2.2, the concentration of normal and branched paraffins decreases with the increase in the oil molecular weight and the boiling point of the cut. Considerable quantities of iso-paraffins have been noted to be present in straight run gasoline, whereas in some types of heavy oils no paraffins are found in the gasoil fraction. In the case of naphthenes and aromatics, they show higher concentration and higher level of condensation along with the increase in the molecular weight and boiling point of the crude oil. It is generally believed that naphthenes in oil



mainly have between five and six member rings conforming the molecules and that the size of the alkyl group they can possess is shorter than those present in aromatics. Except for the lower petroleum fractions, aromatics are usually found in combination with naphthenes and alkyl substitution, especially in the heavier fractions of the oil. Even if one aromatic ring such as benzene is part of a molecule with several naphthenic rings and branched paraffins, the molecule is classified as aromatic (Speight, 1999).



**Figure 2.2. Paraffinic, naphthenic and aromatic hydrocarbon composition in oil for different boiling points (Speight, 1999)**

The overall composition of organic compounds containing nitrogen, sulphur, oxygen, metals (also called organometallic compounds) and inorganic salt in suspension is very low in crude oil. However, they concentrate themselves in the heavier fractions and in the non-volatile residues, which determine their processability. Within this set of organic compounds, those containing nitrogen, high oxygen levels and sulphur are the most important due to their corrosive and harmful characteristic. For that reason, it is a common practice to convert them into easy to remove

molecules. Oxygen is usually present in crude oil in less than 2% mainly as carboxylic acids in naphthene molecules (also called naphthenic acids). Nitrogen, instead, is found in oil as basic and non-basic types of compounds, composed mainly of molecules consisting of pyridine and pyrrole type molecules. In the case of the metals, they can be found in oil either as organometallic surfactants (for Zn, Ti, Ca, Mg) in the water/oil interphase or as oil-soluble compounds (for V, Ni, Fe, Cu). They can generate problems of corrosion and interference with catalytic processes by poisoning the catalyst, which is the reason why their concentration must be reduced (Speight, 1999). Additionally, sulphur is an important contaminant for the refining surroundings and if present in the fuel, it can also cause acid rain.

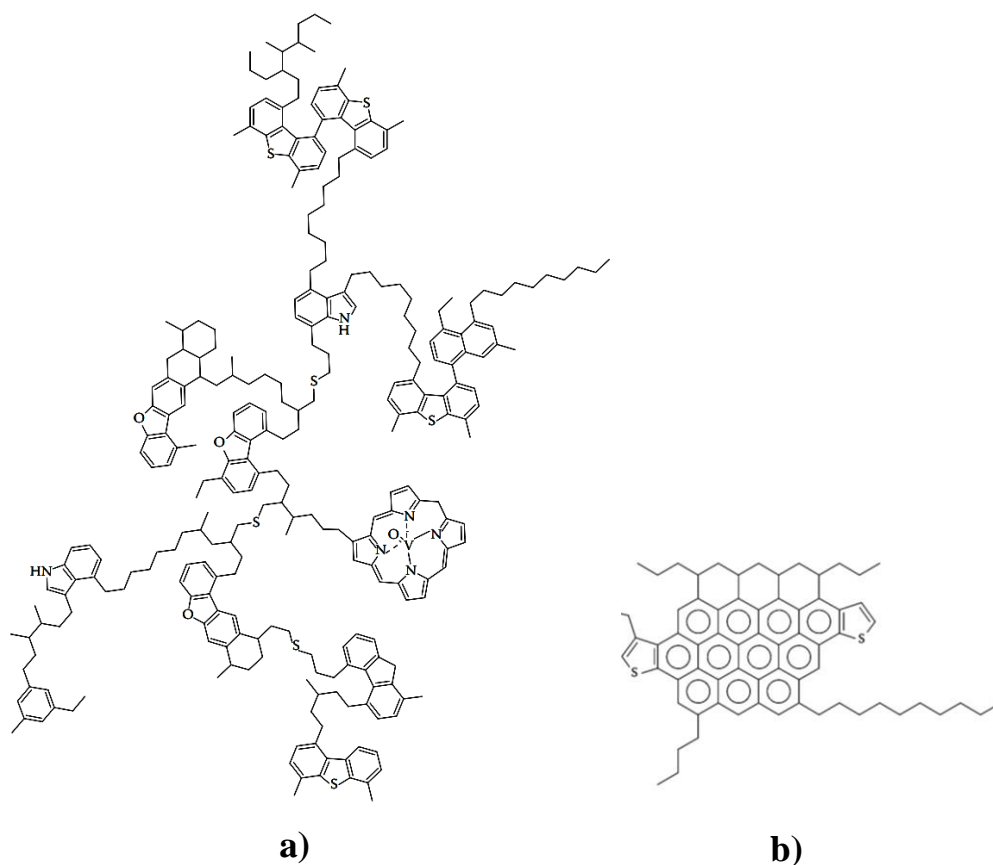
Several analytical techniques allow the fractionation of crude oil into families of compounds with common characteristics. By this means, laboratories are able to compare differences in the composition of these families in crude oils from different origins, as well as the effect of refinery processes in the chemistry of the hydrocarbons. One of the most commonly used separation techniques focuses on fractionation of the crude oil according to a set of molecules of similar boiling point. Every boiling point can be directly correlated with properties such as viscosity and density (Huc, 2011). The heavier the crude oil, the higher the amount of heavy molecules with high boiling point, viscosity and density.

Chemical fractionation of the crude oil by polarity is commonly performed to divide the crude oil into saturates, aromatics, resins and asphaltenes (SARA). Saturates consist of non-polar material constituted by linear, branched and cyclic saturated hydrocarbons (paraffins and naphthenic kind of molecules). The aromatics containing one or more aromatic rings are more polarizable. The latter two, resins and asphaltenes, are the most polar compounds due to their polar substituents. The difference between them lies in the insoluble character of asphaltenes in excess of paraffins such

as heptane or pentane (Fan, et al., 2002). Resins and asphaltenes are very similar in molecular structure, but the latter are characterized with higher molecular weight up to 1650 g/mol (Ancheyta, et al., 2009).

The asphaltene fraction is mainly constituted by aromatic rings with alkyl chains up to C<sub>30</sub>, sulphur compounds (e.g. benzothiophene), nitrogen and metalorganic compounds, ketones, phenols and carboxylic acids. Asphaltenes molecules have been modeled in two different ways (shown in Figure 2.3): archipelago type (a) and continental type (b). The first one is represented as small cores of a few aromatic rings linked to each other by bridging alkanes and sulfur, while the continental type is described as a composition of seven or more aromatic rings conforming the core of the molecule. Both of them aggregate in different ways, the archipelago-type asphaltenes develop planar aggregates in asphaltene solutions. In the case of the continental asphaltenes, they tend to stack and form columns (Ancheyta, et al., 2009).

The stability of asphaltenes is a major issue in the oil industry to avoid plugging and fouling along the different steps involved in the production, transportation and refining of crude oil. Due to the insolubility of asphaltenes in paraffins, crudes with high content of saturates tend to be unstable, while crudes rich in aromatics are more stable (Ancheyta, et al., 2009). The stability of asphaltenes in the crude is also critically related to the amount of resin content. However, it is still not well understood if both fractions work together as a colloidal system or if resins improve the solubilisation of asphaltenes in the crude oil; or if both mechanisms occur simultaneously (Carnahan, et al., 2007).



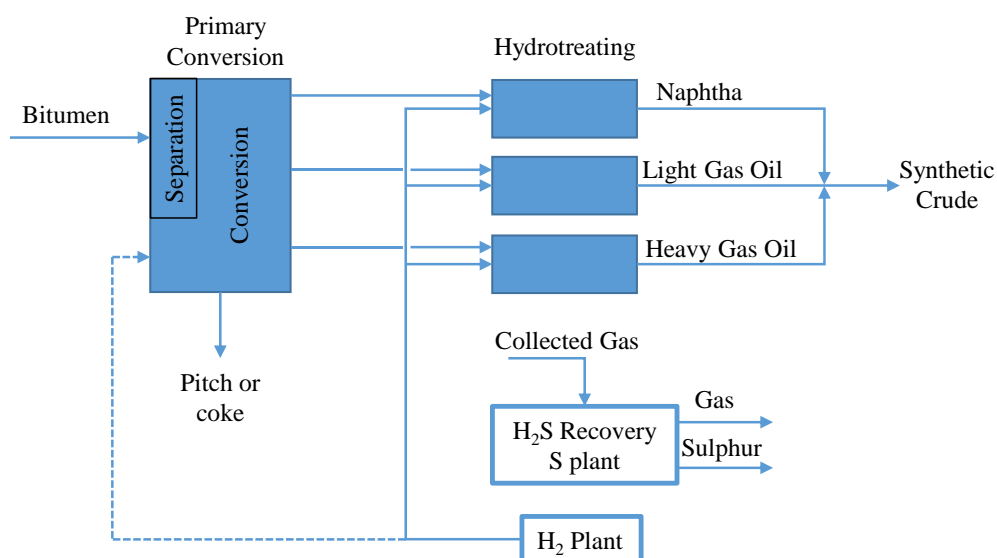
**Figure 2.3. Model molecules for asphaltene type archipelago (a) and continental (b) (Ancheyta, et al., 2009)**

## 2.2 Upgrading

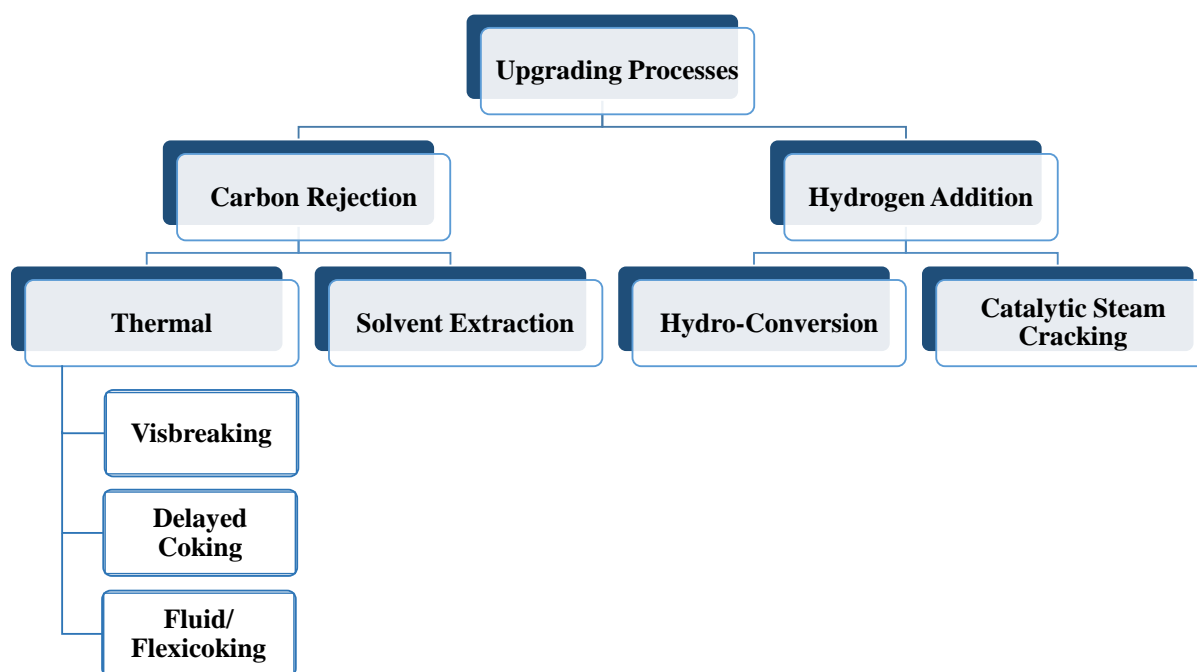
As a consequence of the poor quality of heavy oils regarding °API, viscosity, heteroatoms and residue content; and difficulties encountered regarding transportation, the interest and monetary value of this raw material in the market is relatively low. Therefore, upgrading emerged as a solution to process this material and generate a product that can compete in price with conventional oils. The degree of conversion needed is determined by the targeted market. In the case of the American market, where most of the refineries have been transformed into deep conversion refineries (around 86% of them are equipped with a Fluid Catalytic Cracker), the upgrading should be just enough to meet transportation specification (Huc, 2011).

In general, the upgrading process can be divided into two stages, as it is shown in Figure 2.4. The first stage consists of a primary conversion of the oil with some prior distillation or topping depending of the characteristics of the oil (Speight, 2013). During this stage, heavy molecules are cracked into lower molecular weight molecules and the initial composition of nitrogen, oxygen, sulphur and hydrogen are redistributed within the generated streams. The main goal of the secondary upgrading stage is to remove heteroatoms and saturate aromatics, usually carried out by hydrotreating (Banerjee, 2012). The products of the hydrotreating are mixed together to generate the synthetic crude oil that meets refinery specifications. Moreover, during the first stage of conversion, pitch or coke is produced which is usually piled up, as well as the solid sulphur produced as a consequence of the  $H_2S$  generated along the two stages of the system.

In the primary conversion stage, the light fraction ( $<535^\circ C$ ) is separated from the residue ( $>535^\circ C$ ) with atmospheric and vacuum distillation units. Then, the residue is converted with either one or a combination of the processes presented in Figure 2.5. They are mainly divided into carbon rejection processes and hydrogen-addition processes (Banerjee, 2012).



**Figure 2.4. Typical upgrading scheme (Speight, 2013)**



**Figure 2.5. Upgrading pathways (Banerjee, 2012)**

### *2.2.1 Carbon rejection processes*

The main goal of this kind of processes is to remove heavy carbonaceous material from light hydrocarbons. Therefore, as a result, one stream containing heavy material is produced along with another stream containing the lights generated. This type of process can be subdivided depending on the nature of the separation, which can be either chemical rupture of the molecules by heat or physical separation of the asphaltenes using a solvent (Banerjee, 2012).

#### *2.2.1.1 Thermal processes*

Thermal cracking is one of the oldest conversion processes used in the oil industry to treat heavy hydrocarbons. Its attractiveness lies in the low operating pressures, high temperatures and the lack of need for catalysts, which are usually expensive (Speight, 2013). The chemistry of the process consists in carrying out a set of endothermic chemical reactions that break the side chains of the aromatic complexes and even their ring structure via free radicals. The mechanism starts with the

scission of the bonds C-C, C-S, C-O, C-N and even C-H at high temperatures (above 400°C), which create free radicals. Then, these radicals promote other reactions to occur, such as: activation of surrounding molecules via H-transfer (propagation of free radicals), decomposition of the free radical into olefins, isomerization and cyclization reactions, condensation reactions to form polyaromatic compounds, etc. When two free radical encounters each other, they recombine to form a bond and the reaction concludes (Huc, 2011).

The quality of the products of a thermal process is highly dependent on the operating pressure and temperature. Temperatures greater than 500°C and pressures lower than 100 psi tend to produce lower molecular weight hydrocarbons than those processes operated at temperature lower than 500°C and pressures between 400 and 1000 psi. The severity of the process may be adjusted to the requirements. Mild cracking conditions generate a high amounts of gasoline of poor quality, less gas and decrease coke formation. On the contrary, high severity conditions generate important amount of gas, more coke production and less gasoline (Speight, 2013).

The most common thermal processes can be divided into visbreaking (viscosity breaking) and coking. The first one is undertaken at mild conditions of 450-500°C with residence time of 1-5 min, in order to break the C-C bonds that attach paraffins to the nucleus of the polyaromatic rings. In that way, the main goal of the process is to decrease the viscosity of the oil without getting rid of the heavy fraction. The main disadvantage consists in the instability produced by chemical conversion of the asphaltenes that tend to precipitate (Banerjee, 2012).

On the other hand, coking can be at the same time divided into delayed coking and fluidized coking. Both of them work at high severity for long residence time, aiming to convert 100% of the residue. However, they differ significantly in the way they operate. Delayed coking is carried out in drums that work as batch reactors at 430-450°C, 30-60 psi with long residence time. The feed,

typically vacuum residue, is preheated in a furnace at 490-500 °C, loaded into the drums from the bottom and left it there for hours to promote coking. Fluidized coking, instead, consists of a continuous process, where a fluidized bed riser reactor operating at higher temperatures (about 540°C) with a residence time of minutes, targets the increase in the liquids yields and decrease of the coke formation (Banerjee, 2012).

#### 2.2.1.2 Solvent extraction

Solvent extraction, also called solvent de-asphalting, is a physical process in which the feedstock can be separated into structural families rather than in boiling point as in the case of distillation (Huc, 2011). Therefore, when the bitumen encounters the solvent, the dispersion of the oil components is disrupted and the polar constituents such as asphaltenes and the heaviest resins precipitate (Speight, 2013). As a result, two streams are produced: one called pitch, enriched in asphaltenes and another one called De-asphalted Oil (DAO) mainly constituted by saturates, aromatics and light resins. It is important to note that the solvent de-asphalting unit is not a conversion process, and thus, it must be considered as a preliminary separation integrated to any of the other technologies that convert the heavy fractions of the oil (Huc, 2011).

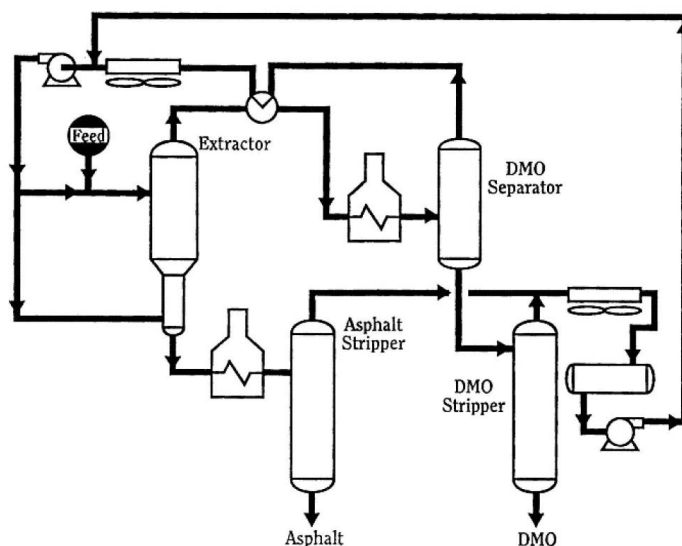
The selection of the solvent is one of the main parameters in the solvent de-asphalting unit. They consist of light paraffins ranging from C<sub>3</sub> up to C<sub>7</sub>, whose selection depends on the quality and the yield of DAO expected. The heavier the solvent, the poorer the quality of the DAO but the higher the yield obtained. Butane is recommended to obtain high quality DAO with an acceptable yield of 40% in the case of processing Athabasca bitumen, while pentane gives a poorer DAO but with yields of 75%. Another important parameter is the solvent to feed ratio, which is proportional to the yield of DAO and inversely proportional to the quality of the DAO produced in terms of metals,



nitrogen and sulphur. With a ratio 4:1 less than 0.05% of asphaltenes can be reached in the DAO, but typical industrial values are around 5:1 (Huc, 2011).

Moreover, the temperature has an important effect in the operation and in the quality of the product obtained. The higher the temperature level, the better the contaminants and asphaltenes removal from the DAO, but the lower the yield obtained toward this stream. The operating pressure, instead, has little effect in the selectivity of the process and it is just fixed slightly above the critical pressure of the solvent (Huc, 2011).

The two most common industrial processes are DEMEX licensed by UOP and ROSE licenced by Kerr-McGee. Both of them work at subcritical conditions for the extraction and supercritical conditions to recover the solvent. The separation of the solvent is performed by slightly increasing the temperature of the product above the critical temperature of the solvent. In Figure 2.6, the schematic of the ROSE process is presented. The feed is mixed with solvent previously recovered and inserted into the extractor to produce DAO (called here De-Metallized Oil, DMO) and asphalt, both still containing the solvent. Then, the streams are heated up and pumped into the separators to recover the solvent, which is cooled down and recirculated at the inlet of the system (Gary & Handwerk, 2001).



**Figure 2.6. Schematic of the ROSE process (Gary & Handwerk, 2001)**

There is an obvious advantage of using this process as an intermediary process in the refinery due to the fact that the residue free of asphaltenes and with lower amount of metals and heteroatoms becomes easier to convert than the original residue. Depending on the quality of the DAO generated, it is a desirable feedstock for a Fluid Catalytic Cracker (FCC), hydrocracker or it can be simply de-sulphurized in a hydrotreater. However, the use of the material rejected is still an issue. The most common uses for the pitch are in power generation where it is used as a fuel, for the production of asphalt, as feed in a partial oxidation unit to produce hydrogen rich gas or in a hydro-visbreaking unit to convert the asphalt into feedstock for other units. In general, the process is relatively low cost and gives the possibility to generate a wide variety of DAO (Speight, 2013).

### ***2.2.2 Hydrogen addition processes***

The hydrogen addition processes aim to improve the quality of the heavy oil by increasing the hydrogen to carbon ratio and removing impurities such as heteroatoms and metals. The typical processes involving hydrogen as reactant consists in treating the feedstock in a reactor with a high

partial pressure of hydrogen in the presence of a catalyst. During oil hydroprocessing several reactions occur, and they can be grouped into three: Hydrocracking, Hydrotreating and Hydrogenation. In the first set of reactions, heavy molecules are cracked into smaller molecules, leading to the formation of free radicals that are further stabilized with hydrogen. The presence of hydrogen avoids condensation reactions between large organic molecules (especially aromatics) that promote coke formation. Within hydrotreating reactions, heteroatoms and metals are removed via Hydrodesulphurization (HDS), Hydrodenitrogenation (HDN), Hydrodeoxygenation (HDO) and Hydrodemetallation (HDM). Hydrogenation reactions target the saturation of aromatics and they are also involved in the final stabilization of the unsaturated molecules produced during cracking (Banerjee, 2012). Oil hydroprocessing favors disaggregation and cracking of asphaltenes, as well as reduction of Conradson Carbon (Huc, 2011).

Table 2.2 shows the main reactions occurring during hydroprocessing. As it can be seen, most of them are exothermic reactions, especially those involved in the saturation of olefins. Reactions involved in the metal and heteroatoms removal are mostly catalytic, while those involved in the hydroconversion or hydrocracking of the feedstock are a combination of thermal and catalytic reactions. Molecular cracking itself occurs mainly because of the effect of the temperature, which makes it an endothermic process. However, the hydrogenation of the free radicals produced during thermal cracking is highly exothermic, giving in general a slightly exothermic process (Huc, 2011).

**Table 2.2. Typical hydroprocessing reactions (Robinson & Dolbear, 2006)**

Reaction Type	Illustration	$\Delta H_R^*$
<b>Minimal C-C Bond Breaking</b>		
Hydrodesulfurization (HDS) †	$R-S-R' + 2 H_2 \rightarrow RH + R'H + H_2S$	-2.5 to -3.0
Hydrodenitrogenation (HDN)	$R=N-R' + 3 H_2 \rightarrow RH + R'H + NH_3$	-2.5 to -3.0
Hydrodeoxygenation (HDO)	$R-O-R' + 2 H_2 \rightarrow RH + R'H + H_2O$	-2.5 to -3.0
Hydrodemetallation (HDM)	$R-M + \frac{1}{2} H_2 + A \rightarrow RH + M-A$	-3
Saturation of aromatics	$C_{10}H_8 + 2 H_2 \rightarrow C_{10}H_{12}$	-3
Saturation of olefins	$R=R' + H_2 \rightarrow HR-R'H$	-5.5
Isomerization	$n-RH \rightarrow i-RH$	n/a
<b>Significant C-C Bond Breaking</b>		
Dealkylation of aromatic rings	$\Phi-CH_2-R + H_2 \rightarrow \Phi-CH_3 + RH$	-1.3 to -1.7
Opening of naphthene rings	$Cyclo-C_6H_{12} \rightarrow C_6H_{14}$	-1.3 to -1.7
Hydrocracking of paraffins	$R-R' + H_2 \rightarrow RH + R'H$	-1.3 to -1.7
<b>Other Reactions</b>		
Coke formation	$2 \Phi H \rightarrow \Phi\Phi + 2 H_2$	+3
Mercaptan formation	$R=R' + H_2S \rightarrow HS-R-R'H$	-3

\* Kilojoules per standard m<sup>3</sup> of H<sub>2</sub> consumed. For exothermic reactions,  $\Delta H_R$  is negative.

† R = alkyl;  $\Phi$  = aromatic; M = Fe, Ni or V; A = metals-adsorbing material

By varying the operating conditions and the kind of catalyst, the hydroprocessing reactions can be selectively adjusted to either favor hydrotreating or hydrocracking reactions. In general, hydrocracking operates at higher pressures and lower Linear Hourly Space Velocity than hydrotreating (for the same volume of oil processed, hydrocracking requires more catalyst), aiming to obtain high conversions of residue (Robinson & Dolbear, 2006). To the effect of the first conversion stage of an upgrader complex, where high levels of residue conversion is desired, hydrocracking is the process of interest.

Hydrocracking catalysts are typically designed to have two functions: a hydrogenating function and a cracking function. The first one is usually given by group VI transition metal sulfides (mostly molybdenum) promoted by group VIII elements (nickel and/or cobalt). The cracking function is given by acidic zeolites (usually Faujasite) or an amorphous silica-alumina support (Speight, 2013). The acid sites present in the hydrocracking catalysts serves as proton donors to attack the

hydrocarbon, in order to follow a cracking via carbonium ion (Greensfelder, et al., 1949). Further development of catalysts for hydrocracking offers the ultradisersion of a bi- or tri-metallic catalyst from the group VI and VIII in the feedstock. As a consequence of the nano scale particle diameter, the surface area available and the activity are increased, while deactivation problems tend to be reduced (Pereira-Almao, et al., 2011).

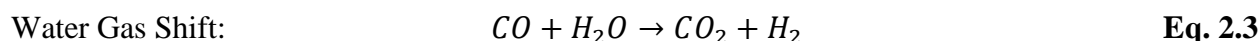
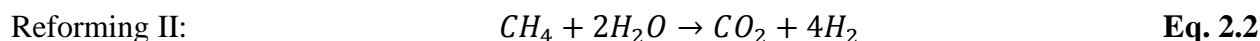
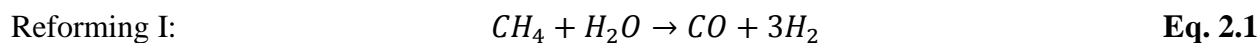
Through the years and because of the changes in the feedstock used, the reactors for hydrocracking have had to evolve. The first kind of reactor was based on a fixed-bed originally designed to treat light oils with low amounts of impurities. As these impurities increased, the plugging of the catalyst pore was often observed, leading to de-activation and frequent shutdowns of the unit. In order to solve this problem, the next generation of reactors consisted in moving beds able to be displaced by gravity from the top to the bottom with the purpose to frequently replace the catalytic bed. On the other hand, the ebullated bed hydrocracker is another type of moving bed reactor that works up-flow with the liquids producing the fluidization of the fresh catalyst incorporated. This kind of reactor was successful at processing vacuum and atmospheric residue at the expenses of the relative high partial pressure of hydrogen required and the high catalyst replacement rate. In order to control the catalyst addition rate, the slurry-phase type of reactor was created in which the micro size catalyst is incorporated in the feedstock along with powder carbon based additives to promote the coke agglomeration and avoid fouling of the system. Therefore, the ratio of catalyst to oil is easily controlled, as well as the residence time in the reactor. This type of reactor works at high temperature aiming to reach conversion higher than 90% (Banerjee, 2012).

Steam catalytic cracking technologies such as Aquaconversion can be also considered part of the hydrogen addition processes; with the difference that hydrogen is not directly supplied into the system, but provided by the catalytic splitting of the water molecule.

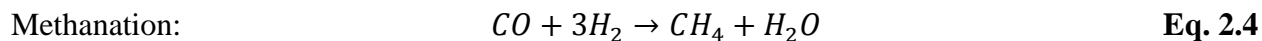
### 2.3 Catalytic Steam Cracking (CSC)

The use of steam for processing hydrocarbons is a common practice in the oil industry. In the thermal cracking of paraffins to produce olefins needed in polymer production, steam works as a diluent to decrease the partial pressure of hydrocarbons in the reactor and thus, favor the production of olefins, which are first-order reactions, but not the condensation reactions, of higher order, that leads to coke formations (Froment, 1992). However, in the steam reforming of methane and light hydrocarbons for the production of hydrogen, the water molecule has an important role as a reactant in the oxidation process of the carbon atoms.

Steam reforming of methane mainly involves the following three reactions, typically performed in the presence of a nickel catalyst:



Methane can be also produced via CO methanation:



The first and third reaction (Eq. 2.1 and Eq. 2.3) are highly endothermic, while the second one is slightly exothermic. Therefore, due to the high endothermic character of steam reforming reactions, the process is usually performed between 820-880°C and pressures of 294-368 psi. Steam reforming of heavier hydrocarbons than methane follows the path: cracking of the molecules to obtain methane and then proceed to its reformation (Fahim, et al., 2010).

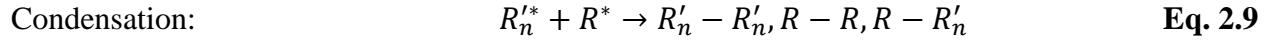
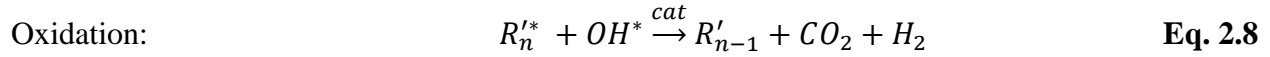
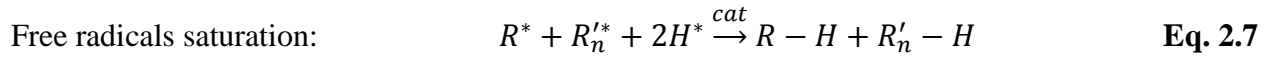
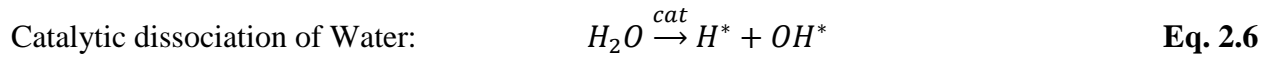
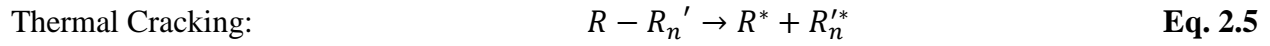
The simplest application of this chemistry to the cracking of hydrocarbons is the de-alkylation of alkylaromatics, which is one of the main pathways to produce benzene and has been industrially

performed under hydrogen atmosphere in the presence of a catalyst. In order to reduce the consumption of hydrogen in the different units in a refinery, intense effort has been allocated into developing a technology able to substitute the hydrogen by steam. Therefore, selective steam reforming of the alkyl group in the molecule, in the presence of a catalyst was developed. One of the main advantages of this process is that not only hydrogen was substituted by water, but also hydrogen was produced in the reaction as a by-product. Several metals from the Group VIII have been evaluated, showing Rh as the most active metal and with an important effect of the support in the activity of such catalysts (Duprez, 1992). In order to avoid full oxidation of the hydrocarbon to CO and CO<sub>2</sub>, the steam reforming conditions were reduced up to temperatures between 350-500°C, pressures between 14.7-427 psi and weight hourly space velocity between 0.3-3 h<sup>-1</sup> (Uchiyama, et al., 1974).

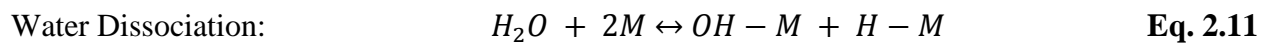
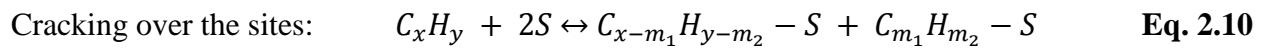
The problems found in the typical thermal conversion processes regarding the amount of solid material generated (in the case of coking) from the crude and the instability of the products in visbreaking, favor the utilization of hydrogen addition processes looking for a better yield and quality products. However, the most common technology in the market is hydrocracking that requires high pressure of hydrogen and special material and equipment to work at those conditions. Therefore, a solution to those issues and based on the previous experience collected with steam processing of light hydrocarbons, steam catalytic cracking was developed to process heavy hydrocarbons with high content of alkylpolyaromatic compounds. The idea is to take advantage of the hydrogen produced by reforming reactions in order to saturate cracked molecules and give stability to the products.

### 2.3.1 Thermodynamics and mechanism

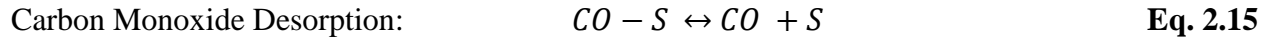
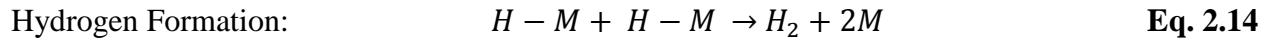
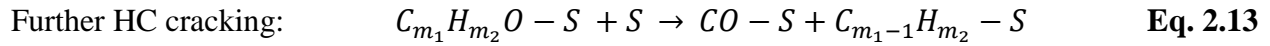
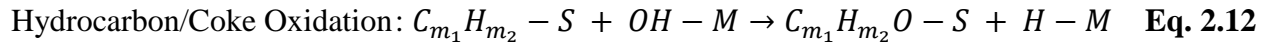
Pereira-Almao, et al., 2013 proposed a set of reactions to describe catalytic steam cracking involving the effect of catalytic pathways in the stabilization of the free radicals produced during the thermal cracking of the hydrocarbons. This kind of mechanism has been used previously to describe hydroprocessing, with the difference that the catalyst dissociates the hydrogen instead of the water molecule (Pereira-Almao, et al., 2013).



The mechanism of reaction usually varies with the type of material used as catalyst, but experiments in steam reforming of iso-octane at temperatures between 310-350°C over nickel supported on alumina, has demonstrated that steam reforming reactions follow a Langmuir–Hinshelwood model where the catalytic cracking require two sites to take place, different from the one required by the water molecules to be split. In that sense, catalytic cracking reactions and water dissociation reactions do not compete for the same sites (Praherso, et al., 2004). The following set of reactions shows the steps involved where each kind of compound is adsorbed, being S and M two different active sites.

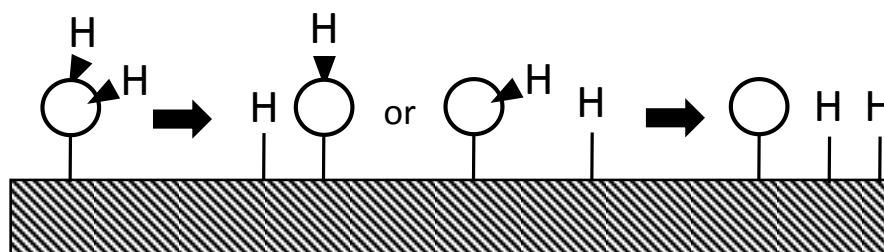






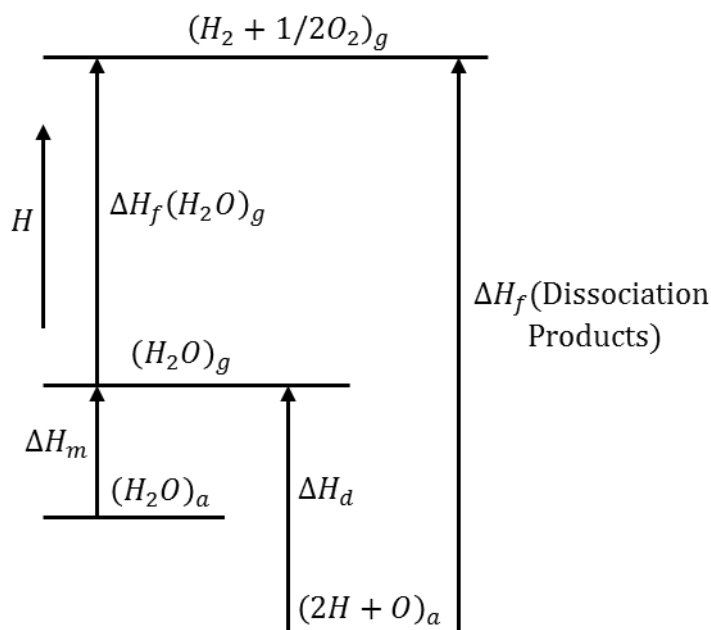
In order to favor the occurrence of the catalytic steam cracking process, two main reactions must be favored: the hydrocarbon cracking (either catalytically or thermally) and the catalytic water dissociation. The hydrocarbon cracking via thermal cracking is an endothermic reaction and it is favored by increase of the temperature. However, it can be improved by the incorporation of an acidic material like those in hydrocracking type of catalysts where the reaction follows the carbenium ion mechanism like in conventional catalytic cracking. This kind of mechanism leads to the production of a large amount of branched paraffins. In the case of aromatic reactants, the carbenium ion mechanism in the presence of hydrogen leads to the de-alkylation or saturation of the aromatic rings into naphthene molecules (Flinn, et al., 1960).

The dissociation of water molecules is a key step in the production of the hydrogen required to avoid the undesirable condensation reactions. Therefore, it is important to understand the chemistry involved in the adsorption and dissociation of the water elements. In Figure 2.7, it is shown the pathway followed by the adsorbed water molecule, which can either split into adsorbed hydroxyl and atomic hydrogen, or further split into atomic hydrogen and atomic oxygen (Thiel & Madey, 1987).



**Figure 2.7. Possible dissociation reactions of adsorbed water (Thiel & Madey, 1987)**

The products and the stability of the products on the surface of the metal are controlled thermodynamically, which controls the products to either recombine to reversibly liberate water or stay stable as individual entities on the surface (irreversible dissociation). Reversible water dissociation is typically observed on oxide surfaces, while irreversible dissociation is observed on metals and semiconductors (Henderson, 2002). Figure 2.8 shows a schematic of the thermodynamic involved in the dissociation of water giving atomic hydrogen and oxygen, omitting kinetic and entropy factors. On the left side, there is a change in enthalpy ( $\Delta H_m$ ) between the free water and adsorbed water, which is the negative of the heat of desorption and can be assumed constant. It has been studied that this parameter does not vary widely among several metals studied. The gaseous state of water molecules (desorbed) can be related to the enthalpy of formation of water ( $\Delta H_f \text{H}_2\text{O}_g$ ) from atomic hydrogen and oxygen. At the right side of the figure, is shown a change in energy between atomic hydrogen and oxygen adsorbed and desorbed ( $\Delta H_f$ -dissociation products), which is related to the energy of formation of the bonds between each atomic hydrogen and oxygen to the metal. In that sense,  $\Delta H_d$  is the enthalpy of dissociation of the water molecules on the surface of the catalyst. Therefore, for a given system, obtaining  $\Delta H_d$  greater or more positive than  $\Delta H_m$ , may imply a non-dissociative adsorption of the water molecule, while having a more negative value supports dissociation on the surface (Thiel & Madey, 1987).

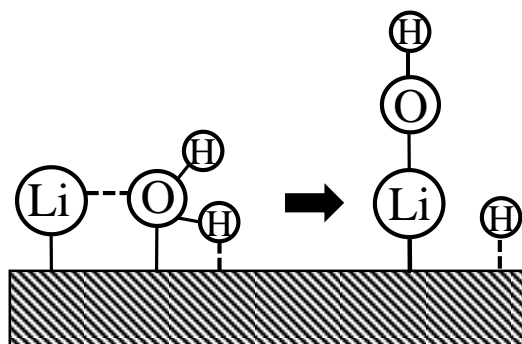


**Figure 2.8. Thermodynamics of water dissociation on a metal surface (Thiel & Madey, 1987)**

The interaction between oxygen and the metal varies more with the type of metal than the interaction hydrogen and metal does. Therefore, the capability of a metal to dissociate water is closely related to its capability to create strong bonds with oxygen. In that sense, most of the Group VIII elements are able to dissociate water, except for some that are relatively inert to form oxides. Some metals such as Co, Ni, Re and Cu are able to dissociate water depending on the morphology in which they are found and the roughness of the surface (Thiel & Madey, 1987). For example, some metallic nickel planes like the Ni (1 0 0), flat and stepped Ni (1 1 0) and stepped Ni (1 1 1) are able to dissociate the water molecules, while some others are not (Henderson, 2002).

Even though the mechanism is not well understood, it is held that alkali used as promoters alters the electronic structure of the metal catalyst favoring the water adsorptive dissociation. In processes where the dissociation of water is the limiting step, it is a common practice to incorporate an alkali such as Cs to the catalyst (Henderson, 2002). Figure 2.9 shows a representation of what

is believed to occur in the adsorption and dissociation of water on a Cu-catalyst containing alkali metals. As it can be seen, the oxygen created a preferential interaction with lithium that triggers the dissociation of the water molecule. As a result, the OH specimen stays adsorbed on the promoter while the H remains on the surface of the metal.



**Figure 2.9. Schematic of the transition state of water molecules on Cu (1 0 0) promoted with Li (Henderson, 2002).**

### ***2.3.2 Technologies***

In 1972 the company Phillips Petroleum Co. patented a method for the upgrading of hydrocarbons based on the in situ generation of hydrogen, via the water gas shift reaction, together with the processing of the oil to produce materials of low molecular weight, having reduced residue and sulfur content. The method consisted of incorporating, simultaneously or in series, two catalytic agents into the oil together with water: one is usually carboxylic salts of alkaline earth metals with the goal of producing the hydrogen from the water. The second agent is in charge of facilitating the reaction between the hydrogen and hydrocarbon constituents, for which carboxyl salts of nickel, cobalt and iron are used. The amount of water incorporated was fixed in a water to oil volume ratio recommended between of 0.2 to 2.5. After mixing, the stream is brought to reaction

condition between 399 and 454 °C and pressure between 300 and 4000 psig to keep most of the oil in liquid phase (Pitchford, 1972).

After several years of research in this field, in 1999 PDVSA-Intevep patented a conversion process technology developed by Pereira-Almao et al 1999, where light hydrocarbons and a reduced level of coke by-products are obtained from catalytic steam cracking of heavy hydrocarbon. Depending on the heaviness of the feedstock, the invention proposed two process' schemes: one for heavy oil and another for extra heavy oil with °API lower than 10. In the first scheme, either atmospheric or vacuum residue is separated from the remaining cuts in order to process it. This residue is passed through a catalyst preparation unit to incorporate the ultra-dispersed catalytic agent into it. Once the feedstock contains the catalyst, steam is integrated into the stream and both pass through a soaker reactor, where the desired catalytic steam cracking reactions take place. The products from the soaker reactor together with the light hydrocarbons obtained in the first separation stage, are recombined in a cyclone, in order to remove coke and catalysts. Different products can be obtained from this scheme such as gas topping, naphtha, gas oil and the bottom. When the feedstock consists of extra heavy hydrocarbons, the technology proposed a similar scheme to the one applied to heavy oil, but targeting transportable synthetic crude oil. In this case, the synthetic crude consists of the products of the catalytic steam cracking unit recombined with the lights from the first fractionation unit, previously desalted to remove catalysts (Pereira-Almao, et al., 1999).

In the catalyst preparation unit, a water in oil emulsion is prepared containing an alkali metal (K and/or Na) and second metal selected from the Group VIII non-noble metal (Ni or Co) or an alkaline earth metal (Ca or Mg) and the mixtures thereof. According to the invention, the steam conversion conditions are reached between 360-520 °C and pressure less than 600 psi, but preferably the operating conditions should be between 410-470 °C with a pressure of 300 psi. The

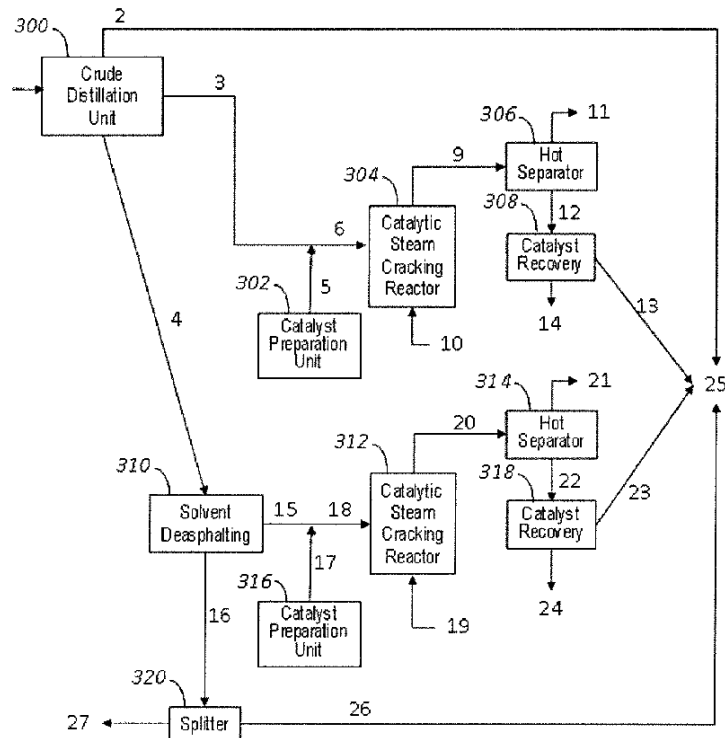
liquid hourly space velocity is kept constant between 0.001-3.5 h<sup>-1</sup> depending on the severity required; and with steam in between 3 to 12 wt. % of the oil. The technology claims to reach conversion of up to 65% of 500°C+ with high selectivity toward middle distillates (Pereira-Almao, et al., 1999).

Nevertheless, the steam conversion of the heavy fractions in the oil, specifically the asphaltenes, tends to generate stability problems for the products. Cracked asphaltenes start precipitating, generating fouling problems in pipelines and vessels. In order to solve this issue, Pereira-Almao, et al., 2013 together with Nexen proposed three possible schemes for upgraders based on the steam catalytic processing of the heavy streams free of asphaltenes. In the first scheme, the heavy oil is fractionated into lights (IBP-250°C), full range gasoil (250-540°C) and vacuum residue (>540°C). One fraction of the vacuum residue is used as fuel and the remaining fraction is recombined at the end of the process with the upgraded product. The gasoil is processed in the catalytic steam cracking reactor, for which the operation varies whether a nanosize catalyst is added prior to reaction or a catalytic fixed bed is used. The liquids are separated from the gases in a hot separator and mixed with the lights and the fraction of vacuum residue determined. In the case of using ultradispersed catalysts, the nano particles are separated from the liquid products before the mixing with the other streams (Pereira-Almao, et al., 2013).

The second scheme for processing asphaltene free streams, consists of topping the crude oil to separate the stream into lights (IBP-250°C) and topped heavy oil (>250°C). The heavy hydrocarbons are once again separated in a Solvent De-Asphalting unit (SDA) into De-Asphalted Oil (DAO) and an asphaltenes rich fraction, which is partially used as fuel. The DAO is processed in a steam catalytic cracking reactor and the products are de-gasified in a hot separator and further mixed with the lights and a certain fraction of pitch. The third scheme, presented in Figure 2.10 is

basically a combination of the previous two schemes, where the vacuum residue obtained in the first stage of the process is de-asphalted and processed via catalytic steam cracking. The lights together with a fraction of the asphaltene rich stream is mixed with the processed gasoil and DAO free of catalyst. The process claims to be able to reduce considerably the viscosity as well as maintaining the stability of the final synthetic crude oil within the three schemes presented. The operating conditions established involved pressure and LHSV constants of 400 psi and 2 h<sup>-1</sup>, respectively. 400 °C was used for processing gasoil and 435 °C for DAO (Pereira-Almao, et al., 2013).

For the purpose of this technology, the nano-catalyst was prepared by pre-mixing an alkali solution (organic or inorganic) with a transition metal inorganic salt or an organo-soluble salt. The metal enriched stream is vigorously mixed with the hydrocarbon to assure the incorporation of the aqueous solution. The developed catalyst preparation methodology, in contrast with Intevep's patent, generates smaller particle sizes by decomposing the emulsions in a controlled manner at high temperature and high flowrates, out of the CSC reactor, specifically in the Catalyst Preparation Unit. Therefore, an increase in the activity per unit mass of catalyst is obtained. The invention also proposes the possible use of rare earth oxides such as Ce, Group IV metals such as Zr oxide and Ti oxide and mixtures thereof together with NiO, alkali metals, CoO<sub>x</sub> and MoO<sub>3</sub> (Pereira-Almao, et al., 2013).



**Figure 2.10. Scheme for catalytic steam processing of asphaltene-free hydrocarbons (Pereira-Almao, et al., 2013).**

## 2.4 Catalyst Development

One of the main challenges for developing supported catalyst for processing heavy hydrocarbons lies in the creation of materials with pore sizes able to handle molecules as big as asphaltenes (size  $> 30 \text{ \AA}$ ), which usually diffuse slowly inside the channels and end up blocking them. As a consequence, active sites inside the channels are lost and de-activation of the catalyst occurs (Banerjee, 2012). In the present research, a variety of materials, described below, were selected to create catalysts of different pore sizes and surface area, carrying the metals of interest to undertake the desired steam cracking reactions.

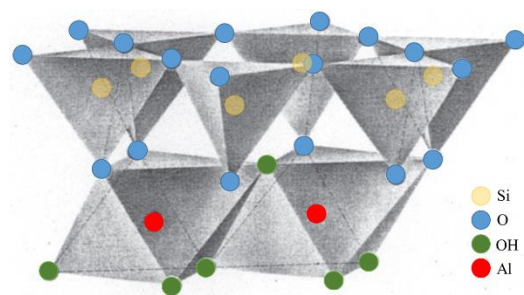


Regarding the catalyst formulations, as for instance in the case of nano catalysts, the use of emulsions containing non-noble metals from the Group VIII (Ni and Co) with alkaline earth metals (Ca, Mg) has been studied with good results toward the production of ultradispersed catalysts (Pereira-Almao, et al., 1999). Further development of these catalysts allowed the preparation of bi and trimetallic catalysts, containing non-noble metals from Group VIII non noble metal and/or two metals from Group VIB (Cr, Mo, W) in the presence of a sulfiding agent (Pereira-Almao, et al., 2011).

For the purpose of this research, bimetallic and trimetallic catalysts were developed. All of the prepared formulations incorporated Ni, which is commonly used in the oil industry for hydrogenation, due to its relative low value, high activity and selectivity (Bartholomew & Farrauto, 2006). The first catalyst (Cat 1) consists of a mixture of kaolin and nano-particles of nickel together with one alkaline (Cs) and one alkaline earth metal (Ba) added as promoters to improve the basicity of the catalyst and to favor reactions involving steam (Hassan, et al., 2013). In the preparation of Cat 2, a hydrotalcite type precursor is used for the formation of a well dispersed mixture of oxides including Ni and Ce dispersed in amorphous aluminium oxide. From the literature, the use of Ce increases the dispersion of nickel, reduces coke formation and increases the activity in steam reforming reactions (Zhang, et al., 2014; Zhang, et al., 2009; Tang, et al., 2014). The third catalyst (Cat 3) consists of a nano-pyroxene material, the sodium-iron silicate Aegirine, with Ce (partially replacing Fe) and adding nickel by impregnating the surface. Catalyst four (Cat 4) is prepared from a Faujasite zeolite X, incorporating Ni and Ce in the cavities of the material by ion exchange of the original Na. Lastly, Cat 5 was prepared by combining the calcined hydrotalcite, as in Cat 2, together with a nano-crystalline cubic molybdenum carbide material.

### 2.4.1 Cat 1: CsBaNi-Metakaolin

Commercial kaolin rocks are constituted of about 5% of impurities and between 90 and 95% of the kaolin group of minerals, whose major species is kaolinite (Kogel, et al., 2002). Kaolinite is a clay mineral, known as a phyllo-silicate, with the molecular formula  $\text{Al}_2\text{Si}_2\text{O}_5(\text{OH})_4$ . Its structure consists of two basic building blocks as shown in Figure 2.11. The upper layer is made up of tetrahedral  $\text{SiO}_4$ , while the bottom layer is an octahedral structure with oxygen and OH group edges and centered on Al atoms (King, 2009). Due to the good packing of the structure, the sheets are hard to separate and thus, most metal sorption activity occurs on the exposed surface area (Miranda-Trevino & Coles, 2003). Calcination of kaolinite at temperatures in the range of 500-800°C, produces the de-hydroxylation of the structure and the formation of a disordered and amorphous material called metakaolin (Siddique, 2008).



**Figure 2.11. Kaolinite structure (King, 2009)**

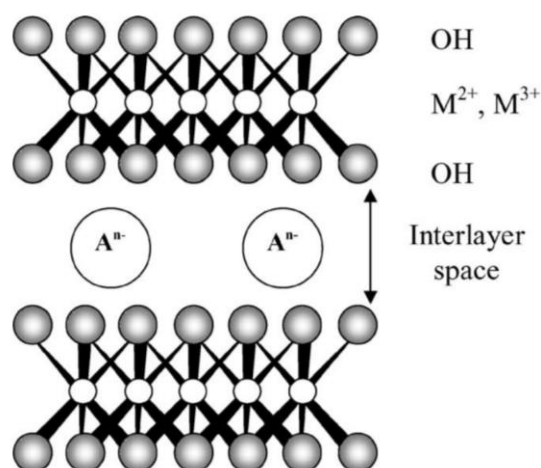
Clays have been extensively used in the petroleum refining industry as supports, matrices of catalysts due to their swelling, adsorption, and ion exchange properties. Before zeolites and aluminosilicates dominated the catalyst market for hydrocracking, acidified kaolin was the main material used. Nowadays, their applications are concerned with the synthesis of zeolite and alumina, as catalyst substrate for the catalytic cracking of petroleum, as adsorbents, ion exchangers, etc. The refractory character of kaolin makes it suitable for processes at high

temperatures and pressures. Besides, it has been demonstrated that the addition of kaolin to FCC catalysts improves the attrition resistance, reduces coke yield and has high tolerance to contaminated metals. They are also excellent supports for Lewis acids or transition metals to be used in organic reactions (Emam, 2013). Hassan et al 2013, evaluated the selective adsorption and further steam gasification of asphaltenes using kaolin loaded with nanoparticles of nickel oxide. Alkaline earth elements (Ca and Ba) were incorporated in the preparation of the adsorbent/catalyst to improve the basicity of the material. The results indicated the positive effect of the catalyst at reduced temperature, at which the asphaltenes crack in a more controlled manner than in thermal cracking. Besides, the production of CO<sub>2</sub> and hydrogen was favored, related to the steam gasification reactions (Hassan, et al., 2013).

#### **2.4.2 Cat 2: NiCe-Calcined Hydrotalcite**

Hydrotalcites are natural anionic clays, also called magnesium-aluminum hydroxycarbonate that can be decomposed during calcination to produce a mix of nano-oxides with high surface area (McKenzie, et al., 1992). They belong to a family of layered double hydroxides (LDHs) with the general molecular formula shown in Eq. 2.16. The divalent and trivalent metals ions ( $M_x^{2+}$  and  $M_y^{3+}$ ) are found coordinated in the double layered hydroxides with octahedral shape, while the compensating anions ( $A^{-n}$ ) are located in the interlayer, as presented in Figure 2.12 (Cantrell, et al., 2005).

LDHs molecular formula	$[M_{1-x}^{2+}M_x^{3+}(OH)_2]^{x+}(A_{x/n}^{-n}) \cdot yH_2O$	Eq. 2.16
------------------------	---	----------



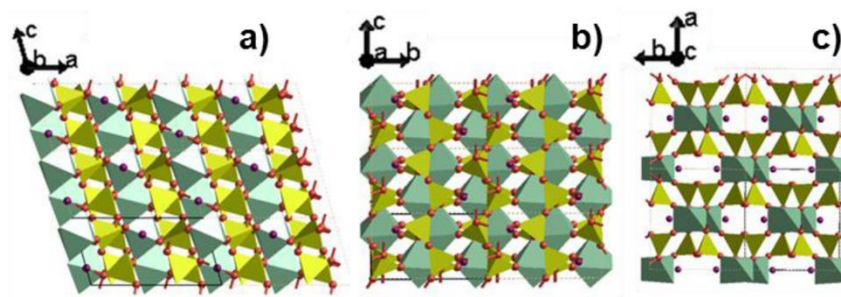
**Figure 2.12. Hydrotalcite structure (Cantrell, et al., 2005)**

The variation of the parameters involved in the molecular formula of the LDHs allows the preparation of various types of synthetic materials. The selection of the metals to be incorporated in the structure, is based on the ionic radius of the metal, which should not be too different from that of  $Mg^{2+}$  (0.65 Å). Several combinations of Mg, Ni and Co as  $M^{2+}$  with Al as  $M^{3+}$  have been used in the literature to prepare hydrotalcites for catalytic purposes. The amount of each cation in the hydrotalcite (x) has been defined to be in the range of 0.2 and 0.33 to obtain pure hydrotalcite, but it can also be extended to a range between 0.1 and 0.5 with the formation of metal hydroxide impurities. There are no limitations regarding the nature of the anion used to compensate the positive charges of the hydroxide layers. However, the size, orientation, number and the strength of the bonds formed determine the separation interlayer space. In the literature, can be found the use of anions such as: inorganics (e.g.  $F^-$ ,  $Cl^-$ ,  $(NO_3)^-$ ,  $(SO_4)^{2-}$ ,  $(CO_3)^{2-}$ ), heteropolyacids and organic acids, the carbonate being the one most commonly used. Those sites in the interlayer not occupied by the anion are filled with water molecules (Cavani, et al., 1991).

The ability to incorporate metals of interest into the structure and the properties of the mixture of oxides after calcination regarding surface area, basicity, thermal stability and small crystal size, have made the hydrotalcite a material suitable for the preparation of catalysts with special use in hydrogenation, polymerization and steam reforming reactions. Catalysts with compositions after calcination of 56.8 wt. % Ni and 9.5 wt. % Al have been prepared in the literature to compare catalytic activity under steam reforming conditions against impregnated catalysts with similar proportion of Ni (61.4% Ni, 19.5%  $\text{Al}_2\text{O}_3$  and 1.31% K). The results showed catalytic improvement at lower temperatures of the coprecipitated catalyst, as well as higher stability and lifetime. Besides, due to the basicity of the mixed oxides, there is no need to incorporate alkali metals into the catalyst (Cavani, et al., 1991). Moreover, the addition of rare earth metals such as La, Zr and specially Ce has been studied, as promoters to improve the dispersion of the metal in the structure, to avoid sintering and to enhance the carbon removal by improving the redox properties of the system. Therefore, steam reforming and hydrogenation reactions are considerably favored (Zhang, et al., 2009; Muñoz, et al., 2012).

#### ***2.4.3 Cat 3: NiCe-Aegirine***

The pyroxenes are a family of minerals with similar crystal structure and general molecular formula  $\text{M}_2\text{M}_1\text{T}_2\text{O}_6$ , where M2 is a five to eight coordinated cation (e.g. Na, K, Li, Ca, Ba, or  $\text{Fe}^{2+}$ ), M1 is a six-coordinated element (e.g. Mg, Mn,  $\text{Fe}^{2+}$ ,  $\text{Fe}^{3+}$ , Al, Cu, Co, Ni, etc.) and T is preferably occupied by Si. Aegirine belongs to this family of compounds with M2, M1 and T sites occupied by Na, Fe and Si, respectively. Thus, the ideal formula of aegirine is  $\text{NaFeSi}_2\text{O}_6$  and the structural shape is presented in Figure 2.13 (Vitale, 2013).



**Figure 2.13. Pyroxene structure showing tetrahedral (yellow) and octahedral (green) layers. M2 cations are represented as purple atoms, M1 cations are grouped in the green octahedral (Vitale, 2013).**

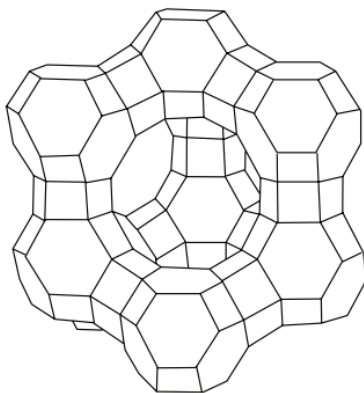
There is little information in the literature regarding the use of aegirine for catalytic purposes, but Vitale, 2013 studied the possibility of exchanging sodium from the crystalline structure by protons, in order to improve the acidity of the material and use it as a hydrocracking catalyst. The experiments processing a model molecule, methyl-cyclohexene, in a reactor at 406°C indicated that the material was indeed able to break the naphthenic rings and to carry out secondary cracking of the produced hydrocarbons. Improvement of the acidity strength by doping the material with Zr showed high activity at lower temperatures, as well as, more selectivity for isomerization and de-hydrogenation. Moreover, experiments to perform hydroxylation of phenol with hydrogen peroxide in presence of aegirine as catalyst, indicated the possibility of using this material to catalyze reactions of organic molecules with steam at high temperatures (Vitale, 2013).

#### **2.4.4 Cat 4: NiCe-Faujasite**

Zeolites are one of the most common used material in the elaboration of catalysts for hydrocracking. As previously mentioned, they support the metals involved in the hydrogenation of molecules, but also their acidity generates the cracking activity required by the process. This type of material came to the industry to substitute amorphous oxides, because of their potential acidity, about 1000 times greater, high surface area and their resistance to coking. Within the wide

range of types of zeolites, Faujasite type Y zeolites are the most commonly used for hydrocracking, while ZSM-5 are mostly used in hydro-dewaxing and shape selective cracking (Ward , 1993).

This type of material is constituted by tetrahedral structures consisting of a cation (e.g. Al, Si, P, Be, Zn, Mg etc.) surrounded by four oxygen atoms. Each of these structures are linked together to form a crystalline framework containing nano-size cavities and channels. Inside the framework, water molecules and easy to exchange cations can be found. The framework in zeolite type faujasite (FAU) consists of linked silicon–aluminum–oxygen with a void volume of about 53%, whose Si/Al ratio define whether it is a Y zeolite (Si/Al around 1.5-3.0) or X zeolite (Si/Al around 1.0-1.4) (Dyer, 2001). In FAU, the framework is constituted by 12 linked tetrahedra that creates a super cage of 12 Å with windows of 8Å in diameter, as shown in Figure 2.14 . The zeolites X and Y are usually prepared in the Na form, which are further ion exchanged with other cations, like for instance ammonium. To produce the acid form, the resultant material is then calcined to decompose the ammonium ions and generate in this way the protons that acidify the structure (Kaduk & Faber, 1995). On the other hand, zeolite X has been of great interest due to the existence of a maximum in the aluminum content and hence, the possibility of exchanging it for cations of interest for the reaction (Lee, et al., 1998).



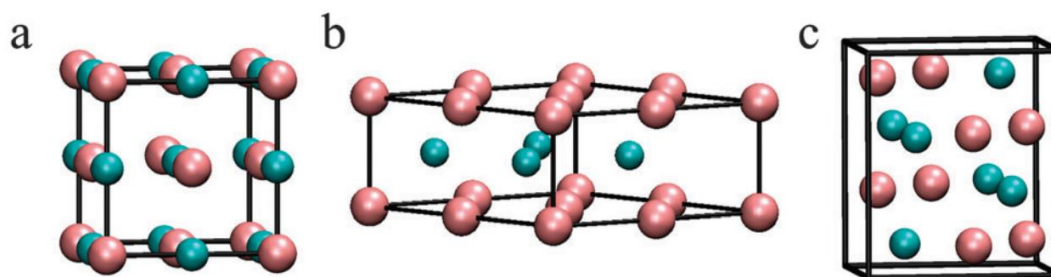
**Figure 2.14. Structure of Zeolite Y (Lutz, 2014)**

#### ***2.4.5 Cat 5: NiCe-Calcined Hydrotalcite+Molybdenum Carbide***

The carburization of Group VI metals like tungsten and molybdenum has been studied since the 70's due to the excellent catalytic properties that the metal develops in presence of carbon, which allows these type of materials to speed up reactions with similar behaviour like those obtained with noble metals like Pt and Pd (Levy & Boudart, 1973). The main interest toward this solid lies in the abundance and low cost of the raw materials used in its preparation compared to noble metals, but specially on their resistance to sulphur and nitrogen poisoning; and their stability under steam (Kaewpanha, et al., 2015; Da Costa, et al., 2001; Xiao, et al., 2000; Dhandapani, et al., 1998). However, research into practical methods to prepare this material at lower temperatures and economically feasible is still carried out. Typically, molybdenum and tungsten carbides are prepared via temperature programmed reaction, where an oxide of the metal of interest, either  $\text{MoO}_3$  or  $\text{WO}_3$ , is thermally treated in presence of a mixture of hydrogen and hydrocarbon until the metal suffers carburization, generating the product of interest. In the case of the molybdenum, this procedure generates the stable hexagonal molybdenum carbide at the end of the process. By using a different precursor such as a cubic oxyhydrate ( $\text{MoOxHy}$ ), the temperature programmed reaction route produces the cubic face of molybdenum carbide. A preparation method to generate this cubic oxyhydrate precursor has been found in the literature, where ammonium heptamolybdate tetra-hydrated is mixed with household sucrose in a solution with water; and then dried out in an oven at  $120^\circ\text{C}$  for 24 h (Vitale, et al., 2015).

In Figure 2.15, the three main stable crystallographic phases for molybdenum carbide are presented, where due to the strongest charge transfer from Mo to C, the  $\beta\text{-Mo}_2\text{C}$  features metallic and ionic character and thus, it is the phase that most activates and stabilizes adsorbed molecules (dos Santos Politi, et al., 2013).





**Figure 2.15. Molybdenum Carbide crystallographic phases: a) cubic ( $\delta$ -MoC), b) hexagonal ( $\alpha$ -MoC) and c) orthorhombic ( $\beta$ -Mo<sub>2</sub>C). Turquoise and magenta spheres correspond to C and Mo atoms, respectively (dos Santos Politi, et al., 2013)**

This phase has been used as a support for different transition metals to carry out methanol steam reforming between 150 and 400 °C. The results showed the complete conversion of methanol for the combination Ni-Mo<sub>2</sub>C at 350°C. The same result is obtained when the temperature reaches up to 400°C for the pure molybdenum carbide ( $\beta$ -Mo<sub>2</sub>C) (Ma, et al., 2014). On the other hand, the hexagonal phase of Mo<sub>2</sub>C( $\alpha$ -Mo<sub>2</sub>C) is also able to hydrogenate completely model molecules such as toluene into methylcyclohexane with no de-activation, at low temperatures of 200°C, low space velocity (WHSV) of 0.35 h<sup>-1</sup> and most important low hydrogen pressures of 2.8 MPa (400 psi) (Frauwallner, et al., 2011). At atmospheric pressure and 90 °C, Rocha Angela S. et al, 2004 was also able to hydrogenate between 20 and 40% of benzene molecules in a batch recirculating apparatus using the same phase of molybdenum carbide, but supported on Y zeolites.

Detailed information about the preparations of the catalysts and their characterization can be found in Chapter Three.

### Chapter Three: Experimental Section

This chapter is intended to explain and provide description of the guidelines followed for the preparation of the catalysts, as well as their characterization. Moreover, properties of the materials used in the experiments, pilot plant description and operating procedure; and methodology for the analysis of the samples generated in the laboratory are also presented within this chapter.

#### 3.1 Catalyst Preparation

By means of the methodology presented below, the preparation of the five catalysts used in this research was achieved. The first catalyst (Cat 1) consists in a mechanical mixture of Ni, Cs and Ba oxides in a calcined kaolinite matrix. The second catalyst (Cat 2) is a combination of magnesium and aluminium oxides together with nickel and cerium oxides, all of them originated from the calcination of a Ni-Ce incorporated hydrotalcite. Cat 3 was prepared from aegirine, where cerium was incorporated in the gel that was hydrothermally treated to produce the pyroxene structure with doped Ce; and nickel was impregnated afterwards. Cat 4 consists of a zeolite matrix type X, submitted to ion exchange to incorporate Ni and Ce into the structure. The last catalyst (Cat 5) is the mechanical combination of Cat 2 with 10% of molybdenum carbide.

##### 3.1.1 Cat 1: *CsBaNi-Metakaolin*

As stated before, the preparation of Cat 1 consisted in the mechanical mixture of the four main components: Cs, Ba, Ni and kaolin as done by Hassan et al., 2013. For that purpose, in a 100 g basis, 6 g of  $\text{CH}_3\text{COOCs}$  (Sigma-Aldrich, 99.9%) and 6 g of  $(\text{CH}_3\text{COO})_2\text{Ba}$  (Sigma-Aldrich, 99.9%) were mixed together with 10 ml of water. Another solution of 20 g of sugar in 10 ml of water was prepared, to work as a porogen in the final extrudates of the catalyst. Then, 65 g of kaolin provided by EMD was mixed with 3 g of NiO in nano particles (<50 nm) provided by

Aldrich with 99.8% purity. Finally, the powder was vigorously mixed with the aqueous solutions, aiming to obtain good homogenization and wetting of the whole material. More water can be added to the mixture to reach the desired consistency of the dough for the extrusion process. The machine used for the extrusion consists of a stainless steel syringe with a piston working with a manual oil pump, in order to control the pressure applied. The dough was inserted into the syringe and the spaghetti shaped catalyst was produced by pressing the piston. The product was dried out overnight at room temperature and then, calcined at 650°C for 8 hours in air, with a heating rate of 10 °C/min. Before the calcination, the oven was programmed to dry further the material at 120°C for 3 h, with a heating rate of 5 °C/min. After calcination, the spaghetti-like materials were cut down into extrudates of 1-3 mm length with an average diameter of 1.5 mm.

### ***3.1.2 Cat 2: NiCe-Calcined Hydrotalcite***

The hydrotalcite precursor for Cat 2 was precipitated by the typical co-precipitation method at constant pH of 11 (Pérez Zurita, et al., 2015). A solution consisting of  $\text{Mg}(\text{NO}_3)_2 \cdot 6\text{H}_2\text{O}$ ,  $\text{Ni}(\text{NO}_3)_2 \cdot 6\text{H}_2\text{O}$ ,  $\text{Al}(\text{NO}_3)_3 \cdot 9\text{H}_2\text{O}$ ,  $\text{Ce}(\text{NO}_3)_3 \cdot 6\text{H}_2\text{O}$  was prepared in their corresponding amounts to give the following respective concentration: 0.8, 0.3, 0.2 and 0.2 M. Another basic solution consisting of NaOH 3.4 M and  $\text{Na}_2\text{CO}_3$  1 M was prepared separately in a beaker. Both solutions were mixed together at a flowrate of 1.6 ml/min under vigorous stirring, followed by an aging time of 24 h at room temperature with constant agitation, to form the gel. Then, aging was continued at 80°C for another 24 h inside an oven. The final gel was filtered and washed several times with distilled water until neutral pH was reached. After this point and avoiding completely drying the material, the hydrotalcite was removed from the filtration system and mixed with sugar to improve the generation of porosity in the catalyst particles. The amount of sugar added corresponds to 30% by weight of the dried hydrotalcite, which is why the amount of dried hydrotalcite to be produced

is needed to be known a priori. The material was slightly dried out aiming to obtain a suitable consistency of the dough to shape it into extrudates. The final spaghetti-like material obtained from the extrusion machine was completely dried out overnight at room temperature and then, calcined at 450°C on air for 16 h with a heating ramp of 10 °C/min. The final material was then cut into extrudates of about 1-3 mm.

### ***3.1.3 Cat 3: NiCe-Aegirine***

The preparation of Cat 3 followed the methodology described by Vitale, 2013 for the preparation of aegirine at low temperatures, where cerium was incorporated during the mineral co-precipitation and nickel was impregnated afterwards. The initial step in the preparation of this catalyst consisted in the preparation of two solutions. One acidic solution with the following concentration: 2M H<sub>2</sub>SO<sub>4</sub>, 0.12 M Ce(NO<sub>3</sub>)<sub>3</sub>·6H<sub>2</sub>O and 0.57 M FeCl<sub>3</sub>·6H<sub>2</sub>O, and another basic solution with 1.19 M of SiO<sub>2</sub>, 0.19 M of Na<sub>2</sub>O prepared from sodium silicate (SiO<sub>2</sub> 26.5 %, Na<sub>2</sub>O 10.6%); and 11.5 M of NaOH. Both solutions were mixed together, adding the acidic one over the basic solution to avoid thickening the mixture, which occurs at pH around 7. Then, the final gel was thermally treated in a Parr reactor at 160 °C with 300 rpm stirring during 96 h, to favor the crystalline growth. Then, the material was filtered, washed with abundant water until no chloride was detected in the water and dried at room temperature overnight.

The acidification of the material was obtained by ion exchange. This procedure allowed every five grams of aegirine to be in contact for about 20 min with 120 ml of a solution of 0.25 M H<sub>2</sub>SO<sub>4</sub> in water. After this time, the material was again filtered, washed with water until no sulfate was detected and dried at room temperature overnight. By empirical experience, these conditions allow the removal of 30 wt. % of the sodium ions previously existing on the surface of the nano-aegirine particles.

After acidification, 4% of nickel was loaded onto the material by wetness impregnation using a solution of  $\text{Ni}(\text{NO}_3)_2 \cdot 6\text{H}_2\text{O}$ . Then, the solid was allowed to dry at room temperature overnight and further calcined at  $500^\circ\text{C}$  for 6 h to generate a yellow powder that was mixed with ludox provided by Aldrich (40% Silica in water), in a weight proportion 1:1.4 to favor the agglomeration and the formation of a suitable dough for extrusion. The catalyst was calcined one more time at  $500^\circ\text{C}$  for 6 h and the extrudates were cut down with similar proportions used before. Due to the use of silica binder, the final concentration of NiCe-Aegirine on the extrudates was about 65%.

#### ***3.1.4 Cat 4: NiCe-Faujasite***

NiCe-Faujasite was prepared following standard methods of zeolite Faujasite synthesis and submitted to ion exchange to incorporate Ni and Ce into the alumino-silicate framework. In order to extrude this powder, each gram of prepared solid was mixed with 0.43 g of kaolin and 0.63 g of ludox described above. After the extrusion was done, the spaghetti-like materials were calcined at  $500^\circ\text{C}$  for 6 h and cut into cylinders of 1-3 mm length. The final concentration of the catalyst in the produced particles was 61 wt.%.

#### ***3.1.5 Cat 5: NiCe-Calcined Hydrotalcite+Molybdenum Carbide***

The precursor of molybdenum carbide was prepared as explained elsewhere (Vitale, et al., 2011), starting from an aqueous solution of ammonium heptamolybdate tetra-hydrate  $(\text{NH}_4)_6\text{Mo}_7\text{O}_{24} \cdot 4\text{H}_2\text{O}$  and household sucrose, which was dried out at  $120^\circ\text{C}$  for 24 h. Then, this precursor material was filled into a fixed bed reactor and converted into cubic molybdenum carbide at  $500^\circ\text{C}$  for 24 h, with a heating rate of  $10^\circ\text{C}/\text{min}$  and flowing 30 ml/min of hydrogen into the system.

In parallel, hydrotalcite was prepared as previously explained, but sugar was not added nor was the extrusion carried out. Instead, after washing, the hydrotalcite was completely dried out and

calcined at the same conditions previously described for Cat 2. Calcined hydrotalcite and molybdenum carbide were mixed together in a proportion 10:1. Then, for each gram of this catalytic mixture, 0.3 g of kaolin, 0.12 g of Ludox and 0.62 g of water were added together to create the right consistency of the dough for the extrusion. In this case, the catalyst was not calcined to avoid dicarbide of molybdenum. The use of silica and kaolin to obtain the dough with the desired properties led to dilution of the catalytic material in the extrudate particles, whose final concentration was 76 wt.%.

## **3.2 Catalyst Characterization**

### ***3.2.1 Textural properties***

The most common technique used to determine surface area is described by the ASTM D3663-84, which is based on the adsorption and desorption of nitrogen at  $-196^{\circ}\text{C}$ . The equipment used to obtain the textural properties was a “Micromeritics TriStar 3000” surface area analyzer. The method consists of a degassing of the sample by flowing an inert material (He) through a glass cell at  $150^{\circ}\text{C}$ , where the solid was placed. Then, the glass cell was submerged in a vessel with liquid nitrogen to cool it down to  $-196^{\circ}\text{C}$ . After reaching that temperature, several injections of nitrogen were performed into the system, fixing the partial pressure of the gas. Each injection step had enough time to allow the system to stabilize and record the amount of nitrogen condensed onto the surface of the material. Once the nitrogen partial pressure to saturation pressure (at  $-196^{\circ}\text{C}$ ) ratio of one is reached, desorption of nitrogen can be started, by decreasing the partial pressure of this gas. Knowing the volume of nitrogen adsorbed at each partial pressure, it was possible to determine the total volume of nitrogen adsorbed in the monolayer by the Brunauer, Emmett and Teller (BET)

equation. Then, with this volume in the monolayer and the cross sectional area of the nitrogen atoms, the surface area of the material was determined (Bartholomew & Farrauto, 2006).

### ***3.2.1 Temperature Programmed Techniques***

This set of techniques aim to determine the surface reactivity of a solid, as well as the energetic and kinetic interaction between molecules and surfaces (Bartholomew & Farrauto, 2006). Within this group of characterization techniques, Temperature Programmed Reduction (TPR) and Temperature Programmed Desorption (TPD) are the most commonly used. Both of them were done using a Quantachrome Chembet 3000 and following the same pre-treatment procedure, in which a known amount of sample (100 mg for TPR and 120 mg for TPD) was placed in a U-tube and introduced into a temperature controlled furnace. A flow of 15 ml/min of argon was allowed to pass through the tube at 200°C for 1 h to remove air and physi-sorbed water. In the last part of the pre-treatment, the tube was cooled down to room temperature, while still passing argon. In the case of TPR, a diluted reducing gas such as hydrogen (10 vol. % in argon) was flowed into the tube, while the system was heated up at a rate of 10 °C/min to 950°C. The composition of the gases at the exit of the U-tube was monitored with a thermal conductivity detector to determine the consumption of hydrogen during the evaluation (Vitale, 2013).

In the case of TPD, before heating the tube up, 15 ml of a diluted basic gas (10 vol. % of NH<sub>3</sub> in helium) was flowed into the system for 1 h to allow the chemisorption of the molecule onto the active sites of the catalyst. Then, with the furnace at about 200 °C, pure helium was flowed through the system to remove the excess of the gas used for the adsorption. After this point, the tube was heated up at rates similar to the one used in TPR. In this case, the detectors can determine the amount of ammonia desorbed, in order to evaluate the desorption profile of the gas attached in the previous step (Vitale, 2013).

In general terms, Hydrogen TPR is used to obtain the characteristic reducibility profile of the catalyst and thus, to determine the most suitable conditions to obtain the total reduction of the metals incorporated. Moreover, the calibration of the gas analyzer allows one to determine the total amount of hydrogen consumed and by balance, the amount of metal exposed for reduction. On the other hand, TPD permits one to determine the acidic or basic properties of a catalysts. In ammonia TPD, this basic molecule interacts with the acid sites on the surface of the catalyst. Therefore, its quantification allows one to obtain the total amount of acid sites and strength, regardless of the type (Lewis or Brønsted) (Vitale, 2013).

### ***3.2.1 Thermogravimetric Analysis (TGA)***

This method consists of analyzing the weight and heat changes experienced by a solid sample, when the latter is submitted to an increase in temperature under the flow of a gas. The equipment used was a DT Q 600 system from “Thermal Analysis Instruments Company”. Within the several functions of this equipment, it was used to determine the amount of coke generated on the surface of the catalyst during reaction. In different runs, fresh and spent catalyst were heated at 20 °C/min up to 800 °C under a flow of air (100 Std. mL/min) to allow the oxidation of the coke and thus, being able to obtain the weight losses. The mass lost obtained between room temperature and 200 °C was assigned to moisture and/or solvent elimination, while the mass lost obtained between 200 °C and 400 °C was considered as oxidation of remaining hydrocarbon. The mass lost obtained between 400 °C and 600°C was attributed to coke and carbon oxidation. By weight difference between the fresh catalyst and the spent one, the percentage of coke present in the catalyst after reaction can be determined.

### ***3.2.1 X-Ray Diffraction (XRD)***

The powder XRD is a technique used mainly to obtain information about the structure of crystalline materials. A primary use of the technique is the identification and characterization of



crystalline compounds based on their diffraction patterns. It consists of analyzing the way in which an X-ray beam, at a certain angle, diffracts when it hits a specific plane of the solid. The angle of diffraction varies within the different planes analyzed, which in general create a unique pattern for crystalline compounds and elements that allow the user to identify and quantify crystalline structures in the analyzed solid by comparison with a powder diffraction database (Bartholomew & Farrauto, 2006). The analyses of the solids were performed in a Rigaku ULTIMA III X-ray diffractometer with Cu K $\alpha$  radiation, evaluating from 5 to 90 2 $\theta$  degree, with 0.02 degree step and a counting time of 0.2 step/s. The powder was placed in a sample holder of 1 mm depth and then topped with a glass sheet. The domain crystal sizes were measured using the software JADE, based on the Scherrer equation (Vitale, 2013)

### ***3.2.2 X-Ray Photoelectron Spectroscopy (XPS)***

This technique is used to carry out chemical analysis onto the surface of a catalyst, determine oxidation states and even determine the dispersion of the oxide phases. The analysis consists of bombarding the surface of the catalyst with X-ray photons that bring as consequence the emission of photoelectrons from atomic core levels, which can be measured as a function of electron energy (Bartholomew & Farrauto, 2006). The equipment used to record the XPS spectra was a Physical Electronics PHI VersaProbe 5000-XPS instrument operating with a monochromatic Al source (1486.6 eV) at 50 W, Pass energy of 23.5 eV and beam diameter of 200  $\mu$ m. The samples were loaded in a custom made sample holder using double faced tape and spectra taken with double neutralization, i.e., a low energy electron beam and low energy Ar<sup>+</sup> beam. The binding energies were reported relative to C1s at (284.8  $\pm$  0.2) eV and peak fitting was performed using the Multipak 9.2.0.5 software.

### 3.1 Carborundum cleaning

Silicon Carbide, commonly known as carborundum, is an inert solid material used in this project to fill the reactor in order to improve thermal transfer at the beginning of it and hold the catalytic bed. This solid was supplied by Panadyne with a particle size of 841 microns. Due to the impurities, like the common presence of iron, a standard cleaning procedure was employed. Every 50 g of carborundum was washed in a rotary evaporator at 45°C with 100 ml of a solution of 10% HNO<sub>3</sub> in water, during 3 hours. After this time, the treated carborundum was filtered and washed with abundant deionized water to get rid of the solubilized iron impurities. Then, more water was added to the carborundum and tested with potassium thiocyanate as indicator. If the color of the solution changes to red, there is still iron that must be washed.

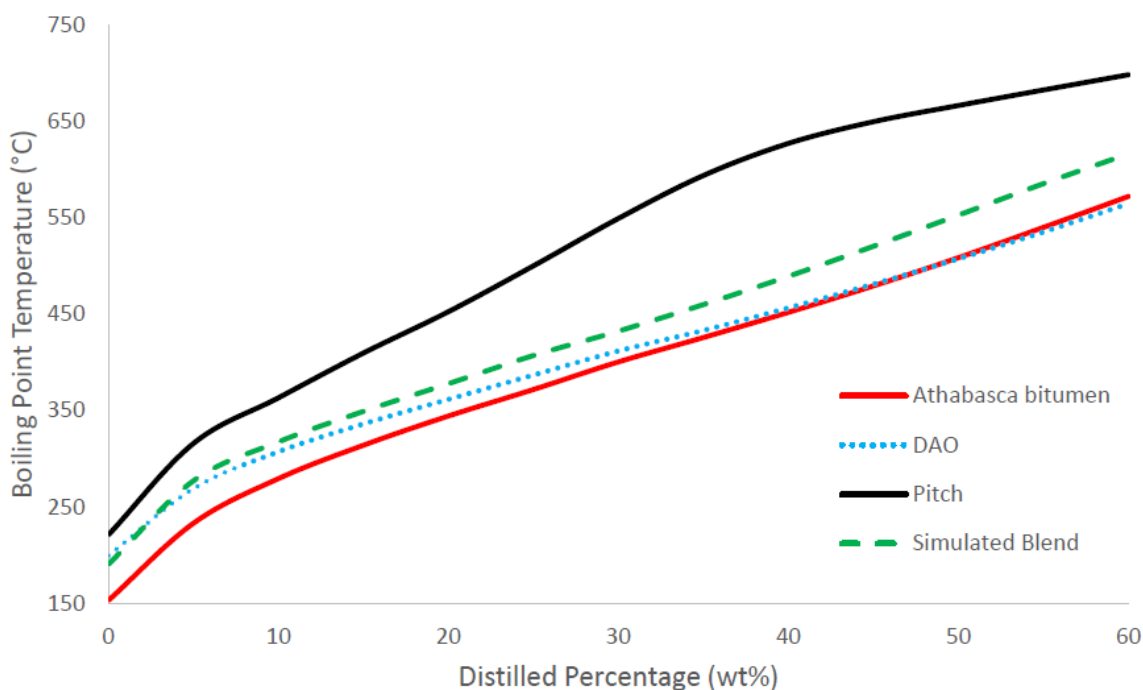
### 3.2 Feedstock

The experiments performed in this research project were done using De-Asphalted Oil (DAO) produced from processing Athabasca Bitumen (provided by Japan Canada Oil Sand Limited, obtained via Steam-Assisted Gravity Drainage), in a bench scale Solvent De-asphalting Unit that existed in the laboratory of the Catalysis for Bitumen Upgrading Group. The heavy oil was processed with pentane as solvent, at 150 °C and 500 psig. The solvent-to-oil ratio selected was 4, aiming to remove as much asphaltenes as possible in order to have good pitch yield, required in another research topic (Da Silva De Andrade, 2014). Therefore, the asphaltene content in the oil was reduced from 17% to 1.4w%, bringing as a consequence an improvement of the oil in terms of °API, viscosity and sulphur content. The production of the DAO was performed in 11 runs under the same conditions with a yield of 73.1%, closing at about 100% mass balance for oil and 90% for solvent. The final DAO has the characteristics shown in Table 3.1.

**Table 3.1. Bitumen and feedstock (DAO) properties**

<b>Property</b>	<b>Athabasca Bitumen</b>	<b>DAO</b>
API Gravity, °API	8.3	12.0
Viscosity @20°C, cP	152,015	10,584
C5-Asphaltenes, wt. %	17.0	1.7
Distillation Cuts, wt. %		
Naphtha, (IBP-190 °C)	1.89	0.06
Kerosene (190-260 °C)	5.32	4.36
Diesel (260-343 °C)	11.89	12.61
LVGO (343-453 °C)	18.29	23.28
HVGO (453-560 °C)	15.65	20.34
Residuum (560+ °C)	46.97	39.36

As it is exposed in Figure 3.1, the theoretical mixing of Pitch and DAO based on their produced weight proportions, reveals a mixing curve above the original one obtained for Athabasca bitumen, especially at the beginning of the distillation curve. As explained by Da Silva de Andrade (2014) in his research thesis, this is a clear indication of light hydrocarbon stripping while removing the solvent used in the operation. As a consequence, about 2.7 wt. % of the light material was removed from DAO during the solvent extraction. At industrial scale, the light hydrocarbon can be separated efficiently from the solvent in order to incorporate it into the DAO or in the final product, improving its viscosity.



**Figure 3.1. Simulated Distillation for the feedstock and products of the SDA Unit (Da Silva De Andrade, 2014)**

### 3.3 Plant description

In order to carry out the set of experiments required to achieve the goals of the thesis, a new bench scale plant was designed, constructed and placed in the laboratories of the Catalyst for Bitumen Upgrading Group at University of Calgary. This plant, named Catalyst Testing Unit (CTU-1) was mainly designed to evaluate small amounts of solid catalysts (between 1-10g) in a fixed bed reactor, under steam catalytic cracking conditions with complex hydrocarbon feedstocks. However, it can be also used to carry out thermal cracking reactions and even hydroprocessing under pressures between 0-490 psi and temperatures up to 500 °C.

The Process and Instrumentation Diagram (P&ID) is presented in Figure 3.2, which can be divided into three main sections: Feed section, Reaction section and Products Sampling section. The whole plant is controlled by a LabVIEW program that allows the user to set 8 different heating loops

(named H-XX), temperature alarms for them, control the gas flow injected into the plant, the operation of the pumps, the pressure of the system and even quantification of the amount of gases exiting the plant. All those parameters can also be recorded by the program in an excel file, saved in the designated location in the assigned computer.

The feed section comprises the units needed to prepare and handle the reactants before entering into the reaction section. It contains two inlets for liquids, two inlets for gases and another one in spare for future uses. One of the two liquid inlets is used to flow oil or any other type of hydrocarbon, by means of the oil pump (500D Syringe Pump-Teledyne Isco) which is constantly heated and supplied with the storage tank (T-2). The heating of T-2 is done occasionally, only when the filling of the pump is required, in which case a variable autotransformer (Staco Energy), already in place, is in charge of controlling the current sent to the heating tape. The second liquid inlet is used for water, which is pumped into the system with P-2 (500D Syringe Pump-Teledyne Isco). Nitrogen, used as carrier gas, and hydrogen used during reduction operations and in case of hydroprocessing operations, are introduced into the plant by means of two SLA5850 Brooks Mass Flow Controllers (MF-1 of 30 Std. ml/min for nitrogen and MF-2 of 200 Std. ml/min for hydrogen). The water pumped into the system by P-2 is initially heated up to its respective saturation temperature, in order to obtain the required phase change. However, a mixer/steam generator was built (M-1), consisting of a 5 cm long tube of 0.95 cm (3/8'') diameter filled with glass beads that generates tortuosity and surface area to assure uniform steam generation. The resulting steam, occasionally with nitrogen when needed, is then blended with the oil and sent to the reaction section. Moreover, this section also includes an adjustable relief valve (set at 490 psi) that opens in case of overpressure, sending fluids to the drainage can.

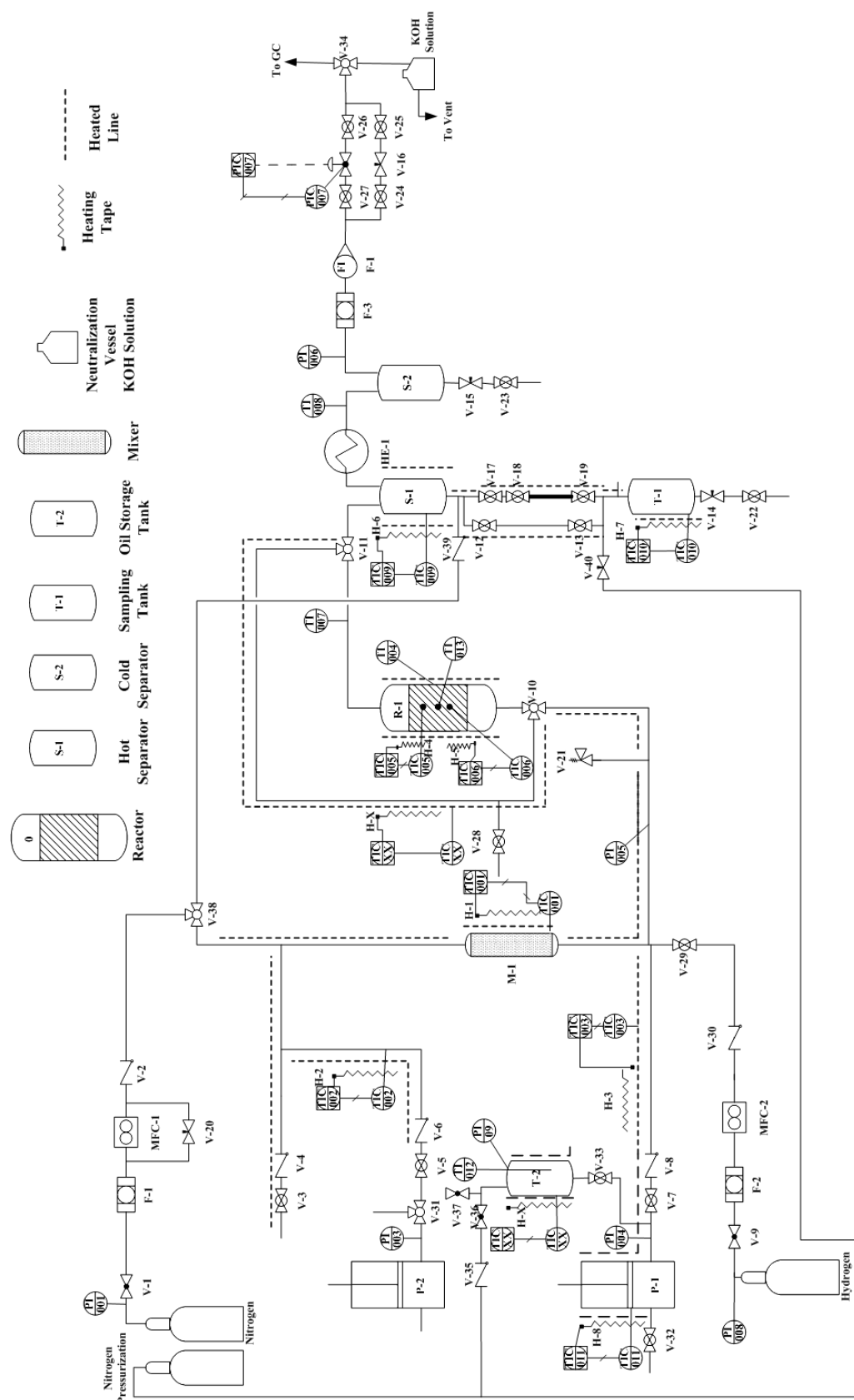
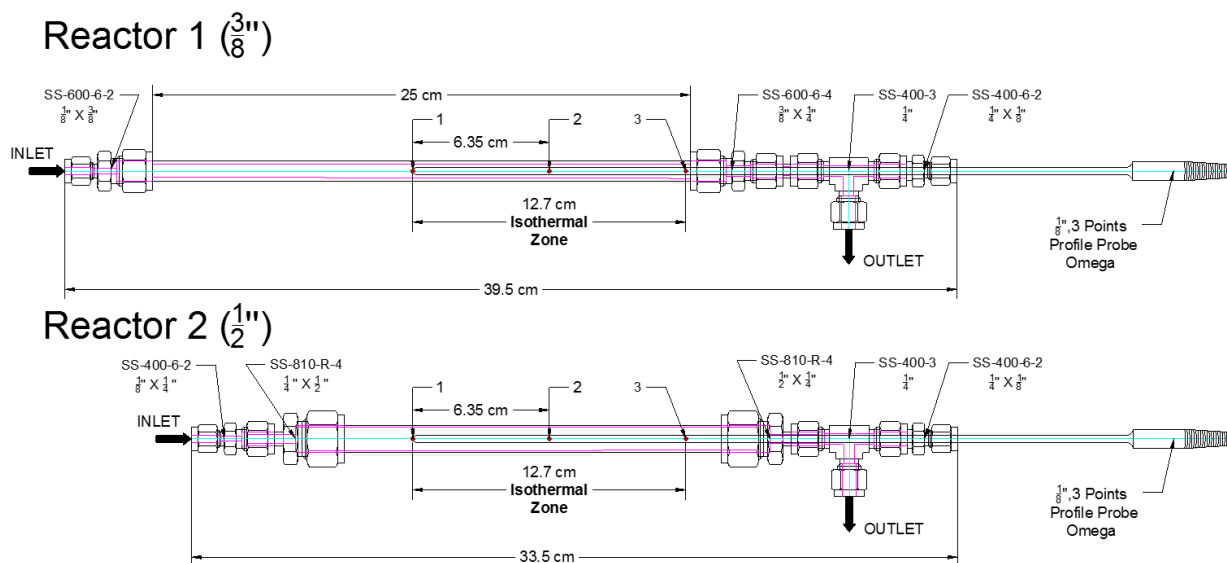


Figure 3.2. P&amp;ID of the Catalyst Testing Unit (CTU-1)

Two reactor arrangements (Figure 3.3) can be used to vary the mass of catalyst needed. Both of them consist of an up-flow stainless steel tube, one of 0.95 cm (3/8'') external diameter with 0.089 cm (0.035'') wall thickness and another one with 1.27 cm (1/2'') of external diameter and the same wall thickness. Including fittings to adapt the reactor to the plant, the arrangement of each reactor results in a 39.5 cm length for Reactor 1 and 33.5 cm for Reactor 2. Based on empirical assessment of the system, it was determined that two heating tapes of 1.27x5.08 cm (0.5x2.0'') were needed to develop 12.7 cm of isothermal zone suitable to set the catalytic bed. The heating tapes were controlled with the internal temperature acquisition points 1 and 3, respectively (shown in Figure 3.3). The temperature at these points was measured with a profile Omega probe of 0.32 cm (1/8'') diameter, placed inside the reactor with three measurement points separated by 6.35 cm. These three points allowed the user to evaluate and control the temperature profile along the catalytic bed. A homogeneous profile was possible to obtain along the whole catalytic bed within 3°C variations, by physically adjusting the heating tapes.

The bottom of the reactor, from the inlet to the isothermal zone, was filled with carborundum to hold the bed and to favor the preheating of the reactants and development of a uniform flow pattern. The small section between the upper fittings and the isothermal section was also filled with carborundum to avoid the upwards movement of the bed because of the pressure. It is important to note that quartz wool was placed at the beginning and the end of the tube to avoid the spreading of solids along the plant. In order to also keep the catalytic bed in place, quartz wool was also added between the carborundum sections and the catalyst extrudates.

The reaction section also includes a bypass system, which can be used during cleaning or special operation to avoid sending fluid through the reactor. When needed, this bypass can be heated by using any of the control loops available with the heating tape and thermocouples already installed.



**Figure 3.3. Reactor assemblies**

The product sampling section of the plant is in charge of managing the products of the reaction in order to be collected and analyzed properly, without affecting the operating conditions of the unit. Once the feedstock was processed in the reactor, gas and liquid products went to the hot separator (S-1), where water and light hydrocarbons in gas phase ( $<205^{\circ}\text{C}$ ) were removed from the heavy products, favored by the injection of a carrier gas into the bottom of S-1. Gases and lights that left the hot separator were chilled in a shell and tube heat exchanger fed with water at  $5^{\circ}\text{C}$ , to favor the condensation of lights and water in the stream. Then, these latter were accumulated in the cold separator (S-2), while gases were removed from the top of it. The gases produced during the reaction together with the carrier gas fed into the system were quantified with a Brooks SLA 5850 series flowmeter (F-1). After quantification, gases passed through the back pressure system, able to work either with a 500 psi Swagelok manual back pressure valve or with an automatic pressure controller (Brooks 5866 series calibrated to work up to 290 psi), operated through the LabVIEW Program. Finally, gases can be either sent to the GC for composition analysis or sent to the vent.



Heavy products remaining in the hot separator were transferred into the sampling tank (T-1) by means of two consecutive automatic valves (V-18 and V-19) working alternatively with a designed volume between them of 3 ml. While the top valve was open collecting sample, the bottom valve remained closed. After a certain amount of time the top valve was closed and the bottom one was opened to transfer the sample, at operating pressure, into T-1. Once the sample transfer was completed, the bottom valve closed and the top one opened to start collecting all over again. The idea of the arrangement is to collect heavy products without strongly affecting the pressure of the system. Every operation of this system generated pressure drops of about 3 psi, which was recovered afterwards by generated gases and nitrogen. Once the product was in the sampling tank, it can be easily removed from it through the collecting valves (V-14 and V-22). The time selected for the automatic operation of the double valve system was assigned depending on the hydrocarbon flowrates.

The lights and water were removed from the cold separator by means of two manual valves that operated alternately as done for the heavy products.

### ***3.3.1 Operating procedure***

The operation of the CTU-1 to evaluate the effect of each condition over the quality of the product, involved two previous steps, i.e. reactor filling and metals reduction operation, before the reaction operation.

#### **Reactor Filling**

Following the schematics presented in Figure 3.3, the tube was disconnected from the lower fittings (either SS-400-6-2 with SS-810-R-4 or SS-600-6-2, respectively) to proceed to its filling upside down. A small amount of quartz wool is inserted through the tube in order to place it at the other end of it (connection between the tube and either SS-600-6-4 or SS-810-R-4). Then,

carborundum previously washed, was added to the reactor until reaching the isothermal zone. At that point, more quartz wool was incorporated before proceeding to fill the isothermal zone with catalyst. In the case of thermal runs, this section was also filled with carborundum. Once all the catalyst was added, more quartz wool was placed and the reactor is completely filled with carborundum. Some room was left free to add more quartz wool into the tube before proceed to tighten it up to the fittings.

The filled reactor was then assembled into the plant and tested for leakage, at 450 psi for 2 hours, constantly looking for leakages with Snoop Liquid Leak Detector from Swagelok.

It is important to know that the amount of catalyst loaded into the reactor, together with the oil mass flowrate to be used, allow the determination of the Weight Hourly Space Velocity (WHSV), by means of the following equation (Eq. 3.1). The inverse of the WHSV provides the contact time between the oil and the catalyst.

$$WHSV[h^{-1}] = \frac{\text{oil mass flowrate}}{\text{mass of catalyst}} \quad \text{Eq. 3.1}$$

### **Reduction Operation**

The used catalysts required some of their elements to be in metallic form, which was achieved by treating the catalysts with a flow of hydrogen under a temperature high enough to produce the reduction of the oxide species. The operating reduction temperature was obtained by performing a Temperature Programmed Reduction (TPR) of each solid. These temperatures can vary from one catalyst to another, however, by previous testing of these solids, all of them proved to be reducible at 500 °C, which was the temperature selected to proceed with the activation. This operation was carried out during six hours at atmospheric pressure and flowing 60 Std. ml/min of hydrogen through the reactor. After the specified time, the hydrogen was purged out of the system with 15

Std. ml/min of nitrogen for at least one hour and the temperature of the reactor was decreased to 250 °C. In order to keep consistency and avoid procedural differences, the reduction operations were always performed before any kind of reaction, even for those cases where no catalyst was used.

During the reduction step, the oil storage tank is heated up to 100 °C to decrease the viscosity of the feedstock and start filling the pump (P-1).

### **Steam Cracking Operation**

Once the reduction operation was performed, the remaining cold sections of the plant were heated up to their respective temperatures. The feed section was heated up to 210 °C (250°C when operating at 400 psi) with H-1, H-2 and H-3 to favor the gas phase of water. The hot separator was heated up to 205 °C (270°C when operating at 400 psi) with H-6 to allow the water separation from the heavy products. The sampling tank (T-1) and pump P-1 were heated to 100 °C with H-7 and H-8 respectively, to keep the oil at low viscosity and improve the quality of the mass balances in the case of T-1.

Once the plant was heated at the expected conditions, either the pressure controller or the back pressure valve were set at the operating pressure and the system was pressurized by means of V-20 (needle valve that bypass MF-1). With the desired pressure established, the MF-1 was set at 5 Std. ml/min and the system was left at these conditions aiming to reach stabilization of the gas flowrate in order to measure the amount of nitrogen fed into the system. After the nitrogen flowrate was obtained, the water pump was set at 25 ml/min for 15 min to fill all the lines in the feed sections. Once the system was filled, the reactor was pre-treated with steam at reaction temperature with a flowrate of 1 ml/min of water for about three hours. Then, the feed section lines were filled with the hydrocarbon feedstock for 15 min at 25 ml/min, before setting the oil flowrate.

Before the automatic operations of the two consecutive valves (V-18 and V-19) that transfer oil to the sampling tank was activated, the hot separator and the cold separator were drained. Four main parameters are involved in the automatic operation of these valves: the time for V-18 (upper valve) to remain open, the delay time between when V-18 closes and V-19 (lower valve) opens, the repeat time in which V-19 closes and V-18 open. Based on practical experience, repeat time and delay time was set at 5 seconds while the time the sample takes to move from the 3 ml accumulator toward the tank (V-19 open) was set to 290 seconds, to favor the complete transfer of the liquid. However, the time V-18 remained open was calculated depending on the hydrocarbon flowrates, aiming to obtain the complete transfer into the sampling tank. By experience, it was established that at least 10% of the 3 ml accumulator must remain empty to assure the total transfer of any extra oil pumped by malfunction of the pump.

### **3.4 Characterization of Samples**

#### ***3.4.1 High Temperature Simulated Distillation (HTSD)***

The High Temperature Simulated Distillation, also named Simdist, is an alternative method to the time-consuming laboratory-scale physical distillation that aims to determine the amount of material distilled at different temperatures (boiling point curve). According to this method, 1 $\mu$ l from a solution consisting of 0.15 g of oil sample in 20 ml of CS<sub>2</sub> was injected into a nonpolar chromatography column placed inside a temperature programmed oven. Hydrocarbons in the column were separated by boiling points and detected and quantified at the exit of the column by a flame ionization detector. By running reference n-alkanes, the chromatographic response was calibrated to obtain a result equivalent to the atmospheric boiling point of the sample aliquots.

According to the literature, with the HTSD method, a crude oil can be analyzed to temperatures up to 732 °C equivalent, with a weight standard deviation below 2% (Villalanti, et al., 2010).

The equipment used to obtain simdist of the liquid sample was an Agilent Technologies Gas Chromatograph, model 7890 A working at conditions described in ASTM-D7169-2005. Chromatograms were analyzed with the software Simdist Expert, from the company Separation Systems Inc.

Based on several repetitions of the same feedstock used in the experiments (DAO), the standard deviation associated to the determination of each one of the distillation cuts of interest was obtained, as shown in Table 3.2. However, due to the absence of naphtha in the DAO used, it was not possible to determine the error for this measurement.

**Table 3.2. Errors in the determination of distillations cuts**

<b>Distillation Cuts</b>	<b>STDV</b>	<b>Rel. Error, %</b>
Naphtha, (IBP-190 °C)	N/A	N/A
Kerosene (190-260 °C)	0.3	7.7
Diesel (260-343 °C)	0.4	3.6
LVGO (343-453 °C)	0.9	4.0
HVGO (453-560 °C)	0.9	4.5
Residue (560+ °C)	2.4	6.0

The main parameter used to evaluate the performance of the reaction was based on the residue conversion, calculated by means of the following equation (Eq. 3.2). It is important to note that the residue in the products is calculated taking into consideration the contribution of gases to the

total mass of products. The typical standard deviation observed for this parameter is between 3 and 5 units of conversion.

$$\text{Residue Conversion}(\%) = \frac{\text{Residue in DAO} - \text{Residue in Products}}{\text{Residue in DAO}} * 100 \quad \text{Eq. 3.2}$$

### **3.4.2 Water content**

Even though the heavy products are stripped from water and light material (boiling < 200 °C) in the hot separator, a small fraction of water still remains in equilibrium and stable in this stream. Therefore, it is necessary to know this fraction, in order to account for it during the characterization of the final products.

The water content was determined with a C20 Coulometric KF titrator from the company Mettler Toledo. The methodology consisted of preparing a solution of 0.4 g of sample with around 9 g of tetrahydrofuran (THF) to dissolve it. The amount of water contained in the THF must be previously determined by adding weighted aliquots of the solvent into the titrator containing Aqua Star® Coulomat A from EMD. Then, the prepared solution was tested in the titrator by adding weighted aliquots and giving to the instrument its respective weight. Knowing the amount of sample and solvent in the solution; and the water content in the solution and in the solvent, it is possible to determine the water content in the original sample by material balance (Carbognani, et al., 2014).

### **3.4.3 Oil density**

The density of the oil was measured with a DD2910/11 Digital Density Meter from Rudolph Research Analytical. The principle of operation of this equipment consists of evaluating and comparing the frequency of oscillation of a glass U-tube when it is empty and when filled with the sample. This variation in oscillation is directly proportional to the mass contained in the fixed

volume. Therefore, with the mass and the volume, the equipment is able to deliver the density of the sample.

In order to measure heavy oil hydrocarbons, it was necessary to dilute the sample in solvent and create a calibration curve. Therefore, each sample was diluted in toluene in concentrations around 0.5wt% and 1wt%. Both solutions and the pure solvent were analyzed in the equipment to determine their density, which were used to create the calibration curve. By extrapolating this calibration at zero solvent concentration, the density of the original sample could be determined and thus, the API gravity with a standard deviation of 0.3 API.

#### ***3.4.4 Microcarbon residue***

The tendency of the bitumen to form coke when it is thermally treated can be determined by standards methods such as Conradson Carbon Residue (ASTM D-189), Ramsbottom Carbon Residue (ASTM D-524) and Microcarbon Residue (ASTM D-4530). Under different conditions, setup and amount of sample, all of those methods aim to determine the amount of residue remaining after evaporation and pyrolysis of the hydrocarbons present in the sample. The advantage of Microcarbon against the other methods is the small amount of sample required to perform the test (Hassan, et al., 2008).

The setup consists of aluminium and stainless steel plate of 10.12 cm diameter with 26 sorted vertical tubes of 1/8'' and 3/4'' length, by which nitrogen can pass through. This plate is placed inside a Barnstead Muffle furnace with temperature controller. On top of the plate, a glass cover is placed to create an inert chamber of nitrogen when the gas starts flowing through the tubes. The initial oxygen in the environment is purged via an orifice (1/8'') on top of the glass cover.

The procedure consisted of incorporating about 20 mg of sample into a 2 cc glass vial and placing it on the surface of the metal plate. With the described setup, up to 26 samples could be analyzed

at the same time. Then, the system was covered with the glass lid and the nitrogen cylinder was opened at a flowrate of 900 ml/min at room temperature and atmospheric pressure conditions. After 45 min purging the oxygen from the system, the furnace was turned on to reach a temperature of 500 °C at 10°C/min. Once the system reached the desired temperature and went through a natural cooling under a nitrogen environment, the vials were removed from the furnace to weight them and then, the calculation of the amount of formed coke is done by weight differences with an error of 1%.

### **3.4.5 Gases**

#### **3.4.5.1 Gas Chromatography**

The molar/volumetric composition of the gases produced during the reactions was determined by Gas Chromatography (GC). For that purpose, an SRI multiple gas analyzer model 8610C with Multiple Gas #3 configuration was connected online to the exit of the plant. The equipment comprises one Flame Ionization Detector (FID), two Thermal Conductivity Detectors (TCD) and one Flame Photometric Detector (FPD). Besides, it also contained one molecular sieve column (model MS13X) of 183 cm (6') and another silica gel column of 183 cm (6'), a combination that separates hydrogen, nitrogen, carbon monoxide, carbon dioxide, and C1-C5 hydrocarbons. A 60 m capillary column (MXT1-60m) was used to separate sulphur compounds from C1-C5 hydrocarbons (SRI-Instruments, 2014).

Hydrocarbons between C1 and C5 were detected and quantified with the FID using a medium gain for its amplifier. Their composition was usually corroborated with the values obtained from the TCD2 at high gain for the amplifier and using helium as a carrier. At the same time, TCD2 was also used to determine the amount of CO, CO<sub>2</sub> and hydrogen (when possible) present in the gas. Hydrogen was also determined by using TCD1 at low gain for the amplifier and using argon as



the carrier in order to increase the thermal conductivity difference between them and thus, being able to sensibly detect small amounts of hydrogen. In general, hydrogen concentrations obtained from TCD1 and TCD2 were compared to corroborate results. Moreover, H<sub>2</sub>S was detected with the FPD at medium gain for the amplifier.

By means of the analyses of standar calibration gases with known and certified compositions, the GC equipment was calibrated. The differences generated between the composition obtained and the certified composition for all the runs performed, is expressed in Table 3.3 as relative error.

**Table 3.3. Relative errors associated with the determination of gases by GC**

Components	Rel. Error, %	Components	Rel. Error, %
H <sub>2</sub> -TCD1	8.2	Propane+Propene FID	2.8
H <sub>2</sub> S-FPD	10.7	Propane-TCD2	3.9
CO-TCD2	5.9	Propylene-TCD2	4.0
CO <sub>2</sub> -TCD2	3.4	n-butane FID	5.0
Methane FID	6.3	iso-butane FID	3.1
Ethane+ Ethylene FID	3.3	1-Butene FID	3.8
Ethane-TCD2	4.1	iso -Pentane FID	4.4
Ethylene-TCD2	4.3	Pentane FID	4.4

#### 3.4.5.2 Mass Spectrometry

For some experiments, the chemical composition of the gases produced in the reaction were also determined via mass spectrometry by means of a Pfeiffer Omnistar quadrupole mass spectrometer (QMS). This equipment takes the gas samples and directs them into a chamber under vacuum

conditions. In this chamber, the compounds were bombarded with electrons to induce their ionization. A quadrupole mass filter, consisting of four parallel rods arranged in the form of a square, was in charge of separating the ions in mass to charge ratio ( $m/z$  or  $m/e$ ), which were then detected by a Faraday detector or a secondary electron multiplier. The current detected can be related to the partial pressure of the compounds or any of their fragments (Pfeiffer-Vacuum, n.d.). In this way, frequent monitoring of the generated gases, separated in mass to charge ratio, can be performed.

#### ***3.4.6 Viscosity***

A Brookfield viscometer model RVDV-II+PRO was used to determine the dynamic viscosity, with a relative error of 5%, at a given temperature on liquid samples placed in the sampling cup. Depending on the viscosity of the sample and the type of spindle used, the rotation speed was varied to obtain a final measurement with a torque between 40-60% of the maximum 0.7187 milli N/m. The temperature of the sample cup was kept constant by means of a Brookfield TC-502 bath.

#### ***3.4.7 Microdeasphalting***

The utilization of this technique allows the determination of the asphaltene fraction in the sample, not soluble in a specific solvent. The procedure consisted of placing approximately 0.4 g of the sample in a 100 ml beaker together with 20 ml of pentane. The mixture was digested for 30 min at 50 °C in a heating plate, keeping the beaker covered with a petri dish to minimize solvent losses. After this time, the content of the beaker was brought to room temperature (about 22 °C) before proceeding to filter the precipitate using a 0.45  $\mu\text{m}$  porous membrane (GH Polypro 47 mm Hydrophilic Polypropylene from Pall Corporation). Then, the membrane with the precipitate was dried in an oven at 100 °C for 5 min, cooled down at room temperature and weighted. By membrane weight differences, before and after the filtration process, the amount of asphaltenes

was determined and related to the initial known mass of sample (Carbognani, et al., 2007). The relative error associated to this procedure is about 20%.

#### ***3.4.8 Elemental analysis (Sulphur and Nitrogen)***

Nitrogen and sulphur contents in the liquid sample was quantified with an Antek 900 Series Nitrogen and Sulphur analyzer. The operation of the equipment consisted in burning at 1100°C a solution of 0.38 g of sample in 2.62 g of toluene. Hydrocarbons are converted into CO<sub>2</sub> and water, while nitrogen and sulphur oxides are detected through the pyro-chemiluminescent technology and Pyro-fluorescent technology, found respectively in the equipment. Each sample was automatically injected several times in order to assure good precision of less than 5% error.

#### ***3.4.9 P-value***

The asphaltenes in oil can show the tendency to flocculate and precipitate causing several problems to the oil industry. The P-value method, developed by Shell, assesses the peptization capacity of the sample that keeps the asphaltenes in suspension; and can be used to calculate and predict the stability of crude oils (Van Den Berg, et al., 2010). The P-value of an oil sample was obtained using Eq 3.3. By titrating the same amount of sample, placed in different vials, using different volumes of hexadecane, the p-value can be determined. After digestion at 100°C for 30 min, each final solution was analyzed in an optical microscope to observe formation of particles. The known volume of hexadecane and mass of sample used gives the P-value of the sample. The higher the amount of solvent required to observe precipitation, the more stable the product is. If the sample with no solvent added shows the presence of asphaltenes, a P-value equals to one is reported. For the purpose of analysis of products, a P-value of 1.15 can be considered as the limit of stability (Higuerey, et al., 2002).

$$P - value = 1 + \left( \frac{\text{volume of Hexadecane (ml)}}{\text{mass of sample (g)}} \right) \quad \text{Eq. 3.3}$$

#### ***3.4.10 Bromine number***

The bromine number is the ASTM standard method widely used in the industry to determine the amount of unsaturated compounds existing in an oil sample and thus, its potential reactivity. The magnitude reflects the grams of bromine that reacts with 100 grams of sample under the given standard conditions of the test. Within the error of the measurement, part of the bromine consumed is also involved in side reactions with sulphur, nitrogen and oxygen containing compounds. The method consists of the coulometric monitoring of the incorporation of bromine molecules into olefins to produce brominated hydrocarbon compounds. The bromine molecules are produced electrochemically in the electrode from the titrant solution and the titration ends when this halogen stops being consumed (Taylor, et al., 1992).

This analysis was performed with a T50 Titration Excellence apparatus provided by Mettler Toledo, which uses Potassium Bromate/Potassium Bromide 0.1 N as titrant. The procedure entails the filling of the respective vessel with enough solvent to wet the tip of the electrode that is going to be inserted after. The solvent was a solution prepared out of acetic acid, dichloromethane, methanol and sulfuric acid. The vessel was then attached to the instrument, introducing the titrant dispenser tube, the electrode and a magnetic stirrer inside. About 0.05 g of sample was required to perform the analysis, which was incorporated into the system as a solution of the oil in dichloromethane. The analysis was always performed at temperatures lower than 3.9°C to inhibit aromatics and heterocyclics side reactions.

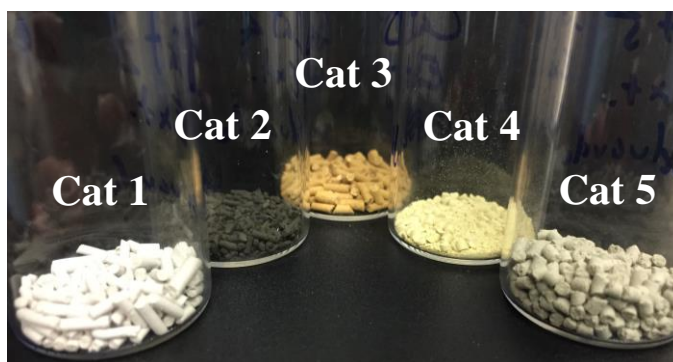
#### ***3.4.11 Total Acid Number (TAN)***

The amount of naphthenic acids present in the crude oil is commonly expressed as the number of milligrams of potassium hydroxide required to neutralize the acidity existing in one gram of crude oil, which is usually defined as Total Acid Number (TAN) (Speight, 2014).

The titration was performed with a T50 Titration Excellence apparatus provided by Mettler Toledo, using a titrant solution of 0.1 M KOH in 2-propanol. A minimum amount of 1 g of sample was placed in a vessel and diluted with 60 ml of solvent prepared out of toluene, 2-propanol and water. This solution was placed in the Titration Excellence autosampler with the electrode and titrant dispenser tube inside. Once the system started pumping titrant, the neutralization reaction was monitored by potentiometry until the reaction was completed. The amount of titrant used for this purpose with its respective concentration and the amount of sample used, gave the final Total Acid Number reported.

## Chapter Four: Catalyst Characterization Results

The synthesis of the catalysts following the methodology presented in Chapter 3, generated the solids presented in Figure 4.1, in which Cat 1 is NiCsBa-Metakaolin, Cat 2 is NiCe- Calcined Hydrotalcite, Cat 3 is NiCe-Aegirine, Cat 4 is NiCe-Faujasite and Cat 5 consists of calcined NiCe-Hydrotalcite plus Mo<sub>2</sub>C. Once the catalysts were prepared, they were analyzed via nitrogen adsorption/desorption, temperature programmed reduction and desorption, X-ray diffraction and X-ray photoelectron spectroscopy. The results obtained by these techniques are presented in this chapter, as a way to understand the physical-chemical properties of the synthesized solids.



**Figure 4.1. Catalysts after preparation**

### 4.1 Nominal metal composition for each catalyst

Based on the employed reactant weights in the preparation of each catalyst, their purity, their expected consumption and the final metal oxidation states, the expected metal concentrations were calculated and presented in Table 4.1. As shown, the catalyst prepared from the calcination of hydrotalcite (Cat 2) is the one containing the highest amount of Nickel with about 19%, followed by its combination with molybdenum carbide (Cat 5). The nickel content in the latter is about 3.8 times greater than that in the Cat 1 and about 5.4 times greater than in the one with the lowest

content. The same trend is observed in the catalyst containing Ce, Cat 2 and Cat 5 have the highest concentration, while Cat 3 and Cat 4 contain about the same Ce concentration. These results are important to bear in mind, since the active sites (Ni and Ce) of Cat 2 and Cat 5 are in considerable larger proportion in comparison with the other prepared catalysts. It is also important to note that the proportion of active phases selected for the preparation of Cat 5 (10 parts of calcined hydrotalcite per part of  $\text{Mo}_2\text{C}$ ), leads to a ratio Ni and Ce to  $\text{Mo}_2\text{C}$  of 1.9 and 2.6, respectively.

**Table 4.1. Nominal weight percentage of active metals in prepared catalysts.**

	Metal Weight Concentration, %				
	Cat 1	Cat 2	Cat 3	Cat 4	Cat 5
Nickel	3.4	18.9	2.6	2.4	13.0
Cerium	-	26.6	6.5	6.9	18.3
Cesium	6.0	-	-	-	-
Barium	4.6	-	-	-	-
$\text{Mo}_2\text{C}$	-	-	-	-	7.0
Iron	-	-	12.0	-	-

## 4.2 Textural properties

As shown in Table 4.2, the synthesis of the solids generated catalysts in a wide range of specific surface area, pore volumes and pore width. As expected, the greatest surface area was obtained for the zeolitic material (Cat 4) with  $283 \text{ m}^2/\text{g}$ , while the smallest surface area of  $14 \text{ m}^2/\text{g}$  was achieved by using clays in the preparation (Cat 1). Cat 1 exhibits mesoporous distribution with an average pore width of  $205 \text{ \AA}$  and with a small percentage of pores close to the micropore range. Cat 2 is characterized by a wide pore distribution with some of them close to the micropore range, but with main porosity in  $100$  and  $200 \text{ \AA}$ . Cat 3 and Cat 4 exhibit a clear bimodal pore distribution, both

centered at similar values. In the case of Cat 3, the pore distribution is centered on 35 and 100 Å, while in Cat 4, it is centered in 35 Å and 90 Å. The variation in the preparation of Cat 2 to generate Cat 5, modified the surface area and the pore distribution of the solid generated. As it can be observed, Cat 5 is characterized by lower available surface area, probably because of the incorporation of kaolin. However, the pore distribution is also wide in this case, but shifted toward big pores with the average at 165 Å.

Regarding pore volume, Cat 2 and Cat 5 contain the largest pore network in terms of volume per gram of catalyst. In the case of Cat 1, the pore volume obtained was very small, indicating the characteristic low porosity of this solid.

**Table 4.2. Textural properties of catalysts\***

	Cat 1	Cat 2	Cat 3	Cat 4	Cat 5
BET Surface Area, m <sup>2</sup> /g	14	232	180	283	117
Pore Volume, cm <sup>3</sup> /g	0.08	0.59	0.39	0.14	0.56
Type of Porosity	Bimodal	Trimodal	Bimodal	Bimodal	Multimodal
Main Pore Widths, Å	35/205	30/100/200	35/100	35/90	35/65/85/165
Avg. Pore Width, Å	205	81	75	70	165

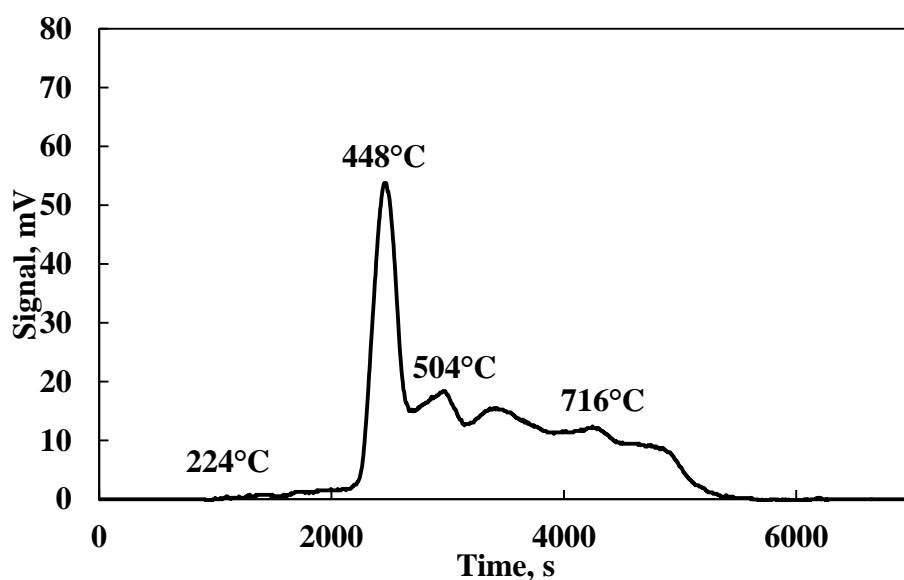
\*Adsorption/Desorption curves and pore distribution curves can be found in Appendix B

### 4.3 Temperature Programmed Reduction (TPR)

The reducibility of the metals contained in each catalyst was evaluated via TPR, from which results are presented in the following charts (Figure 4.2 to Figure 4.6). Cat 1's reduction profile (Figure 4.2) exhibits an initial small reducibility at 224°C, but with a main signal centered at 448 °C and continuous hydrogen uptake between 504°C and 716 °C. In the case of Cat 2 (Figure 4.3), a considerable amount of hydrogen was consumed between 210 and 533 °C, but the main reduction



took place at higher temperatures, centered at 897 °C. Cat 3 (Figure 4.4) shows a wide distribution of hydrogen uptake in the range 315-775 °C with a main hydrogen uptake centered at 658 °C. Cat 4 (Figure 4.5) exhibit reducibility starting from 303 °C, but a bimodal reduction behaviour is observed, centered at 468 and 798°C, respectively. Finally, Cat 5's profile (Figure 4.6) behaves very similar to the one obtained for Cat 2. However, the main signal, centered at 895°C, decreases in size and new small signals are found centered between 191°C and 726°C. In general, all the catalysts showed a certain consumption of hydrogen associated to the presence of the metals incorporated and thus, their capacity to be reduced. Based on the initial temperatures for hydrogen consumption, Cat 1, Cat 2 and Cat 5 appear to contain metals arranged in such a way that are easier to reduce. In the case of Cat 4 and Cat 5, due to the stability of the metals in the crystalline structure, the initial temperature to favor their reduction is about 100 °C higher. As a whole, the catalysts showed a certain degree of reduction by the temperature of 500°C, which was the one selected to carry out the operation of hydrogen pre-treatment.



**Figure 4.2. H<sub>2</sub>-TPR for Cat 1**

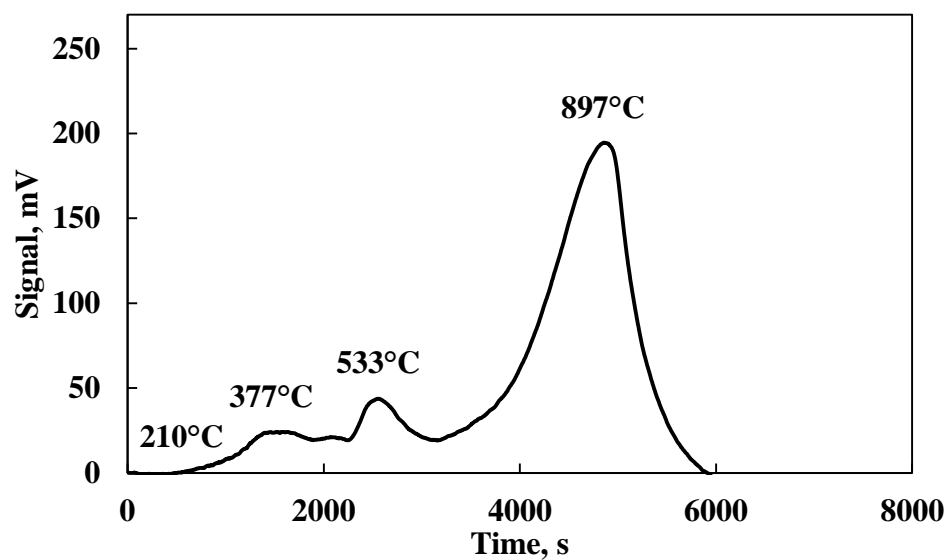


Figure 4.3. H<sub>2</sub>-TPR for Cat 2

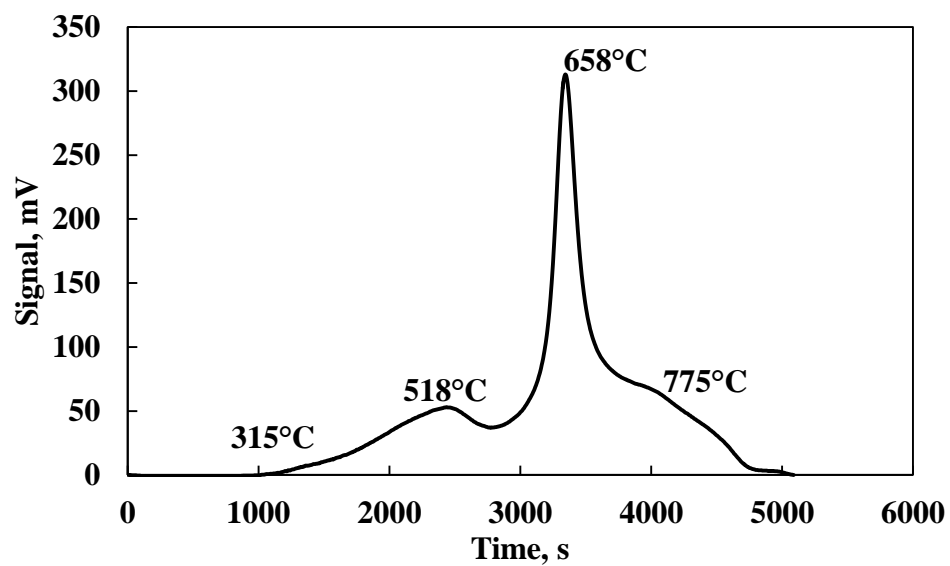
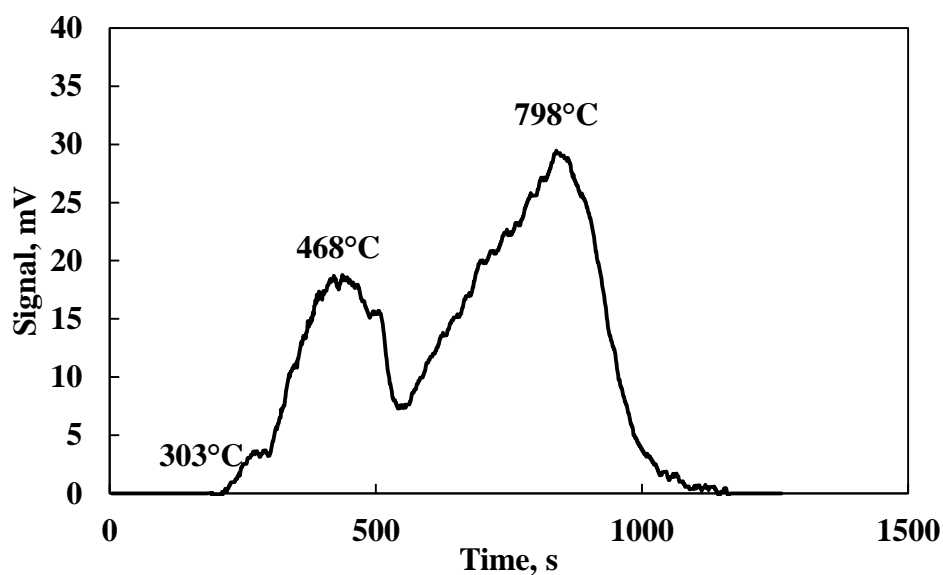
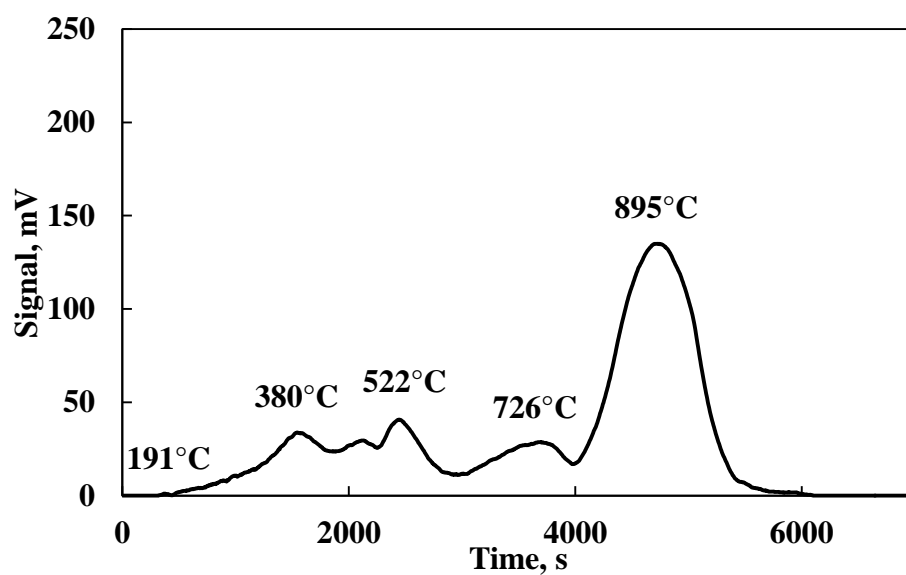


Figure 4.4. H<sub>2</sub>-TPR for Cat 3



**Figure 4.5. H<sub>2</sub>-TPR for Cat 4**



**Figure 4.6. H<sub>2</sub>-TPR for Cat 5**

Based on the H<sub>2</sub>-TPR results and using the corresponding calibration, the total hydrogen uptake was calculated and presented in Table 4.3. In the same table, the total dispersion is also presented, calculated by comparing the experimental hydrogen consumption with the theoretical hydrogen

required to reduce the nominal amount of metals loaded. According to this table, the catalyst prepared from hydrotalcite (Cat 2) showed the highest hydrogen uptake, which is directly related to the amount of exposed metal active sites available to perform the reactions. However, based on calculations for dispersion, only 60 % of the metal loaded is exposed to interact with hydrogen. In Cat 5, where Ni and Ce from Cat 2 were diluted, the consumption of hydrogen is lower.

Moreover, due to the conservation of their crystalline structures, modified faujasite (Cat 4) and specially the modified aegirine (Cat 3), showed the best dispersion of the metals among all the catalysts. The use of a nano powder of NiO in the preparation of Cat 1 influenced the achievement of a good dispersion of the metal, giving a value of 70%.

**Table 4.3. Hydrogen uptake per gram of catalyst**

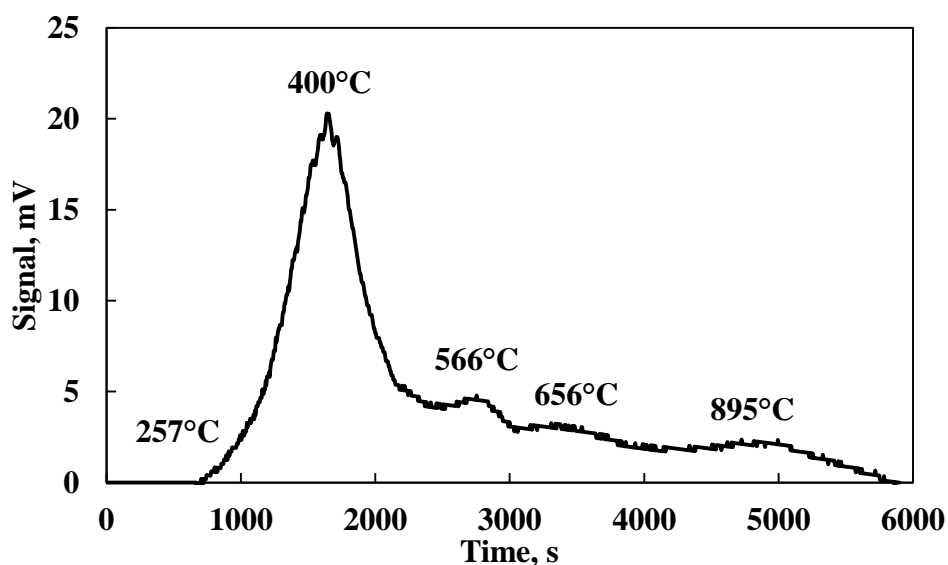
Catalyst	Hydrogen Uptake, $\mu\text{mol-H}_2/\text{g Cat}$	*Dispersion, %
Cat 1	398	69.0
Cat 2	2487	59.6
Cat 3	1663	95.4
Cat 4	509	77.0
Cat 5	1567	54.5

\*Calculated from theoretical reduction of total metal existing in the catalyst

#### 4.4 Temperature Programmed Desorption of Ammonia (TPD)

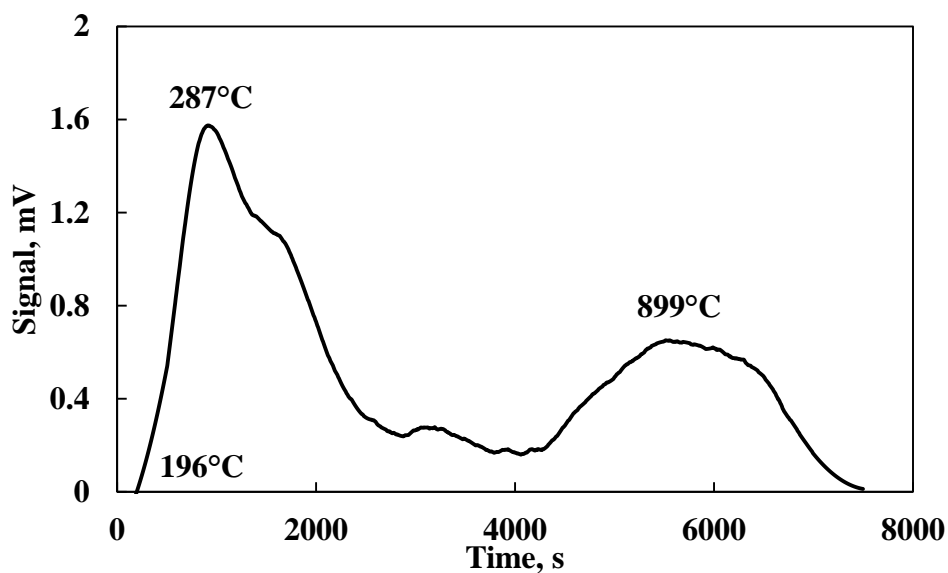
The evaluation of the catalysts via ammonia TPD allowed the determination of their total acidity (Bronsted and Lewis) and their possibility to undertake catalytic cracking of hydrocarbons. In the case of Cat 1, the adsorption of ammonia on the surface of the catalyst could not be achieved, as a clear indication of the absence of acid sites in the catalyst. This result agrees with previous

findings, where catalysts prepared from alkaline earth metals with metakaolin evaluated by CO<sub>2</sub>-TPD; showed the basic properties of this kind of materials (Hassan, et al., 2013). The result for Cat 2 is presented in Figure 4.7, where it can be observed that the starting point for ammonia desorption occurred at 257°C, reaching a main signal centered at 400 °C. This catalyst also shows the presence of a stronger type of acid sites, found at temperatures between 566-895°C. The presence of acid sites in a catalyst prepared from calcined hydrotalcite is not unforeseen, since Al<sup>3+</sup>-O<sup>2</sup> sites are created with moderate Lewis acidity. Besides, the increase in the acidity depending on the aluminum content has also been studied (Cantrell, et al., 2005). Furthermore, the incorporation of nickel into the preparation of the catalyst favors the generation of medium and strong acid sites, due to the formation of surface nickel aluminate spinel, where the nickel ions can occupy the holes in the octahedral and tetrahedral spinel lattice, which polarizes the structure and thus, affects the acidity of the material. Further substitution of Al<sup>3+</sup> by Ni<sup>2+</sup> is also possible, affecting the net positive charge, which leads to an increase in acidity (Stanislaus, et al., 1989).



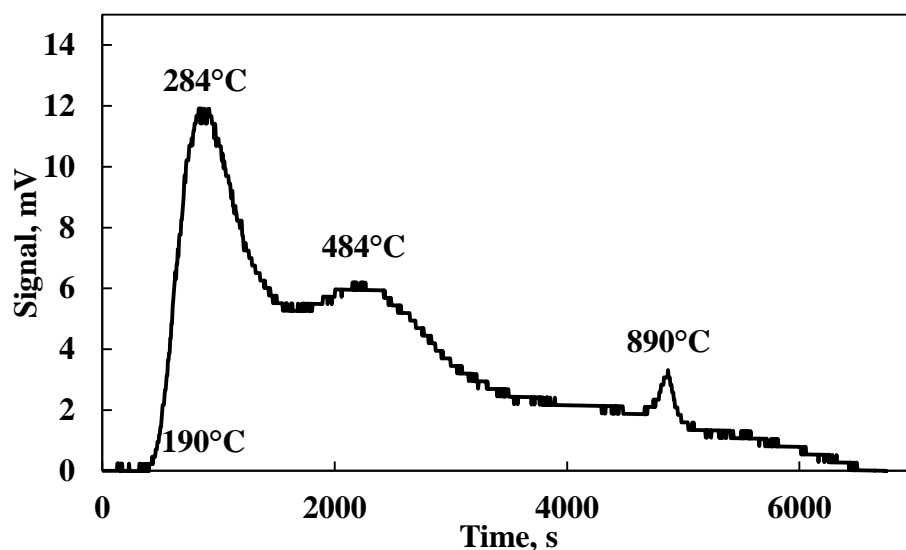
**Figure 4.7. NH<sub>3</sub>-TPD for Cat 2**

Cat 3 (Figure 4.8), in comparison with Cat 2, showed weaker acid sites that started desorbing ammonia at 196°C and presented a maximum at 287°C. However, Cat 3 contains a proportion of acid sites of similar strength to those in Cat 2, the desorption of which took place with a maximum centered at 899°C.



**Figure 4.8. NH<sub>3</sub>-TPD for Cat 3**

Desorption of ammonia in Cat 4 (Figure 4.9) occurred in a similar way than for Cat 3 for the first 1500 s of evaluation. The initial desorption and the maximum peaks were reached at about the same temperature, which indicates similar strength in acid sites. However, the strength of the following sites was different in both cases. In the case of Cat 4, the rest of the acid sites desorbed steadily between 484 and 890°C, with a signal in each mentioned temperature.

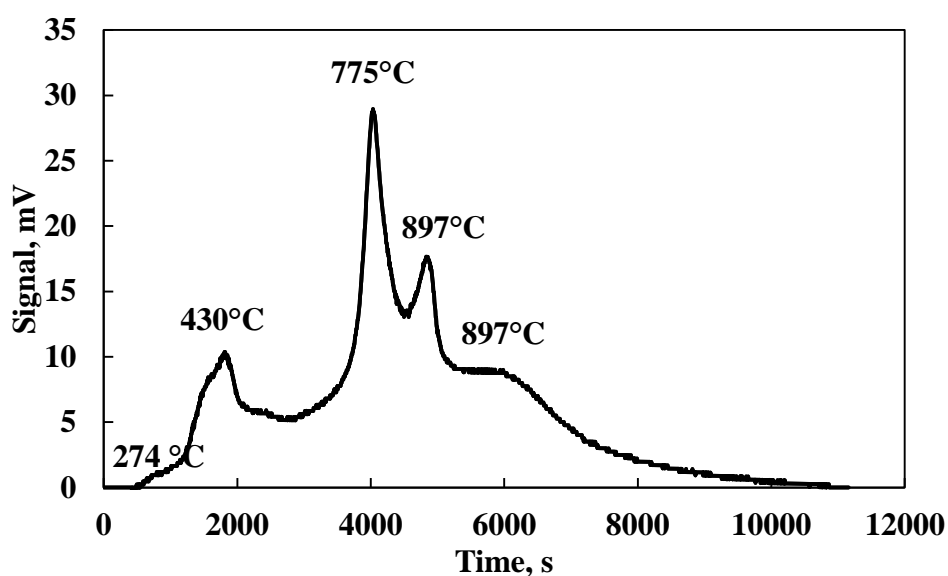


**Figure 4.9. NH<sub>3</sub>-TPD for Cat 4**

The modification done to the preparation of Cat 2 to synthesize Cat 5, plus the addition of extra components, altered considerably the profile obtained for the desorption of ammonia, indicating a noticeable change in total acid distribution. The initial temperature of desorption and peaks occurring at the beginning of the evaluated catalysts remained very similar, giving a maximum centered at 430 °C in this case. However, different stronger sites were developed in Cat 5, showing peaks of desorption centered at 775 and 897 °C. This modification of desorption profile can be attributed to the interaction created by the incorporation of the silica solution to the calcined hydrotalcite, rich in amorphous alumina. By this means, the alumina was hydrolyzed and submitted to a condensation process with hydroxyl groups of the incomplete polymerized silica solution. As a consequence, a deficiency of positive charge was created in the four-coordinated aluminium atom, which generates a Lewis acid site (an electron pair acceptor). In solution, this pair of electrons is donated by water (Tamele, 1950). On the other hand, due to this alumina-silica interaction, an increase on the strength of the acidity is expected after a thermal treatment, such as

the one conducted before reaction. The increase in temperature can be a factor in the formation of strong Brønsted sites, generated by the migration of aluminum atoms and substitution into the silica structure, which generates a negative charge that requires compensation by protons (Hensen, et al., 2010).

In general, all the catalysts show the existence of strong acid sites that desorb at temperatures ranging between 890-900°C, which by comparison of signals, Cat 5 seems to contain the highest proportion of this type of acid sites.



**Figure 4.10. NH<sub>3</sub>-TPD for Cat 5**

Table 4.4 represents the final total amounts of desorbed ammonia obtained for each catalyst. From these results, the catalyst containing the highest amount of acid sites was Cat 5, followed by Cat 4 and Cat 2. Except for Cat 1 that contains no acidity, Cat 3 is the one with the lowest amount of acid sites, due to the fact that most of the acidity was induced via ion exchange of sodium, restricted to a maximum of 30% exchangeable. Originally, the prepared aegirine only accounted for Lewis type acidity. In the case of Cat 4, the acidity comes from Brønsted acids generated by the



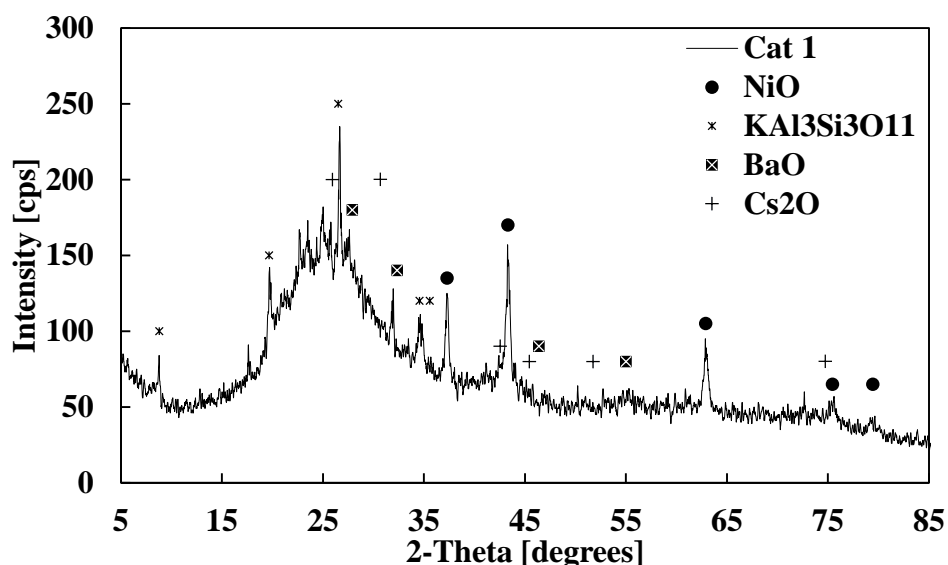
hydroxylation of the compensation cations. Besides, ion exchanged rare earths like Ce are also able to present Lewis acidity when zeolites are dehydrated (Ward, 1969).

**Table 4.4. Ammonia desorption quantities for catalysts evaluated**

Catalyst	Ammonia Desorbed, $\mu\text{mol-Ammonia/g Cat}$
Cat 1	17
Cat 2	2134
Cat 3	374
Cat 4	2205
Cat 5	5631

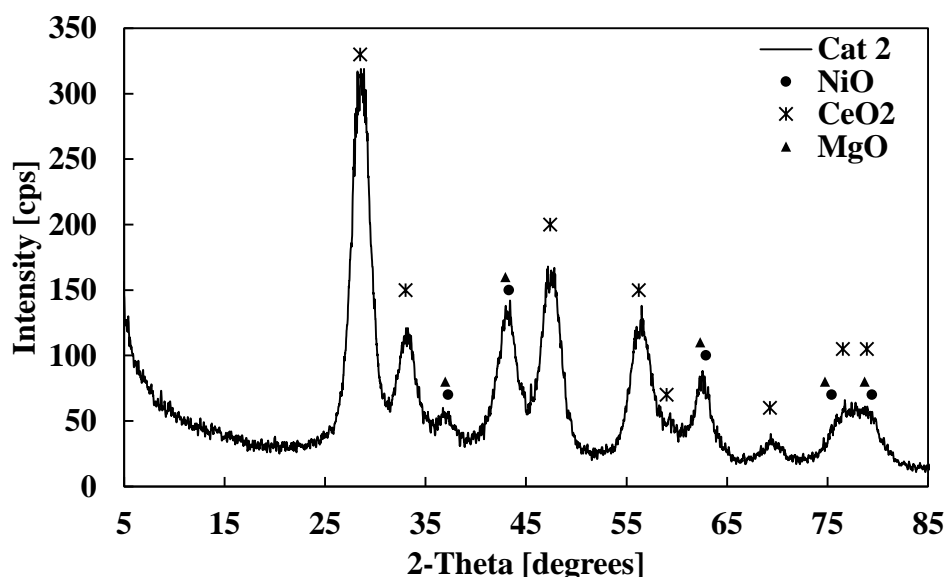
#### 4.5 Powder X-Ray Diffraction (XRD)

The powder analysis for Cat 1 via XRD generated the result presented in Figure 4.11. Due to the calcination conditions used for Cat 1, the kaolinite added to the catalyst becomes amorphous (known as metakaolin) and it was no longer observed in the XRD diffractogram. However, some traces of existing contamination with a crystalline potassium aluminosilicate remained stable even after the treatment at 650°C. The presence of Cs oxide (PDF#00-009-0104) could not be assessed with the XRD, probably due to the low concentration present in the material, but some Barium oxide (PDF#01-071-3780) can be suggested as present in the diffractogram at about 55 degrees of 2-theta. Nickel oxide (PDF#01-075-0269) is also clearly identified in the diffractogram with large and thin peaks, giving a crystalline domain size in the range of  $12\pm 4$  nm.



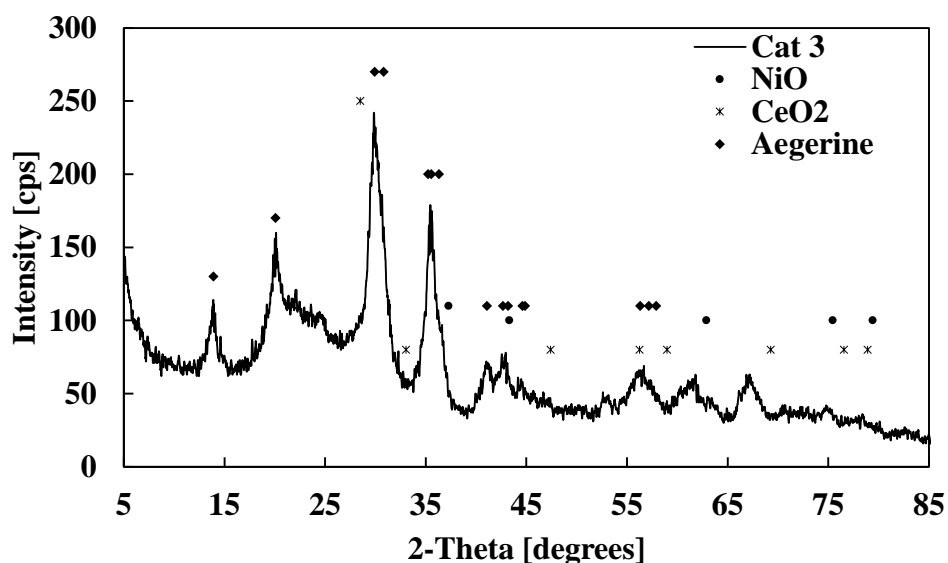
**Figure 4.11. XRD diffractogram for Cat 1**

Figure 4.12 presents the diffractogram obtained for Cat 2, as well as the location of the peaks that represent NiO, CeO<sub>2</sub> (PDF#01-075-7750) and MgO (PDF#01-077-2364). As can be concluded from the wide shape of the peaks, there is a clear evidence of the formation of small crystalline domain sizes of about  $4 \pm 1$  nm for cerium oxide in the structure of the catalyst. It is hard to determine the presence of NiO, since its respective peaks overlap with those of MgO. However, both of them are found along the whole spectrum with an average size of  $4 \pm 1$  nm. In the search for the contribution of aluminum oxide, no match could be found with the data base, probably due to the formation of an amorphous phase for this oxide.



**Figure 4.12. XRD diffractogram for Cat 2**

The XRD diffractogram for Cat 3 shown in Figure 4.13, represents clearly the crystalline structure of the Aegirine (PDF#00-034-0185) with average crystalline domain size of  $7 \pm 2$  nm. The methodology followed for the preparation of Cat 3, incorporated cerium atoms inside the crystalline framework, reason why it should not be clearly found the presence of cerium oxide in the diffractogram, unless some cerium remained outside of the structure and sintered into larger material than 3 nm, which is the smallest size detectable for mixed compounds with the XRD methodology followed. In such a case, as occurring with nickel oxide, identifying them becomes a very difficult task due to the population of the chart with peaks corresponding to the aegirine. Moreover, the proper wet impregnation of the aegirine with nickel nitrates generated a well dispersed nickel making NiO, if present, not identifiable by XRD.



**Figure 4.13. XRD diffractogram for Cat 3**

The XRD diffractogram of the modified faujasite, as provided, is presented in Figure 4.14 for a range from 5 to 35  $2\theta$  degrees. In agreement with the literature, little modification in the structure of the zeolite was obtained after Ni and Ce were exchanged (Wang, et al., 2009; Wang, et al., 2009). A shifting of the peaks towards the left is observed, indicating an expansion of the unit cell in the zeolite. No Ni or Ce oxides were found in the XRD diffractogram, as evidence of the successful ion exchange or the generation of very small crystalline domain size oxides. Due to the common large crystalline domain size of zeolitic materials ( $>200$  nm), this parameter could not be determined using the Scherrer equation. As expected, the incorporation of kaolin and silica for the preparation of Cat 5 generates an amorphous phase in the bulk of the catalyst that is represented in the XRD diffractogram as a reduction in the intensity of the zeolite peaks (shown in Figure 4.15) and the appearance of a hump between 15 and 35  $2\theta$  degrees.

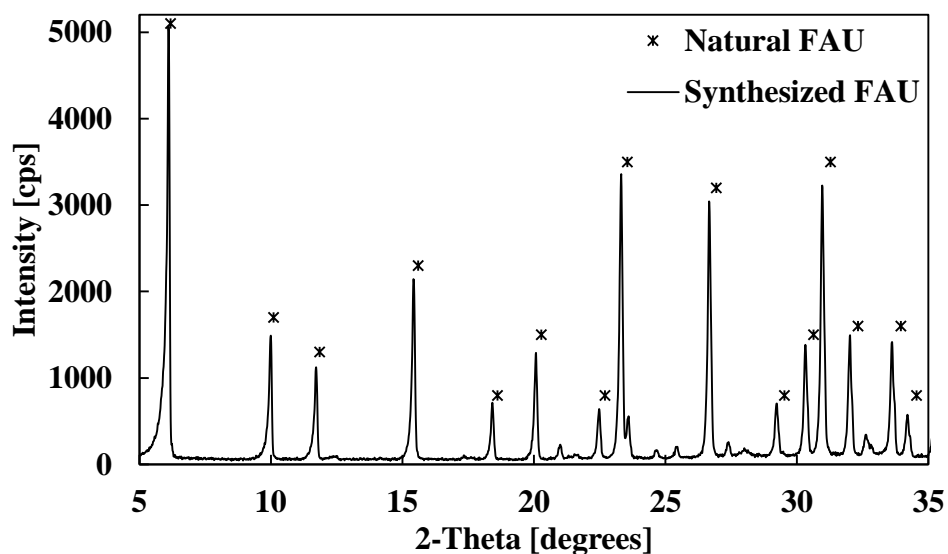


Figure 4.14. XRD diffractogram for as provided FAU.

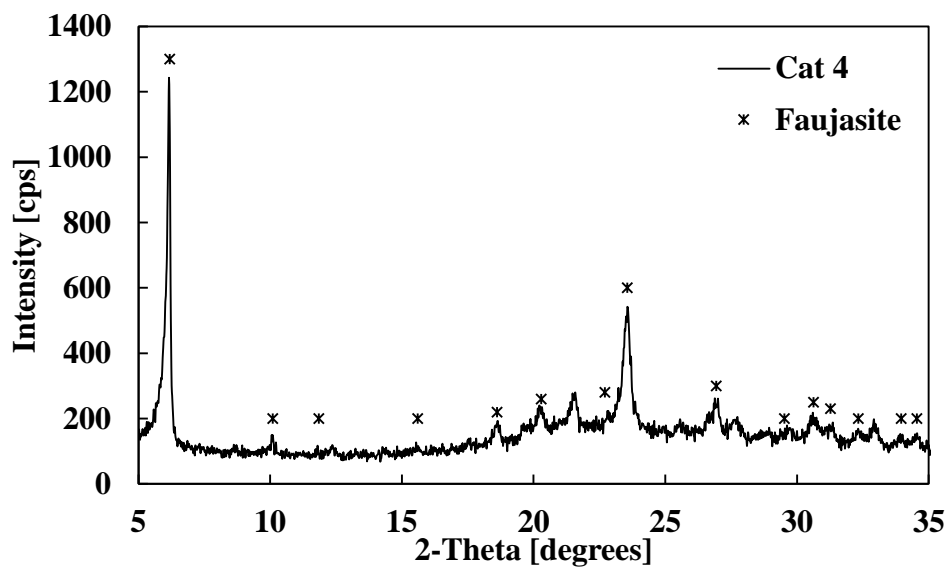
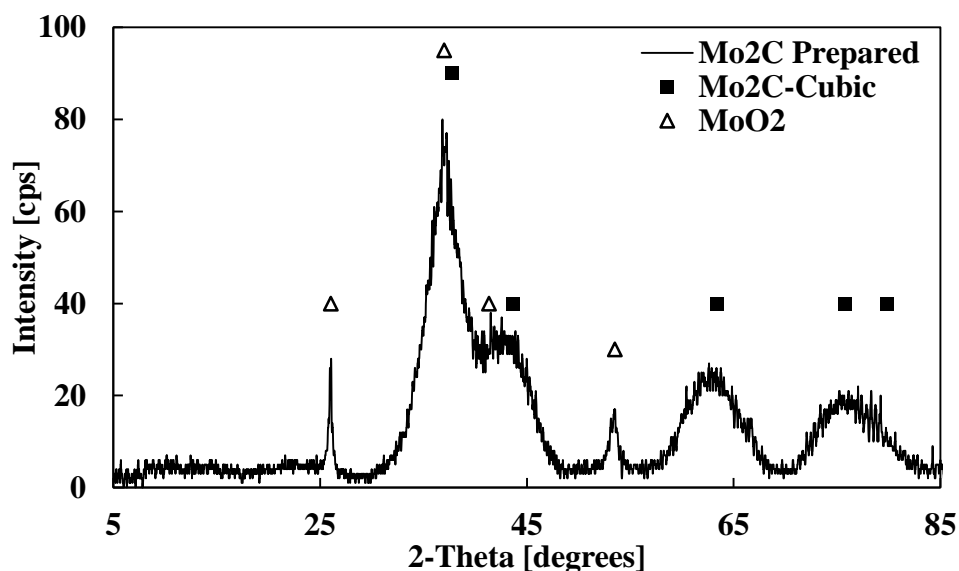


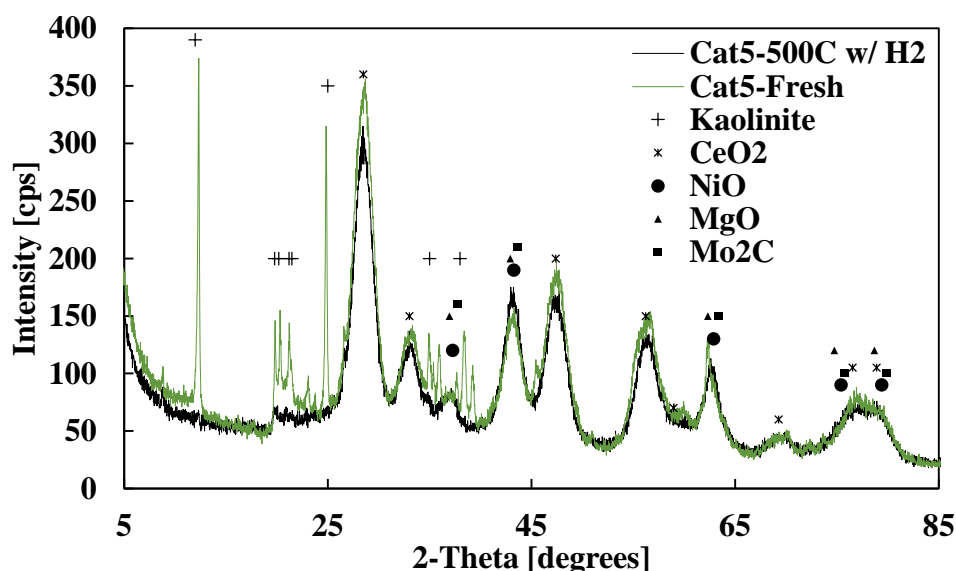
Figure 4.15. XRD diffractogram for Cat 4.

The thermal treatment of the precursor used to prepare molybdenum carbide, generated the diffractogram presented in Figure 4.16. As it can be concluded, molybdenum carbide with the cubic phase (PDF#00-015-0457) was obtained with very small crystalline domain size of  $1.8 \pm 0.3$  nm. However, the thermal treatment was not 100% effective, since traces of  $\text{MoO}_2$

(PDF#01-073-1249) were observed as side product. The preparation of Cat 5, by mixing the NiCe calcined hydrotalcite with molybdenum carbide, kaolin and silica generated the product analyzed in Figure 4.17. In the same figure, it is also presented the XRD pattern obtained for the catalyst after reduction with hydrogen at 500 °C, as done during the operation in the pilot plant. The results highlight the presence of kaolinite in the catalyst bulk of Cat 5 fresh, which was dehydroxilated after the thermal treatment producing the amorphous metakaolin. Once the kaolinite was converted into metakaolin, the final XRD pattern for Cat 5 looks very similar to the one obtained for Cat 2, where cerium oxide is easy to identify, as well as nickel/magnesium oxide. In this case, Mo<sub>2</sub>C peaks also overlap with those peaks of Nickel and Magnesium oxide, which makes it hard for identification.



**Figure 4.16. XRD for Molybdenum Carbide.**



**Figure 4.17. XRD diffractogram for Cat 5 fresh and treated in hydrogen at 500°C**

#### **4.1 X-Ray Photoelectron Spectroscopy (XPS)**

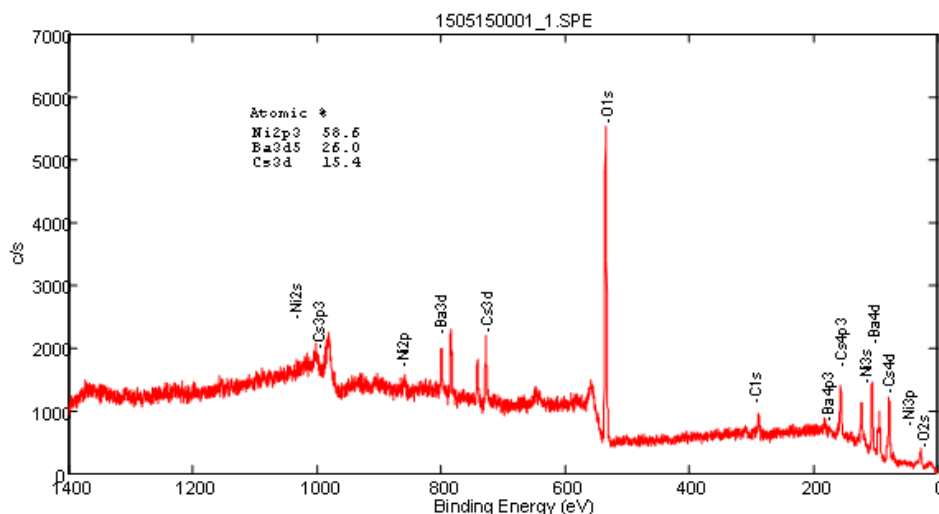
The analysis of the catalysts via XPS allowed the elemental quantification of the different metals used in their preparation. This quantification was achieved by performing a survey scan over the surface of the catalyst with a maximum depth of 4-6 nm and a minimum spot analysis of 10  $\mu\text{m}$ , which results were used to generate charts similar to the one presented in Figure 4.18. In this case, the peaks observed are sharp and intense which shows the high superficial concentration of all the elements present in the sample. The concentration of the metals in the surface of each catalyst is presented in Table 4.5.

The experimental superficial atomic ratios of Cat 1 corresponds, in terms of the proportions, to the theoretical atomic composition calculated using the nominal data for Ni, Cs and Ba (42%, 33% and 25% respectively) but do not correspond to the absolute values. Since this catalyst is the result of a mechanical mixture of their components, the result obtained is expected. The differences can be interpreted in terms of an enrichment of the surface with Ni and Cs. In the Ba 3d region the

calcined sample shows a Ba  $3d_{5/2}$  peak at 780.85 eV attributed to BaCO<sub>3</sub> (Moulder, et al., 1995). The Cs  $3d_{5/2}$  spectrum of the sample exhibits a peak at 724.7 eV that is an intermediate magnitude between the values found for thin surface layers of cesium oxide and peroxide on various substrates (725.2 and 724.5 eV for Cs<sub>2</sub>O and Cs<sub>2</sub>O<sub>2</sub>, respectively) (Larichev, et al., 2007).

For the Ni-Ce containing catalysts, their metal proportions were calculated and compared with the one obtained from the respective nominal values (shown in Table 4.5). These results show the occurrence of metal migration to the surface of the catalyst, which is observed as an increment in the composition of some metals and a decrease of some others. In the case of Cat 2, the Ni/Ce proportion is strongly reduced by about 92%, while in Cat 3 the same behaviour is observed but in lower proportion (about 47% reduction). As a consequence, the surface of the catalyst is enriched with Ce atoms. On the contrary, for Cat 4 and Cat 5 the experimental Ni/Ce ratios are much higher than the nominal one, which is an indication of the high nickel content on the surface of the solids. For Cat 4, the content of nickel on the surface was increased almost ten times with respect to the nominal value, while in Cat 5 the increase was about 6 times. It is interesting to note that the slight variation in the preparation of Cat 5, with respect to Cat 2, generated as a consequence the population of the surface of Cat 5 with nickel atoms.





**Figure 4.18. Survey scan for Cat 1**

**Table 4.5. Experimental surface atomic composition of metals on the catalysts**

Cat.	Ni (%)	Ba (%)	Cs (%)	Al (%)	Mg (%)	Ce (%)	Si (%)	Fe (%)	Zr (%)	Mo (%)	Ni/Ce (Nom.)	Ni/Ce (XPS)
1	58.6	26.0	15.4	-	-	-	-	-	-	-	-	-
2	<0.1	-	-	63.3	36.1	0.7	-	-	-	-	1.7	0.14
3	0.3	-	-	-	-	0.6	95.5	2.9	0.6	-	0.95	0.5
4	2.3	-	-	18.9	-	0.3	78.5	-	-	-	0.83	7.7
5	1.0	-	-	53.9	44.0	<0.1	-	-	-	1.0	1.7	10

#### **4.1.1 Decomposition of Ni 2p<sub>3/2</sub>**

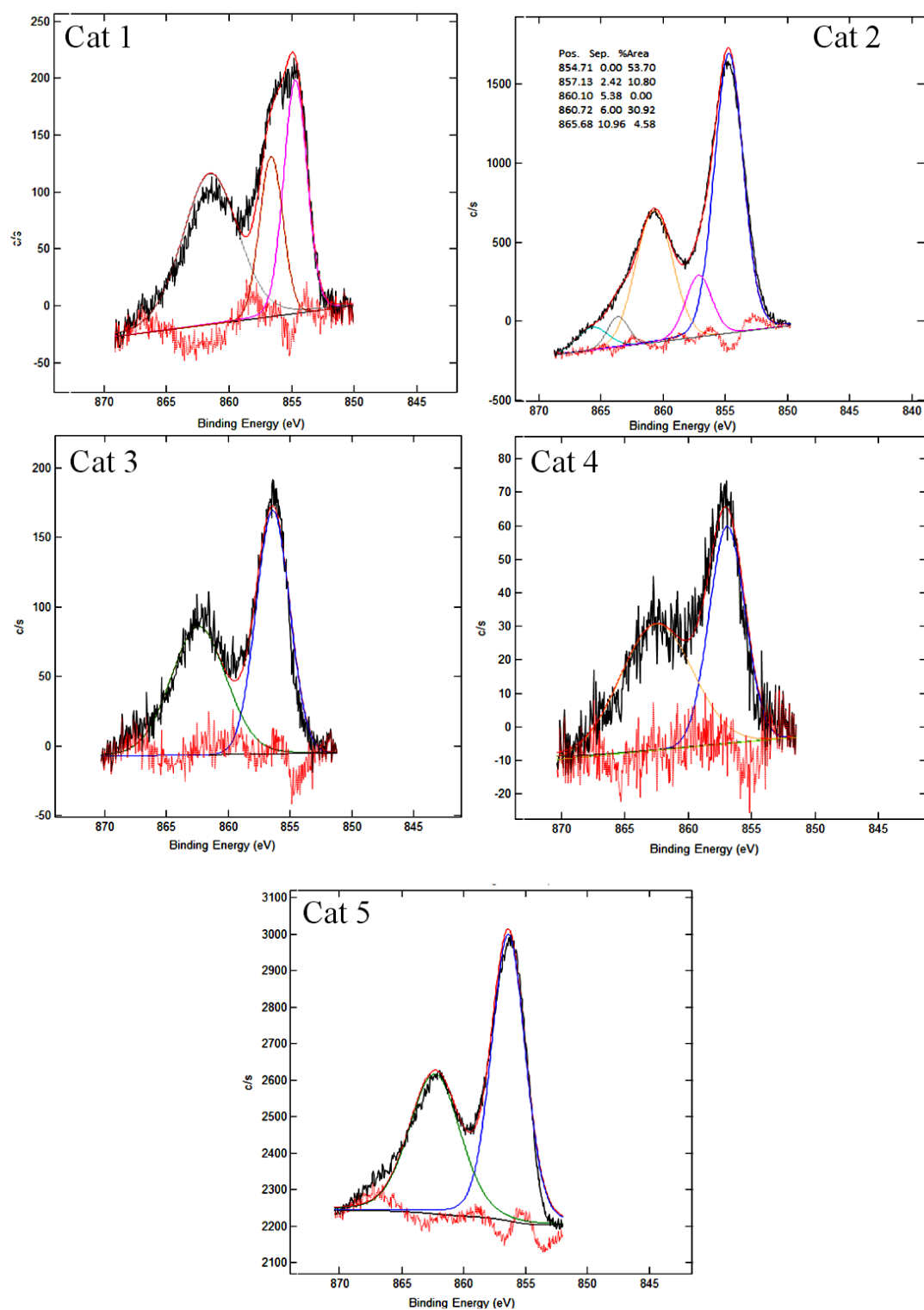
Figure 4.19 represents the XPS spectra for Ni 2p<sub>3/2</sub> for each one of the catalysts evaluated. The binding energy values are presented in Table 4.6. In all cases, the Ni 2p spectra correspond to nickel in the Ni<sup>2+</sup> state. The presence of intensive “shake up” satellites located 6 eV apart from the main peak supports this assignment (Khasin, et al., 2006). In the case of Cat 1, the spectrum shows a Ni 2p<sub>3/2</sub> at 854.70 eV which can be assigned to Ni in bulk NiO (Andonova, et al., 2011). For

Cat 2, two Ni  $2p_{3/2}$  peaks were observed at 854.71 and 857.13 eV, which shows the presence of two different Ni species. The first signal can be attributed to Ni in NiO, as also observed from Cat 1. The additional signal at 857.13 eV with an error of 1 eV, could be attributed to Ni forming a spinel-like structure with alumina ( $\text{NiAl}_2\text{O}_4$ ), which gives a binding energy of 856.1 eV (Andonova, et al., 2011). The proportion of these two species is 5:1 for NiO:  $\text{NiAl}_2\text{O}_4$ . It has also been found that Ni can form an MgO-NiO solid solution that shifts the signals toward higher binding energy (Hu & Ruckenstein, 1997). Cat 4 also shows a peak with binding energy at 857.1 eV, assigned to Ni in  $\text{NiAl}_2\text{O}_4$ .

The spectra of Cat 3 and Cat 5 show Ni  $2p_{3/2}$  peaks at 856.1 and 856.3 eV, respectively. These values are more than 1eV higher than the binding energy reported for Ni in NiO. However, it has been reported similar binding energies for Ni-catalysts obtained from silicate intercalated hydrotalcite and assigned to a Ni species that is difficult to reduce (Basile, et al., 2009).

**Table 4.6. Binding energy for Ni  $2p_{3/2}$  in all the catalysts evaluated**

Catalyst	Ni $2p_{3/2}$ Binding Energy (eV)
1	854.7
2	854.7 – 857.1
3	856.1
4	857.1
5	856.3



**Figure 4.19. Decomposition of Ni 2p<sub>3/2</sub> for all catalysts**

#### ***4.1.2 Decomposition of Ce 3d<sub>5/2</sub>***

The XPS spectra of Ce 3d<sub>5/2</sub> signal for Cat 2, Cat 3, Cat 4 and Cat 5 can be found in Figure 4.20. It is well known that the Ce 3d<sub>5/2</sub> spectrum is composed of three signals in the case of CeO<sub>2</sub> and two signals for Ce<sub>2</sub>O<sub>3</sub> (Romeo, et al., 1993). In the case of the charts presented in Figure 4.20, it is possible to observe the existence of five signals, indicating the partial reduction state of Ce atoms present in these samples. However, the detailed characterization of these signals becomes a difficult task, since up to ten peaks are detected, taking into account the spin-orbit coupling. In the case of Cat 2 and Cat 5, an additional signal due to a Ni 2p satellite is also observed at  $\approx 878.39$  eV. The detailed binding energy obtained for each of the signals detected is presented in Table 4.7. According to this table and using the Ce<sup>3+</sup>/Ce<sup>4+</sup> ratio, Cat 3 is characterized with the lowest content of Ce<sup>3+</sup> and Cat 4 with the highest. Therefore, Cat 4 followed by Cat 5 might have higher activity for water activation at the initial stage of the process among the Ce containing catalysts, while Cat 3 might have the lowest capability.

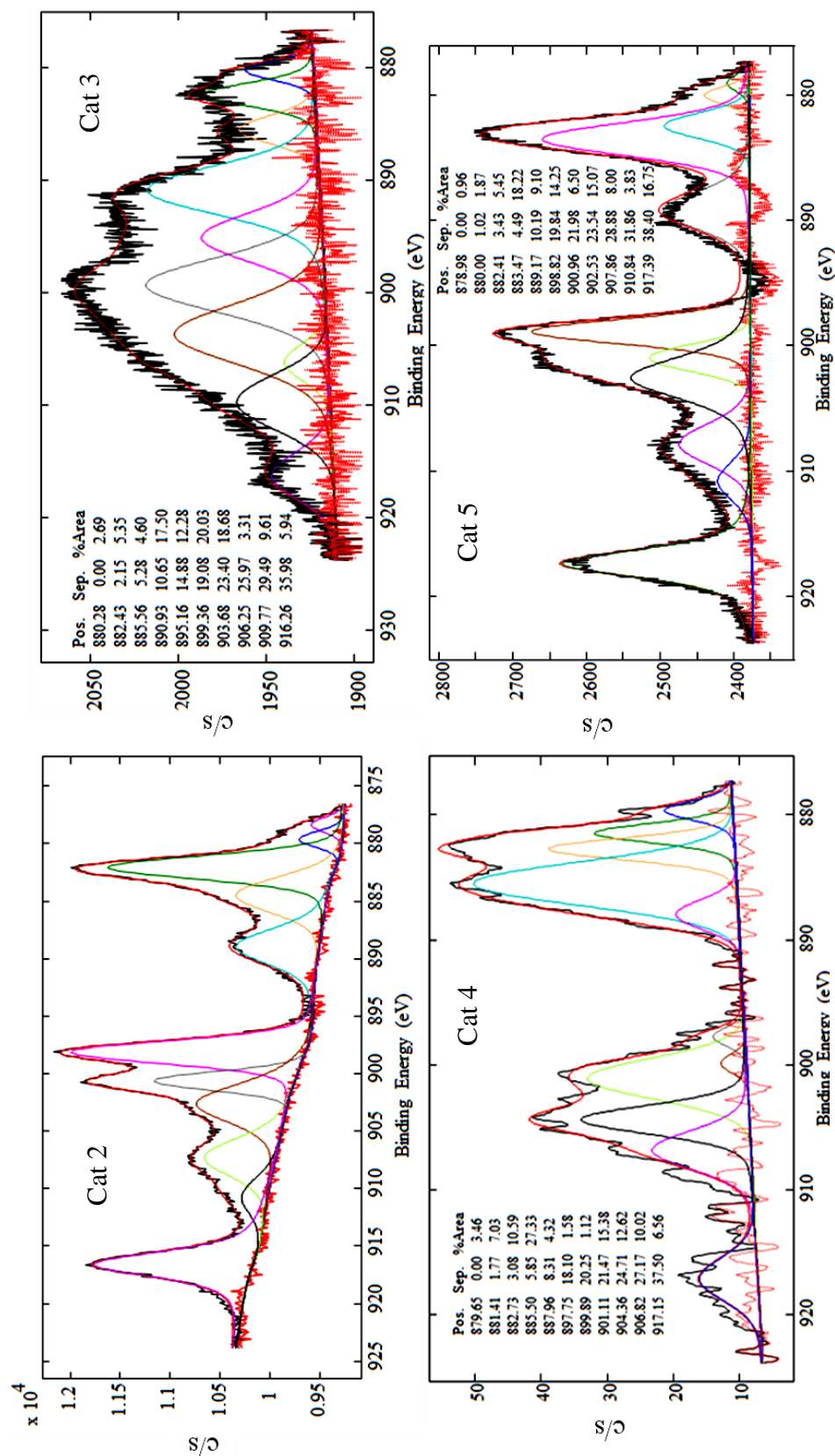


Figure 4.20. Decomposition of Ce 3d

**Table 4.7. Binding energies for Ce 3d<sub>5/2</sub> signals**

	Binding energies, eV					
	Cat 2	Cat 3	Cat 4	Cat 5	Ce <sup>3+</sup> in CePO <sub>4</sub> *	Ce <sup>4+</sup> in CeO <sub>2</sub> *
Ce <sup>3+</sup>	879.66	880.28	881.41	800.00	880.9	-
	884.48	885.56	885.50	883.47	885.2	
	898.16	895.16	897.75	898.82	899.1	
	907.25	906.25	904.36	902.53	903.4	
Ce <sup>4+</sup>	882.09	882.43	882.73	882.41	-	882.7
	888.96	890.93	887.96	889.17		888.5
	900.66	899.36	899.89	900.96		898.3
	902.59	903.68	901.11	907.86		901.3
	910.58	909.77	906.82	910.84		907.3
	916.57	916.26	917.15	917.38		916.9
Ce <sup>3+/</sup> Ce <sup>4+</sup> ratio	0.66	0.30	1.01	0.75	-	-

\*Beche, et al., 2008

From this detailed analysis of the adsorptive, structural and surface chemical characteristic of the five catalyst tested, it can be concluded that Cat 2, Cat 3 and Cat 5 could have hydrogenating capabilities at temperature lower than 400°C (from TPR), in particular Cat 5 in which Ni migrated in abundance to the surface of the catalyst (from XPS). Also, Cat 5 could have higher tendency to hydrocarbon cracking (from TPD). The complexity of the superficial Ce<sup>+n</sup> signals makes it difficult to derive conclusions on the water activation possibilities of the catalysts, making the reactive and stability evaluation of the catalysts a necessity.

## Chapter Five: Pilot Plant Operations

The analysis of all the data obtained from the evaluation of Cat 1 (NiCsBa-Metakaolin), Cat 2 (NiCe-Calcined Hydrotalcite), Cat 3 (NiCe-Aegerine), Cat 4 (NiCe-Faujasite) and Cat 5 (Cat 2+Mo<sub>2</sub>C) in the pilot plant, is presented in this chapter and divided into three main sections. The first section aims to give information about the effect of some studied parameters on the conversion of residue in thermal cracking operations. The second section focuses on the evaluation of the catalysts, their performance, analysis of the products and variation in operating conditions. Finally, the third section takes into consideration the best result obtained during the catalytic steam cracking evaluation to assess the achievable improvement at the end of the upgrading scheme proposed.

The most frequent main sources of error during pilot plant operations can be experienced during the acquisition of the data, handling of the products or by failure of the equipment. For that reason, Table 5.1 was created based on the mass balance calculations done for each sample obtained in the plant. The oil mass balance accounts for the mass of oil pumped into the system in comparison with the mass of heavy hydrocarbons, light hydrocarbons and gases obtained as products. As can be seen, close to 100% of the oil pumped was consistently recovered as products with a small variation of 6% between all the samples analyzed. This reflects the good performance of the pump and the proper acquisition of the samples. Besides, it was determined by experience that to obtain such a good mass balance for oil in the constructed system, a minimum of 11 g of heavy hydrocarbons was needed, regardless of the time needed to produce it. In that way, remaining oil in the pipes and any drop of oil spilt out of the collector vessel, would not be significant for the mass balance determination.

The results obtained for the water mass balance were lower than expected, since in general 81% of the water was recovered with an important variation of 16%. These low recoveries for water are related to the very little amount of water injected and handled at the end as product. In most cases, the time selected only allowed the recovery of as much as 1 ml of water sample. Therefore, any minimum amount of water lost by handling or evaporation would mean an important variation in the mass balance. Additionally, the mass balance for water does not account for the amount of water consumed during reaction, which is transferred to the hydrocarbon products and the gases. Therefore, this might be another reason for the obtained low mass balance for water. Nevertheless, the employed syringe pump for water and oil are very reliable. They work by volume difference and thus, the volume of fluid pumped into the plant is exactly the same as that obtained from the volume variation in the syringe. Notwithstanding this, in general, 97% of all the reactants injected into the system were recovered at the end of the process, with a small variation of 8% among all the samples evaluated.

**Table 5.1. Average mass balances obtained along all the performed runs**

	Thermal Runs	Catalytic Runs	All Runs
Avg. Oil Mass Balance, %	103±6	100±6	101±6
Avg. Water Mass Balance, %	76±15	85±16	81±16
Avg. Global Mass Balance, %	102±5	96±8	97±8

### **5.1 Thermal steam cracking**

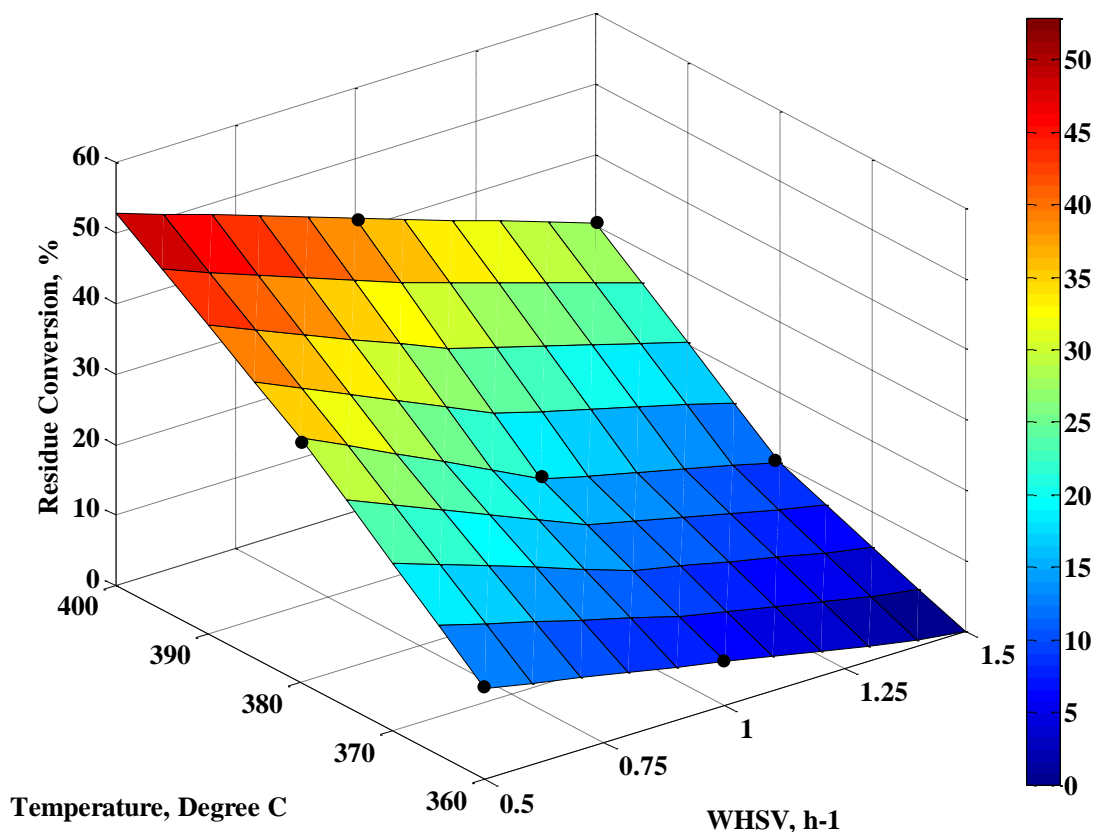
The proper evaluation of the catalytic activity of the solids developed in the laboratory, requires an initial understanding of the residence time and thermal effect on the conversion of molecules existing in the used feedstock, especially on those heavy molecules located within the residue



fraction ( $>560^{\circ}\text{C}$ ). In order to obtain this knowledge, it was necessary to operate the designed plant with the 3/8" reactor free of catalyst and filled only with an inert material (washed carborundum). In this way, flow patterns and residence times of the oil in the reactor were kept relatively constant, by having solids that approximately simulate the catalytic bed but with no effect on the conversion of the hydrocarbon molecules. In order to obtain a weight hourly space velocity (WHSV) of reference for each used flowrate for the thermal runs, a mass of catalyst of 3.5 g was assumed for the calculations, which together with its corresponding oil flowrate, allowed the determination of a value for WHSV that can be used to compare with catalytic runs.

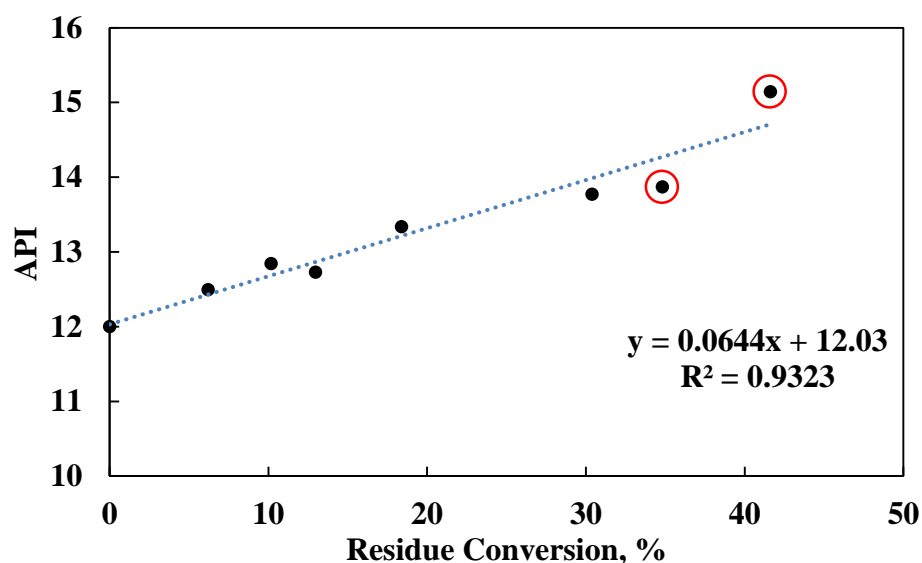
As shown in Figure 5.1, the thermal experiments involved seven runs (black dots) with temperatures in the range of  $360\text{--}400^{\circ}\text{C}$ , and with space velocities between  $0.5$  and  $1.5\text{ h}^{-1}$ . Intermediate values were linearly interpolated, while conversion at  $360^{\circ}\text{C}/\text{WHSV}=1.5\text{ h}^{-1}$  and  $400^{\circ}\text{C}/\text{WHSV}=0.5\text{ h}^{-1}$  were linearly extrapolated from the experimental data obtained. The surface chart is in agreement with what is expected, increases in space velocity leads to lower residence time of the oil in the reactor and thus, less time for the molecules to be cracked. On the other hand, increases in temperature favor the rupture of C-C, C-H and C-heteroatom bonds by producing free reactive radicals, which is reflected in a reduction of the residue content in the oil. Therefore, the final conversion of residue and product distribution is highly dependent on the severity of the process, expressed as residence time-temperature combination (del Bianco, et al., 1993). It is also interesting to note the sensitivity of the system toward temperature changes, especially over the residue conversion. Taking the point  $380^{\circ}\text{C}/\text{WHSV}=1.0\text{ h}^{-1}$  as reference, large variations in space velocity of about 50% can lead to a decrease in conversion of 8 points or an increases of 16 points. Conversely, improvements in the residue conversion of 23 points or reduction of 12 points can be achieved with a variation in the temperature as small as  $20^{\circ}\text{C}$  (3% variation in Kelvin units). For

that reason, it is important to have a good control of the temperature during the operation of the reactor in order to obtain the degree of thermal cracking expected for each condition.



**Figure 5.1. Effect of temperature and residence time over the residue conversion in thermal cracking**

The results of the analytics performed to the products generated in the plant are presented in Figure 5.2 to Figure 5.5 (API, viscosity, asphaltenes and microcarbon vs. residue conversion). According to the results obtained, the API can be estimated from a linear regression with an  $R^2$  of 93%. The final two points of the chart, seem to deviate slightly from the trend generated by the rest of them. The very final point corresponds to a conversion of 42% of residue, where the presence of precipitated asphaltenes was observed by optical microscope analysis. Therefore, the analytics of this sample might be affected by the fact that it was not completely homogeneous.



**Figure 5.2. API variation with residue conversion**

It was found that the logarithm of viscosity is linearly related to the conversion of residue with an  $R^2$  of 96%. On the other hand, the determination of the asphaltene content in the products can be estimated by a linear regression with respect to the residue conversion, with an  $R^2$  of 93%. In this case, the sample corresponding to a conversion of 42% was discarded, since the trend was notoriously affected by it. Finally, it was also determined that the tendency of the oil to produce coke (microcarbon) is affected linearly by the achieved conversion. The linear regression is able to predict the microcarbon with an  $R^2$  of 92%. In this case, the last point was once again omitted, due to the interference generated in the trend obtained by the rest of the points.

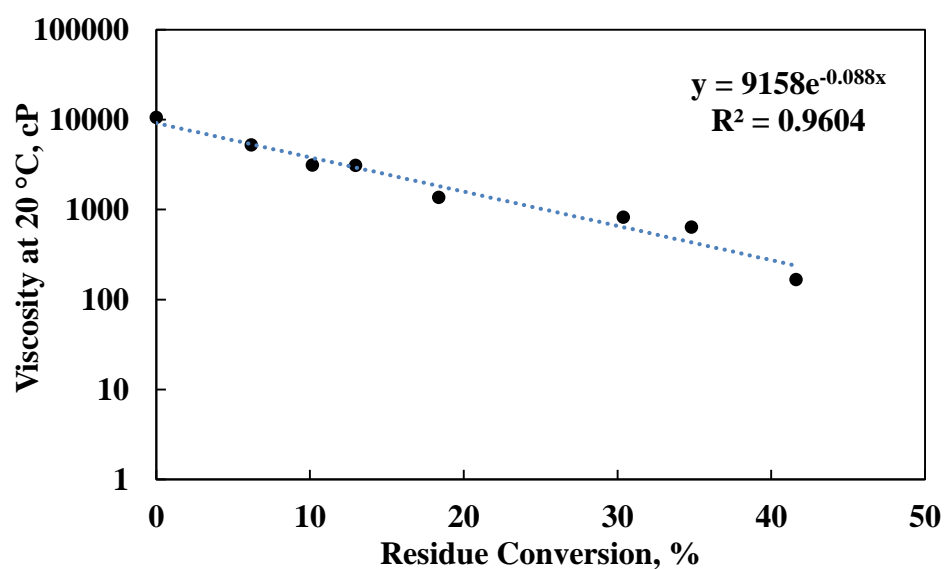


Figure 5.3. Log of viscosity variation with residue conversion

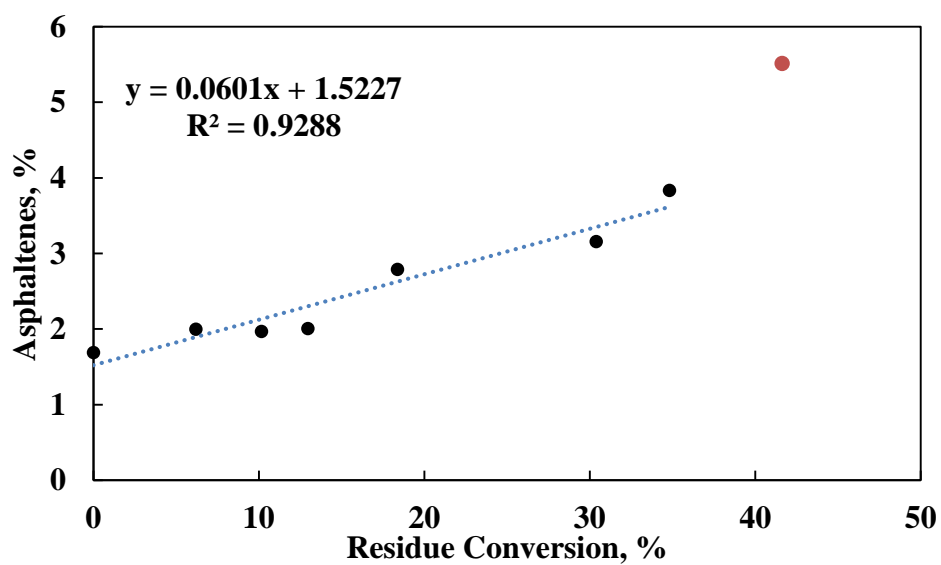
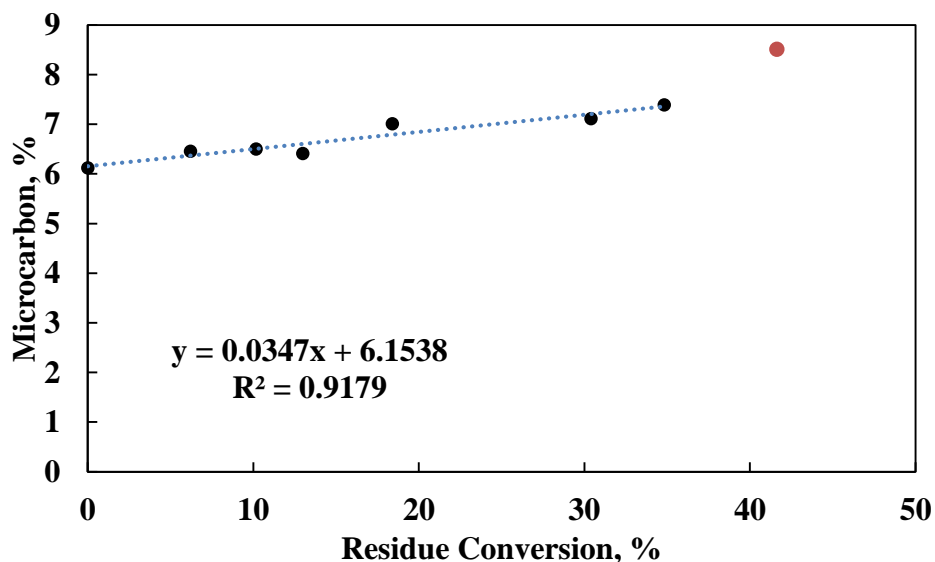


Figure 5.4. Asphaltene content vs. residue conversion



**Figure 5.5. Microcarbon vs. residue conversion.**

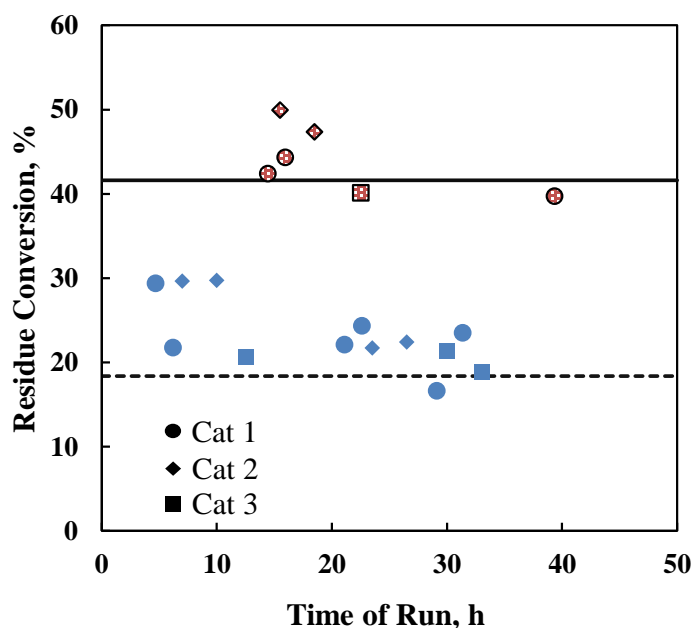
## 5.2 Catalytic steam cracking

### 5.2.1 Preliminary catalyst screening

The first set of catalytic experiments was designed to evaluate three different kinds of catalyst (Cat 1, Cat 2 and Cat 3) initially developed in the laboratory and believed to have promising characteristics to perform water splitting and thus, to be used to undertake reactions of steam cracking of hydrocarbons. Each catalyst was tested in the pilot plant using De-Asphalted Oil (DAO) and water in a weight proportion 1 to 0.05 and at a pressure of 1034.2 kPa (150 psi). For these experiments, the flowrates of DAO and water, and the weight of catalyst loaded were kept constants to work at a weight hourly space velocity (WHSV) of  $1 \text{ h}^{-1}$  in the case of Cat 1 and Cat 2. Due to the need of incorporating a binding agent (silica) in the preparation of Cat 3 to shape it into extrudates, the active catalytic material was reduced by 35%, which ended up giving a WHSV of  $1.6 \text{ h}^{-1}$  for this catalyst. The initial operating temperature used in these experiments was  $380^\circ\text{C}$  followed by an increment of  $20^\circ\text{C}$  to reach  $400^\circ\text{C}$ . After collecting samples at this last

temperature, the reactor was cooled down to 380 °C to evaluate possible de-activation of the catalyst.

The results of these experiments in terms of residue (560°C+) conversion against time are presented in Figure 5.6. As can be seen, Cat 1 shows strong de-activation of 26% in the first 6 hours of reaction at 380 °C, giving a conversion slightly higher than the thermal run evaluated at the same conditions. When evaluated at 400 °C, Cat 1 was not able to improve its catalytic activity and practically all the conversion generated was produced by the effect of temperature. Returning back to a temperature of 380 °C, no significant improvement was observed for Cat 1, which kept converting residue in a similar proportion obtained in the first stage of the experiment. In the case of Cat 2, the solid remained stable during the first 10 hours of operation giving catalytic conversion with an advantage of 10 points above the thermal one. The same extra catalytic activity was observed at 400 °C, since about 7 points were observed above the 42% of conversion generated by the thermal effect. This good performance could be explained by its characteristic acidity and higher amount of active sites in comparison with the other catalysts, for which de-activation would take longer. After three hours of operation at 400 °C, the de-activation was favored, which was confirmed in the third stage of the experiment, where the activity of Cat 2 went from 30% conversion (first stage) to about 22%. Presumably, this de-activation is caused by the high temperatures that induced coke formation and blocking of the pores and active sites. Cat 3 did not perform better than the other two catalysts evaluated. Due to operational problems, the first sample was collected after ten hours of operation and by that time, the catalyst seems to be already de-activated or not active enough to give significant extra conversion besides that obtained by the thermal effect. This behaviour was observed along the whole experiments and especially at 400 °C.



**Figure 5.6. Effect of temperature and catalyst type on residue conversion. Blue symbols correspond to runs at 380 °C and patterned red symbols at 400 °C. The respective thermal conversions are also shown at 380 °C (dotted line) and 400 °C (continuous line).**

Even though the three catalysts experienced de-activation by the end of the tests, the compositions of the gases generated during the reaction differ considerably from that obtained for the thermal runs. As observed in Figure 5.7 for the reactions at 380 °C, in the final stage of the experiments, the three catalysts showed an important concentration of hydrogen in the generated gases, between 20 to 36 times more hydrogen was produced during the catalytic test in comparison with the thermal test, which confirms some activity is still remaining in the catalyst. Moreover, the increased levels of CO<sub>2</sub> in the catalytic test in comparison with the thermal tests, showed the occurrence of steam reforming reactions. However, the production of hydrogen is very high and the ratio H<sub>2</sub>/CO<sub>2</sub> is much higher than 4, which is the ratio for methane steam reforming. Therefore, in addition to steam reforming, dehydrogenation to produce aromatics and partial oxidation reactions are also taking place.

The good dispersion of Ce and Ni in Cat 3 allows the generation of hydrogen in similar proportions obtained for Cat 2, whose nominal content of active metals was considerably higher (about 7 times for Ni and 4 times for Ce). Furthermore, it is interesting to note that this similar proportion of hydrogen was also obtained despite the fact that Ni is in lower atomic proportion for Cat 2 with respect to Cat 3 (about 3 times) on the surface of the catalyst, according to XPS analysis. At the same time, Ce is in similar proportion on the surface of both catalysts. Consequently, it can be concluded, based on xps analysis, that the hydrogen production is more dependent on the cerium content than on the nickel content. In general, the generation of hydrogen is significantly better performed by the use of a Ni-Ce combination, like in Cat 2 and Cat 3, than by the use of alkaline and alkaline earth metals with Ni (the case of Cat 1).

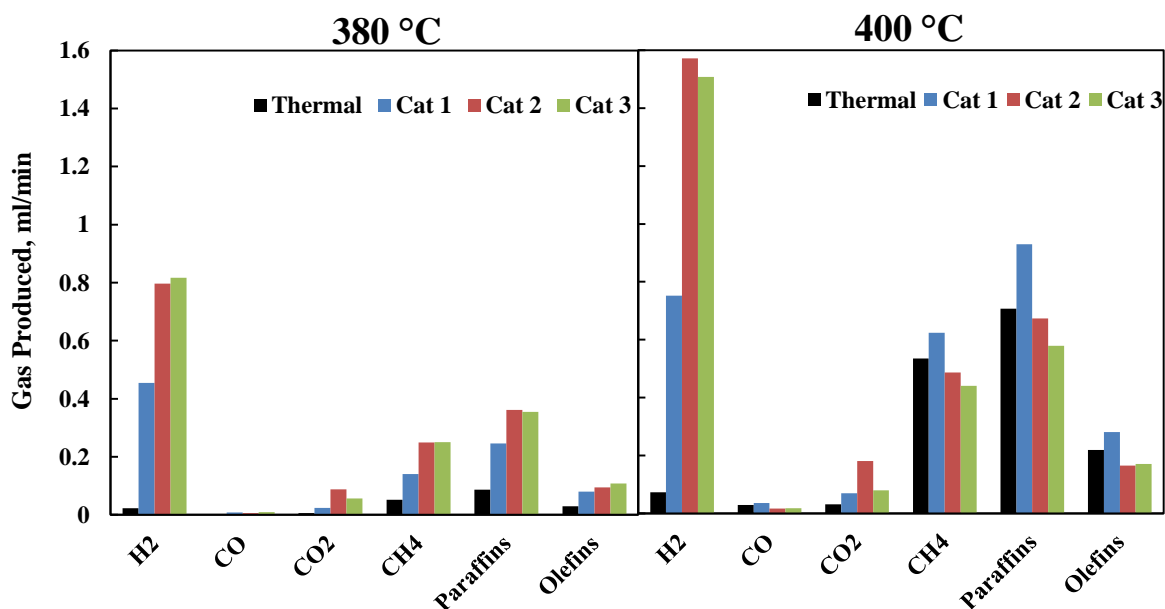
Moreover, the gas analysis indicates that the use of the evaluated catalysts also improves the cracking activity, since methane and some others hydrocarbon compounds in the range of gases up to C<sub>5</sub> (saturated compounds denoted as paraffins and unsaturated as olefins) are produced in the reaction. The improvement in the methane production can be attributed to hydrogenolysis and methanation type reactions. Among the three catalysts tested, Cat 1 seems to be the least active at this temperature, due to its lower capacity to produce hydrogen and other gases in general, while Cat 2 and Cat 3 behave in a similar way.

At 400 °C, while Cat 2 and Cat 3 increase the production of hydrogen 97% and 84% respectively, Cat 1 increases it by 65%, which reveals it to be less active for water dissociation and hydrogenation. Instead, the increase in temperature seems to favor Cat 1 to be more selective for the production of hydrocarbon gases, probably generated via hydrogenolysis.

In comparison with the runs at 380 °C, where differences in the hydrocarbon gas production could be observed between the catalytic run and the thermal run, at 400 °C the main production of these



compounds is probably due to the effect of the temperature. On the other hand, despite the amount of hydrogen produced in the catalytic runs, it was also observed the production of olefins implying the absence of a hydrogenating function that would take advantage of the produced hydrogen to saturate these olefins.

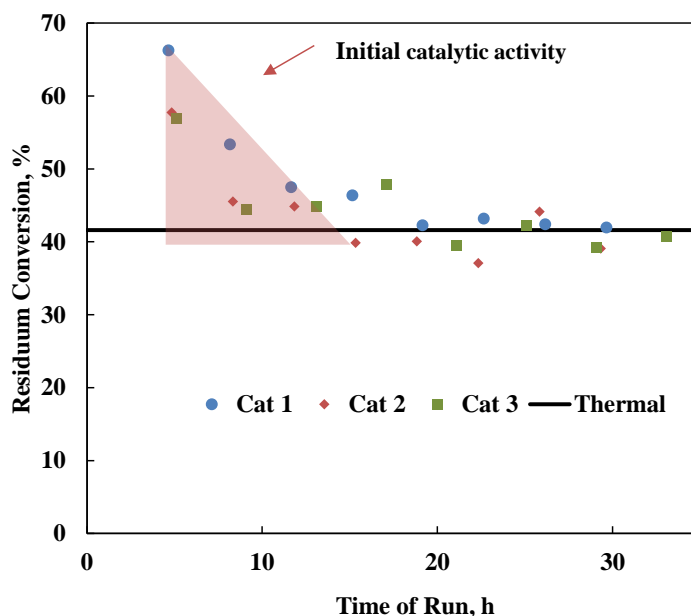


**Figure 5.7. Components gas flowrate reached at the end of each temperature for the catalytic runs, in comparison with the thermal runs.**

It is interesting to note that although Cat 3 is producing as much hydrogen as Cat 2, the latter is the one that is favoring more the carbon-oxygen bond formation (oxygen coming from the water molecules), evidenced by the generation of CO<sub>2</sub>. Therefore, the oxygen in Cat 2 experiments is leaving the system as CO<sub>2</sub> molecules, whilst it is expected that the products of Cat 3 might contain an important amount of oxygenated hydrocarbons compounds (e.g. aldehyde, ketones) in comparison with those remaining in Cat 2 products. Analyses for these compounds are extremely difficult and expensive. Thus, Cat 3 was discarded at this catalysts screening stage.

### 5.2.2 Catalyst stability and product comparison

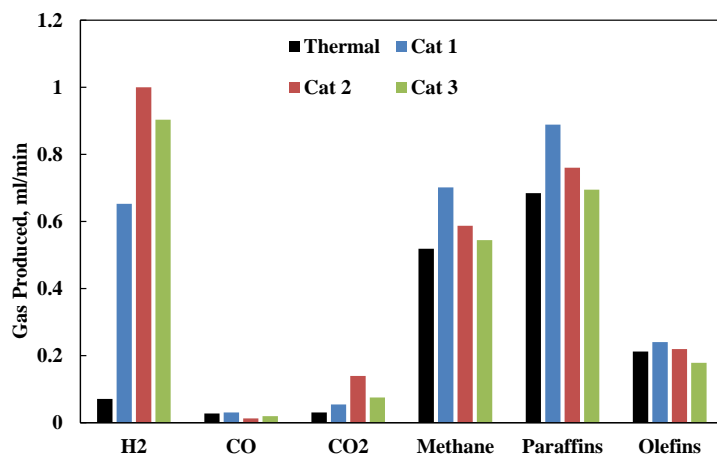
In the previous experiments was evaluated the conversion obtained for each catalyst submitted to a variation of temperatures for a short period of time on stream. In this section, the catalysts were submitted to a constant temperature of 400°C during longer periods, to evaluate the performance of the catalyst and the de-activation profile generated by each one of them. In this case, in order to compare properly, all the reactors were loaded with catalytic material ensuring a WHSV of 1 h<sup>-1</sup> for each test. The results of this experiment are presented in Figure 5.8 in terms of conversion of residue. As can be seen, all the catalysts presented an initial activity higher than 57%, which is 16 points above the thermal conversion of residue. However, after 15-20 hours all the catalysts experience a strong de-activation until reaching the activity obtained in the thermal run.



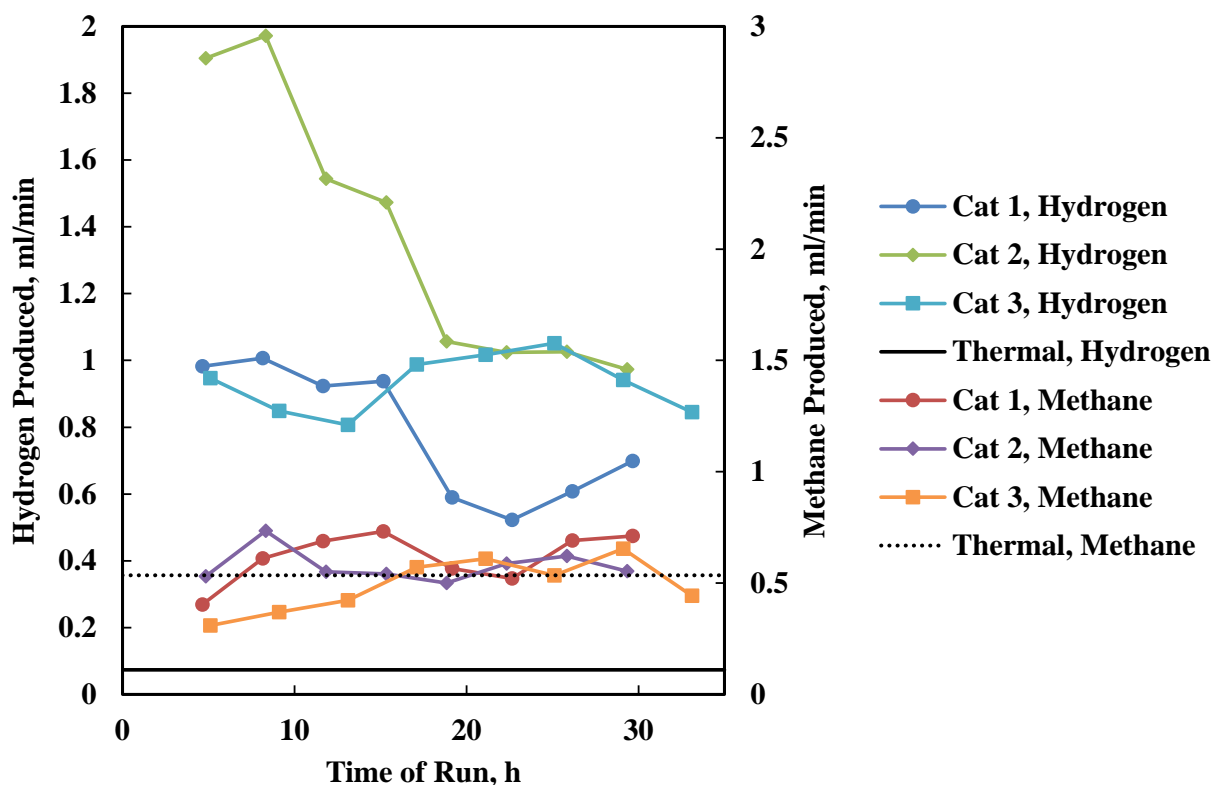
**Figure 5.8. Deactivation profile of the catalyst tested at 400 °C and WHSV=1 h<sup>-1</sup>.**

Since the catalysts were submitted for a longer period of time at 400°C, it is expected to lose more active sites by the end of the experiment in comparison with that obtained in the catalytic

screening. However, similar trends in the production of each type of gas are also observed, as shown in Figure 5.9. Cat 2 and Cat 3 dominate the production of hydrogen, while Cat 1 has a certain selectivity for hydrocarbon cracking, which generates higher amounts of olefins, paraffins and methane. Figure 5.10 represents the profile of de-activation from the hydrogen and methane production points of view. The production of methane remains stable during the whole experiment at magnitudes similar to that obtained for the thermal run, which is an indication of the strong effect of temperature on the hydrocarbon cracking to produce gases. Cat 1 shows a slightly higher activity for methane production. However, there are important differences in the production of hydrogen. At the beginning of the experiment, Cat 2 was able to produce almost double the amount of hydrogen produced by the other two catalysts, but after 25 hours of reaction the hydrogen production equals the value obtained for Cat 3. Cat 1 remained stable during the first 15 h of reaction, followed by a loss of water splitting activity on average of about 30%. Even though Cat 3 loses 22% of activity toward residue conversion, the activity for water dissociation remains stable along the whole experiment. This is an indication of the stability of the water splitting sites.



**Figure 5.9.** Gas production at stabilization (400 °C and WHSV=1 h<sup>-1</sup>).



**Figure 5.10. Hydrogen and methane production evolution with time (400 °C and WHSV=1 h<sup>-1</sup>).**

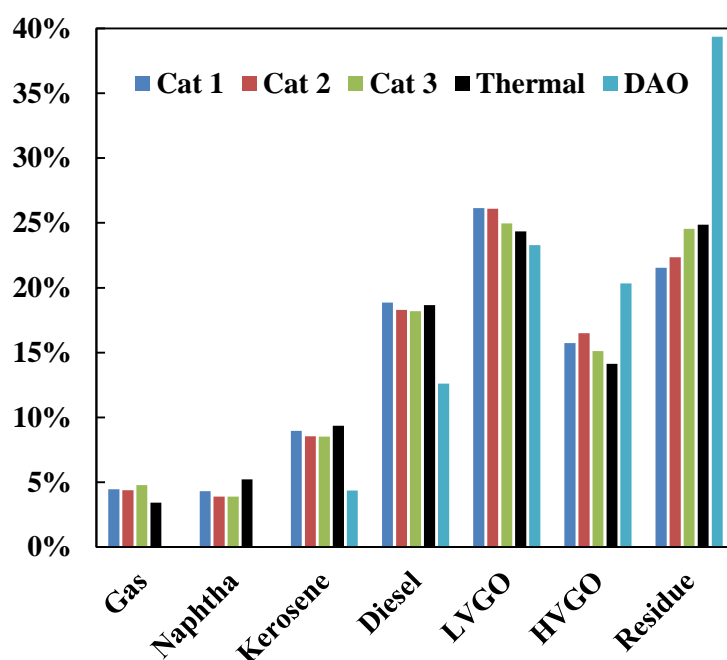
The recovered catalysts, after each reaction, were cleaned with toluene and dichloromethane in order to remove any trace of the hydrocarbon feedstock. With the purpose of determining variation in their physical properties, they were analyzed via TGA and nitrogen adsorption/desorption. The results are presented in Table 5.2, where the loss in the surface area available for reaction is clearly seen, presumably due to the formation of coke and blocking of the pore network. Cat 1 and Cat 3 experienced about 85% surface area reduction, while Cat 2 experienced the highest reduction with 94%. On the other hand, it was determined by TGA in air, that Cat 1 and Cat 2 were the solids with the highest coke content. In the case of Cat 3, the percentage of coke obtained was very small. It is presumed that the high acidity found in Cat 2 and the severe conditions regarding temperature, might have favored the production of coke on the surface of the catalyst, and thus, blocking of the

pores network. In the case of Cat 3, containing also acidity but in lower proportion and a good dispersion of the metals (especially cerium with coke oxidation properties), benefited from the prevention of carbon deposition on the surface of the catalyst. In the case of Cat 1, the probable lower activity for water dissociation and lack of a function for coke removal, such as that of Ce, there did not appear to be any means for avoiding coke formation.

**Table 5.2. Catalyst properties after reaction**

	Cat 1	Cat 2	Cat 3
BET fresh, m <sup>2</sup> /g	14	232	180
BET spent, m <sup>2</sup> /g	2.16	13.9	26.3
Coke accumulated, %	20.3%	20.3%	6.0%

Heavy and light liquid products obtained at the end of the experiments were mixed and analyzed via simulated distillation in order to obtain the product yields for the different distillation cuts. The results of these analyses together with the gas yields are presented in Figure 5.11, where it is possible to see a general reduction in the residue and Heavy Vacuum Gas Oil (HVGO) content either thermally or catalytically to generate lighter cuts. However, there are no important differences in the product distribution generated by the use of a catalyst in comparison with the thermal run. The minor trends observed in the chart indicate that catalytic runs tend to be more selective to the production of heavy hydrocarbons in the range of Light Vacuum Gas Oil (LVGO) and HVGO; and favor the production of gases. Contrariwise, the free radical cracking of hydrocarbons, occurring thermally, tends to generate lighter material, which is reflected in the improved proportion of products generated in the range of naphtha and kerosene (Greensfelder, et al., 1949; Hsu & Robinson, 2006).



**Figure 5.11. Product Distribution at similar conversion for Cat 1, Cat 2 and Cat 3 (400 °C and WHSV=1 h<sup>-1</sup>).**

The liquid products were characterized in order to understand the improvement obtained in the quality of the products at the end of the reactions. The results of these analyses are presented in Table 5.3. In general, there was a considerable improvement in the viscosity and API gravity of the DAO originally fed into the system, either catalytically or thermally processed. There is a clear improvement in terms of API and viscosity for the product obtained thermally in comparison with the ones obtained catalytically, which confirms the trend previously discussed for Figure 5.11, where the thermal run favors the production of light hydrocarbons that decrease the viscosity and increase the API in higher proportions. The content of asphaltenes and the indicators for olefin content and potential for coke formation (microcarbon) gives values very similar for all the cases evaluated, except for Cat 3 which exhibits a slightly lower degree of unsaturation than the thermal run. Therefore, despite the fact that the ability of the catalysts to produce hydrogen was proved, this element was not fully involved in the saturation of olefins and prevention of condensation

reactions to decrease the amount of coke produced and the content of olefins in the catalytic products.

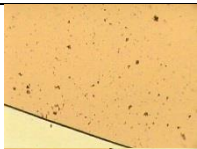

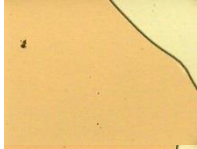




**Table 5.3. Product properties for similar conversions for Cat 1, Cat 2 and Cat 3 (400 °C and WHSV=1 h<sup>-1</sup>).**

	Cat 1	Cat 2	Cat 3	Thermal	DAO
°API	14.5	14.3	14.2	15.1	12.0
Viscosity at 20°C, cP	223	299	209	166	10584
Asphaltenes, wt. %	5.6	4.8	6.0	5.5	1.7
Microcarbon, wt. %	8.5	8.2	8.4	8.5	6.1
Desulphurization, %	10.7	10.0	11.6	11.9	-
TAN, mgKOH/g	1.07	0	0	1.07	3.3
Bromine No., gBr/100g	25.9	25.2	20.0	22.7	14.1

The conversion of carboxylic acids present in the feedstock was also observed, which was revealed by a decrease in the total acid number (TAN) of the samples. Cat 2 and Cat 3 were the more selective catalysts for this type of reaction, lowering the TAN value to zero. The decarboxylation and reduction of oil acidities by means of processes that involve the use of MgO and more specifically, hydrotalcites containing catalysts has been studied in the literature. With this type of catalyst, the basic character of magnesium assists in the adsorption of acids. Then, these molecules can be cracked and thus, de-carboxylated. Moreover, catalysts containing nickel on alumina have also shown promising results for this purpose (Speight, 2014). In the case of Cat 1 containing nickel nano particles, no improvement was observed in comparison to the intrinsic TAN reduction obtained by the use of temperature, which implies that the Ni-Ce combination found in Cat 2 and Cat 3 seems to be the most favorable combination to favor the TAN reduction.

Microscopy analysis of the products determined the stability of the asphaltenes in the products. As can be seen in Table 5.4, the product obtained thermally was affected by the amount of light hydrocarbons (naphtha) produced, influencing the peptization value of the asphaltenes and favoring their precipitation. In the case of the catalytically generated products, the asphaltenes were stable in the hydrocarbon, up to a P-value of 1.15, at which the products of Cat 1 and Cat 3 precipitated. Among the three catalysts, Cat 2 seems to generate a product that meets with the previous established minimum peptization values.

**Table 5.4. P-Value of products (400 °C and WHSV=1 h<sup>-1</sup>).**

	P-Value	
	1.0	1.15
Cat 1		
Cat 2		
Cat 3		
Thermal		

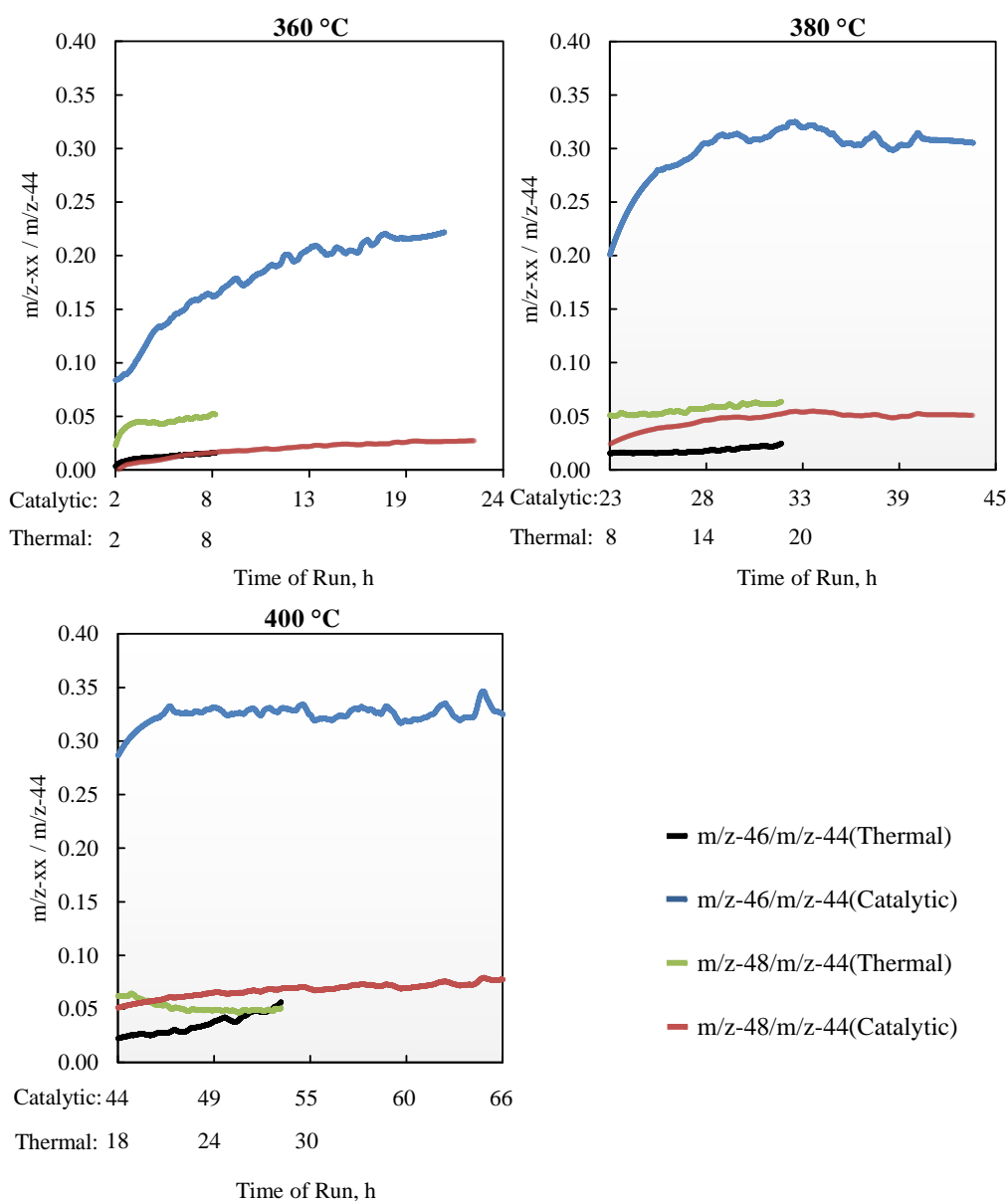
### ***5.2.3 Experimental demonstration of catalytic water splitting***

Due to the better quality of the products generated by Cat 2, the latter was selected to perform the water splitting verification experiments. These experiments consisted in processing the feedstock in the reactor, both thermally and catalytically, using a solution supplied by Marshall Isotopes-



Israel with 50 vol. % of isotopic water ( $\text{H}_2\text{O}^{18}$ ) and 50 vol. % of distilled water ( $\text{H}_2\text{O}^{16}$ ). By using labeled water, it can be confirmed if the oxidation to produce  $\text{CO}_2$  observed in steam processes comes from using internal oxygen contained in the reactant feedstock (decomposition of carboxylic acids and other oxygenates) or from the oxygen and hydroxyl radicals generated during water dissociation, which react with terminal carbon atoms from hydrocarbon radicals to produce labeled  $\text{CO}_2$ . In the first case, mostly  $^{16}\text{O}=\text{C}=^{16}\text{O}$  is going to be found in the gas products since  $^{16}\text{O}$  is the most abundant isotope (99.756%) , while in the second case several combinations of  $\text{CO}_2$  are going to be present in the gas products ( $^{16}\text{O}=\text{C}=^{16}\text{O}$ ,  $^{16}\text{O}=\text{C}=^{18}\text{O}$  and  $^{18}\text{O}=\text{C}=^{18}\text{O}$ ). A similar procedure has been found in the literature, showing satisfactory results for the dissociation of water using ultra-dispersed catalysts during steam catalytic cracking reaction at 440 °C (Fathi, 2011).

The monitoring of the gases produced during reaction, via quadrupole mass spectrometry, generated an ion current signal in amperes for each molar mass with time (shown as mass to charge ratio  $m/z$ ), which was used to compare the evolution of the three targeted compounds  $^{16}\text{O}=\text{C}=^{16}\text{O}$  ( $m/z$ -44),  $^{18}\text{O}=\text{C}=^{16}\text{O}$  ( $m/z$ -46) and  $^{18}\text{O}=\text{C}=^{18}\text{O}$  ( $m/z$ -48). With this information it was possible to create a profile for the signals ratio between each molecular weight ( $m/z$ -XX) against the molecular weight 44 ( $m/z$ -44), associated to regular  $\text{CO}_2$ , as presented in Figure 5.12 for reactions carried out at 360°C, 380°C and 400°C. These ratios allow one to estimate the amount of isotopic  $\text{CO}_2$  produced per molecule of regular  $\text{CO}_2$ . However, it is important to highlight that according to mass spectra for  $\text{CO}_2$  and propane, about 76% of  $\text{CO}_2$  molecules and 8% of the propane molecules are ionized and detected as  $m/z$ -44. Therefore, final ratios were recalculated using GC analysis and gas flowrates measurements in order to approximately remove the contribution of ions generated from decomposition of propane, in the signal  $m/z$ -44. The final results are presented in Table 5.5.



**Figure 5.12.  $m/z-xx / m/z-44$  ratios for experiments at 360, 380 and 400 °C**

As shown in Figure 5.12, the gas analysis via mass spectrometry shows differentiation in the production of isotopic  $\text{CO}_2$  when a catalyst is used in comparison with the production of  $\text{CO}_2$  in the absence of it at all temperatures studied using the same labeled water. At 360 °C, an induction period is observed for the catalytic runs, in which probably an equilibrium concentration of  $^{16}\text{O}$  and  $^{18}\text{O}$  is established at the surface of the catalyst due to water molecules that start adsorbing and

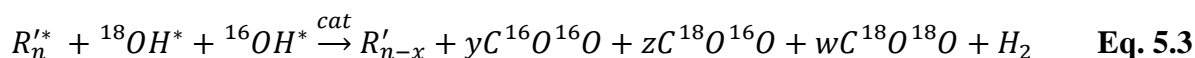
dissociating on the surface of the catalyst. Additionally, this induction period can also be related to the diffusion and concentration of the produced labeled carbon dioxide molecules. After this period, the catalyst starts dissociating water at a constant rate. This behaviour was experienced at each temperature evaluated for the catalytic run, whilst the thermal run had the tendency to produce labeled CO<sub>2</sub> at a stable but lower rate during most of the time evaluated. Moreover, the double oxidation of carbon with labeled oxygen during the catalytic run does not seem to be very significant, since the results obtained are in the same range of values achieved by the thermal runs (about one order of magnitude lower than in the case of single oxygen labeled CO<sub>2</sub>).

**Table 5.5. Recalculated signal ratios for CO<sub>2</sub>**

m/z-xx/m/z-44	Catalytic			Thermal		
	360°C	380°C	400°C	360°C	380°C	400°C
46/44(CO <sub>2</sub> )	0.24	0.35	0.40	0.02	0.03	0.09
48/44(CO <sub>2</sub> )	0.02	0.06	0.09	0.06	0.09	0.09

The final ratios presented in Table 5.5 state that among all the catalytic experiments, between 2.5-4 molecules of isotopic CO<sub>2</sub> (m/z-46) were produced per 10 molecules of regular CO<sub>2</sub> generated. In the case of the thermal runs, between 2 and 9 molecules were generated per 100 molecules of CO<sub>2</sub>. Therefore, that is one order of magnitude difference in the generation of <sup>16</sup>O=C=<sup>18</sup>O (m/z-46) between the catalytic evaluation and the thermal evaluation. In conclusion, these results confirm the hypothesis where the dissociation of water molecule takes place on the surface of Cat 2 used in this work. In the case of these experiments, the following reactions best describe the results obtained, where the production of <sup>18</sup>O=C=<sup>18</sup>O (m/z-48) is negligible. This mechanism is a

simplification of more complex chemical exchange processes occurring between the metal oxides of the catalyst and the water dissociating on the surface of them.



With  $y + z + w = x$ .

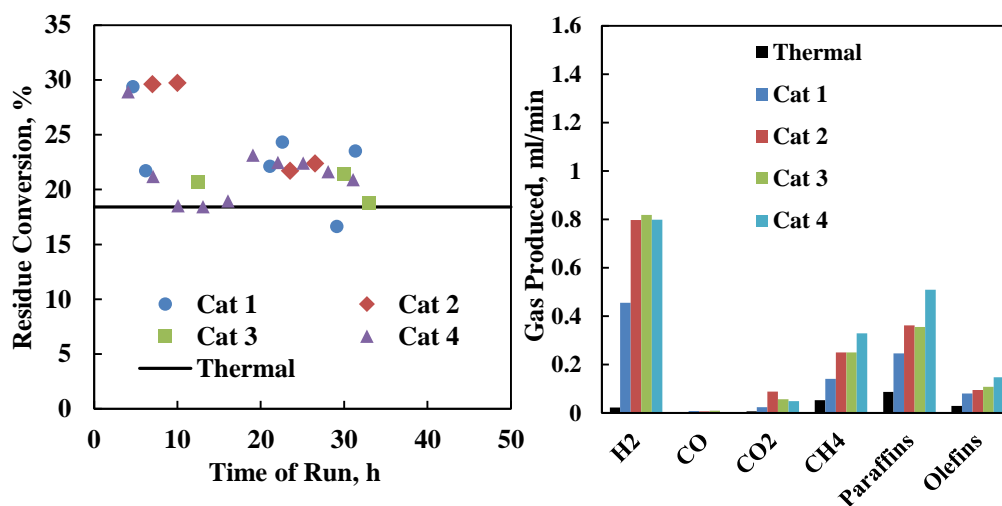
Regarding the effect of the temperature, it is interesting to note a considerable increase in the signal for m/z-46/m/z-44 between 360 °C and 380 °C of about 49%, against an increase of just 13% between 380 °C and 400 °C. This result leads one to consider the water dissociation on the surface of the catalyst to be considerably improved by the temperature within the range 360-380 °C, but not significantly improved after this point. At higher temperature than 400 °C, the relative percentage increase in the production of labeled CO<sub>2</sub> might reach a plateau or diminish.

### ***5.2.4 Operational and catalyst improvements***

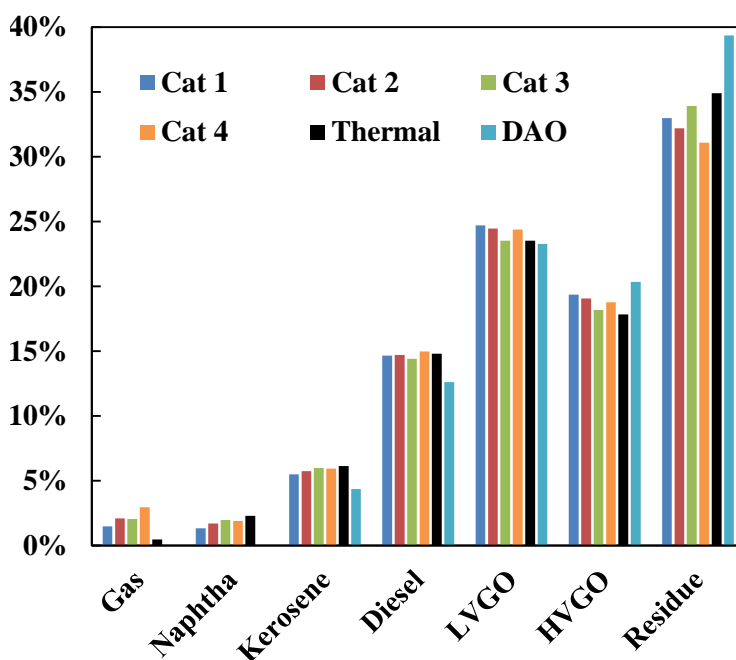
#### **5.2.4.1 Cat 4 evaluation**

Based on gas chromatography analysis and the results from the water splitting verification experiments, the capability of the tested catalysts to dissociate water and generate the required hydrogen to avoid condensation reactions, was proved. However, on overall, there was not important evidence for improvements in the quality of the products by taking advantage of the produced hydrogen. The results also indicated that the catalysts lost their activities for residue conversion, in a relatively short period of time, probably due to coke formation on the surface of it, favored by the high temperatures. For these reasons Cat 4 was developed, aiming to work at

lower temperatures to avoid coke formation but targeting the improvement or holding the activity toward residue conversion by the addition of acid sites. The results of the evaluation of this catalyst at 380°C and WHSV=1 h<sup>-1</sup> is presented in Figure 5.13, which shows a rapid decrease in conversion in the first 10 hours of reaction followed by a recovery of the activity. At the end of the reaction, the conversion obtained with this catalyst is very similar to that obtained for Cat 2, which is slightly above that obtained thermally. However, the presence of acid sites in this catalyst, indeed improved the cracking activity, as more methane and gas hydrocarbons lighter than C<sub>5</sub> were detected by GC. Besides, as presented in Figure 5.13, the overall yield toward gas production is also increased.



**Figure 5.13. Results for Cat 4 evaluation at 380°C and WHSV=1 h<sup>-1</sup>.**



**Figure 5.14. Product distribution for Cat 4 in comparison with Cat 1, 2 and 3.**

#### 5.2.4.2 Operating conditions evaluation

Due to the low operational flows used in the plant, to be able to evaluate small amounts of catalyst, a carrier was used to improve the transportation of the reactants through the lines and assure the right feeding of the reactor. This carrier is also important to push the reaction gases out of the system and to accelerate their arrival to the online GC. However, the presence of a carrier could be a detrimental factor to the good performance of the reaction, especially for the hydrogenation reactions. It has been observed that hydrogen is at least partially produced by the water dissociation, however, the dilution of this product together with the low pressures might be slowing down the hydrogenation reactions, avoiding their occurrence in a significant rate and favoring the de-activation of the catalyst. In order to evaluate the degree of dilution obtained before proceeding to carry out exploratory runs, water was used as a reference compound in the analysis of different scenarios for operations at 380°C, 150 psi and WHSV=0.5 h<sup>-1</sup>, simulated by the VMG® simulation

package and assuming no reaction. The first case evaluated the typical operation where 5 Std. ml/min of nitrogen was fed into the plant. In the second scenario, no nitrogen was used as carrier but the gas velocity was kept constant by increasing the mass ratio water to oil to 18%. In the third case, no nitrogen was used and the typical water to oil proportion of 5% was kept.

The results of these simulations are shown in Table 5.6, where the influence of the carrier can be observed, which leads to a high gas volumetric fraction of 98.3%. Therefore, the reactor basically follows a spray flow pattern, where mostly gas was flowing inside of it together with a few drops of oil. In molar fraction, out of 85.6% of gases present in the reactor, just 21.4% consisted of water and the rest of it was considered nitrogen and gas hydrocarbons.

**Table 5.6. Process simulation for different scenarios and using WHSV=0.5 h<sup>-1</sup>**

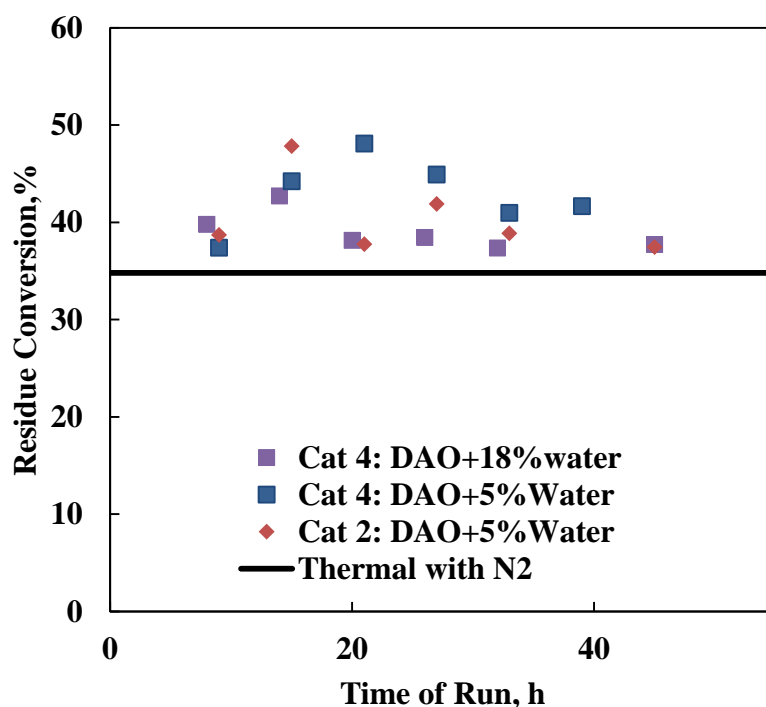
Description	Case I	Case II	Case III
	DAO+5 ml/min N <sub>2</sub> as carrier +5% Water	DAO+18% Water	DAO+5% Water
Temperature, °C	380	380	380
Pressure, psi	150	150	150
Gas volume flow (Volumetric fraction), ml/min	1.52 (98.3%)	1.51 (98.2%)	0.43(93%)
Liquid volume flow, ml/min	0.03	0.03	0.03
Liquid molar fraction, %	14.4	14.3	43
Gas molar fraction, %	85.6	85.7	57
Water molar fraction in gas, %	21.4	78.2	48.5

In the second case, it was observed that by using 18% of water respect to oil mass flowrate, the flow pattern can be kept constant, but the molar concentration of water in the reactor is improved

to 78.2%. In case III, there is just a reduction of 5% in the volume fraction occupied by gases. However, in comparison with Case I, Case III increased the concentration of water molecules in the gas phase by 27 points. Therefore, by using the Case III conditions during the reactions, the produced hydrogen is expected to increase its molar concentration in similar proportions to water and thus, the hydrogenation reaction can be favored.

In order to evaluate the real effect of these variables on the conversion of residue and stability of the catalyst, the reactor was filled up with Cat 4 and operated as in Case II and Case III at  $WHSV=0.5\text{ h}^{-1}$ . The results are presented in Figure 5.15, as a chart representing the residue conversion obtained vs. time. As it can be observed, when using 18% water, slightly higher conversions are obtained in comparison with the thermal run at the same conditions. However, when the gas flow was decreased and only 5% of water was used, the conversion was slightly improved to obtain about 42% residue conversion, which is about 7 points above the conversion obtained for the thermal run. This improvement for Cat 4 under Case III conditions can be attributed to the reduction of the gas velocity and improvement in the concentration of the hydrogen produced. Cat 2 was also evaluated, but its performance was not considerably better than the thermal run, just about three points above the thermal conversion.





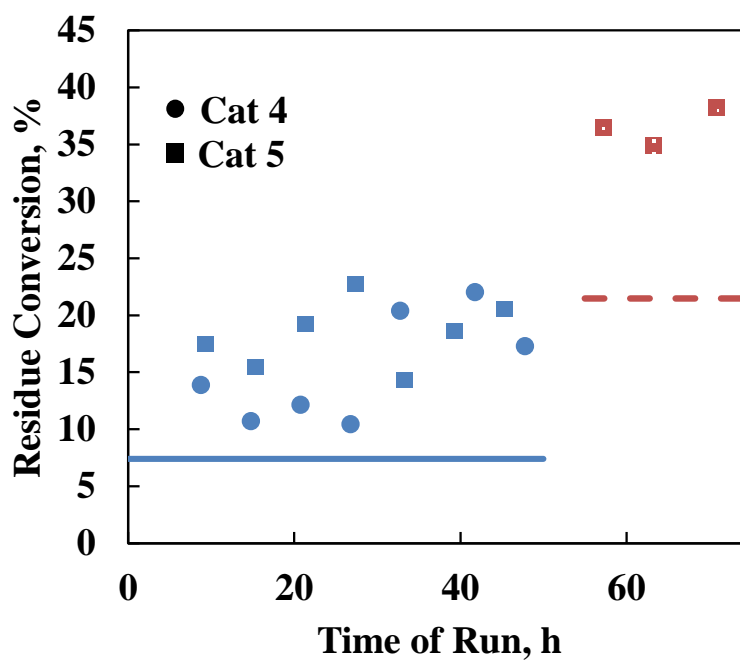
**Figure 5.15. Experimental results for water content/parameter variations**

#### 5.2.4.3 Further improvements in operation and catalysts

Based on the previous experience acquired when evaluating the effect of the carrier in the conversion obtained in the reactor, the following experiments were performed feeding nitrogen at the hot separator, in order to keep carrying the reaction gases out of the plant, but without affecting the internal flow dynamics and concentration of reactants inside the reactor. On the other hand, to keep avoiding the formation of coke on the surface of the catalyst, the operating temperature was decreased to a range between 350°C and 370°C, while the amount of catalyst was increased up to 6 g by the incorporation of a bigger reactor of a half inch (Reactor 2, Figure 3.3). All these changes allow one to undertake reactions at  $WHSV=0.25\text{ h}^{-1}$ .

For this section, another catalyst was incorporated into the evaluation. In this case, the objective was to take advantage of one of the previous catalysts evaluated in the first stage of this research

which proved to produce good quantities of hydrogen and incorporate a function that improves the lack of hydrogenation observed so far. Therefore, Cat 5 was developed such that the mixture of oxides existing in Cat 2 are combined with active sites of molybdenum carbide, as the hydrogenating function recently developed in the Catalyst for Bitumen Upgrading (CBU) group. The results of the evaluation of this new catalyst, together with Cat 4, are presented in Figure 5.16. As it is shown, important differences can be observed for both catalysts in comparison with the thermal run under the same condition. By the end of the experiment at 350°C, Cat 4 and Cat 5 were 9 and 13 points respectively above the thermal run, which is a considerable gain in conversion. Cat 5 was also evaluated at 370 °C and the difference in the obtained conversion was almost constant, giving this time 15 points above the thermal run. The analysis of the products, presented in Table 5.7, also reflects the benefits obtained catalytically, where the viscosity is reduced by more than one half with respect to the thermal products. It is also evidenced, probably due to the hydrogenation function incorporated in Cat 5, that properties like asphaltenes content, micro carbon and bromine number are lower in Cat 5 as compared with Cat 4, while the desulphurization reactions were also improved by Cat 5. However, Cat 4 is considerable better catalyst for the conversion of carboxylic acids that give the acidity to the oil. At 370 °C Cat 5 improved even more the viscosity and the API of the products, while just slightly affecting the other properties due to the extra conversion obtained.



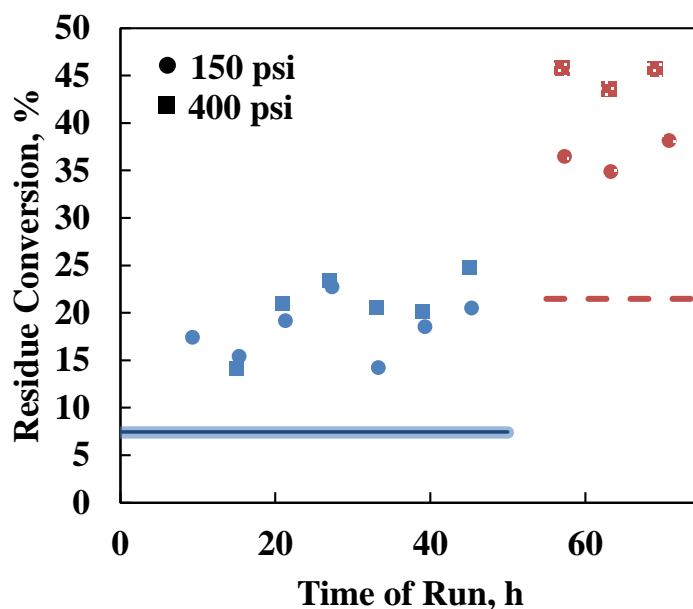
**Figure 5.16.** Evaluation of Cat 4 and Cat 5 at 150 psi. Blue symbols refer to runs at 350°C and patterned red symbols at 370°C. Lines correspond to the thermal runs.

**Table 5.7.** Properties of products (Thermal and Catalytic) evaluated at 150 psi

	DAO	Thermal		Cat 4	Cat 5	
	-	350°C	370°C	350°C	350°C	370°C
API	12	12.6	13.8	12.9	13.3	14.5
Viscosity	10,584	4,505	860	2,167	1,937	309
Asphaltenes, %	1.7	1.6	3.1	2.8	2.0	4.2
Micro carbon, %	6.1	6.3	6.9	7.0	6.8	7.7
Desulphurization, %	-	0.9	6.8	7.9	8.5	15.5
TAN, mg KOH/g	3.3	2.6	1.9	1.1	2.0	1.8
Bromine No., gBr/100g	14.1	19.3	22.1	21.7	19.3	23.3

Pressure was another factor of interest that was evaluated. Hydrogenation reactions are industrially carried out at higher pressures. Therefore, an increase in the magnitude for this variable could improve the activity and stability of the catalysts. For that purpose, another set of reactions were carried out only with Cat 5 at 400 psi, using a WHSV=0.25 h<sup>-1</sup>. Figure 5.17 and Table 5.8 represent the results obtained when evaluating the effects of the pressure on the conversion and on the properties of the products generated by Cat 5. In general, it is shown that at 350°C, no important differences are observed between the operations at these two pressures. At 400 psi the conversion is improved by just 4 points. It is interesting to note that the two thermal runs performed at this temperature experienced exactly the same conversion, which indicates that the pressure creates no effect in the thermal conversion of residue for this pressure range. Nevertheless, the experiments performed at 370 °C at 150 psi and 400 psi clearly differentiate the gain in conversion obtained because of the pressure effect for Cat 5. At 400 psi, the conversion is improved by almost 10 points, which leaves the catalytic operation at 400 psi about 24 points above the thermal run.

Due to the extra conversion gained at higher pressures, the viscosity is considerably improved, while the API remains at about the same value obtained at 150 psi. It is commonly observed, the viscosity magnitude is significantly affected by the conversion achieved, while the API is not as much. For that reason, minor variations in conversion can be easily detected in the viscosity, while the API might not vary as much for the same sample.



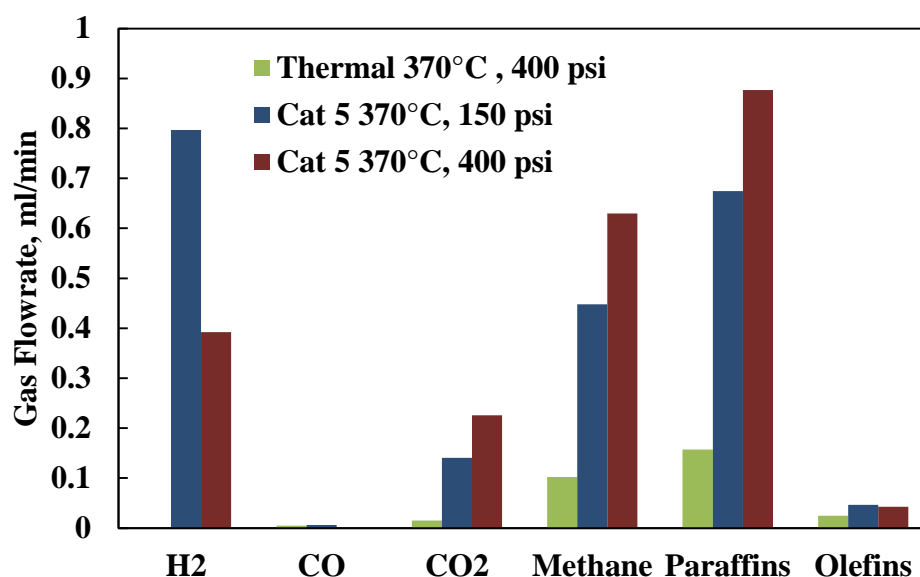
**Figure 5.17. Pressure effect on residue conversion for Cat 5 evaluated at 350°C (blue symbols) and 370 °C (red symbols). Straight lines correspond to their respective thermal runs. Light blue for thermal at 150 psi and dark blue for thermal at 400 psi.**

**Table 5.8. Product properties evaluated at 150 psi and 400 psi with Cat 5.**

	DAO	Thermal			Catalytic			
Temperature, °C	-	350	350	370	350	370	350	370
Pressure, psi	-	150	400	400	150	400	150	400
API	12	12.6	12.8	13.8	13.3	13.3	14.5	14.4
Viscosity	10,584	4505	4220	860	1937	1502	309	232
Asphaltenes, %	1.7	1.6	1.9	3.1	2.0	2.0	4.2	4.3
Micro carbon, %	6.1	6.3	6.3	6.9	6.8	6.6	7.7	7.5
Desulphurization, %	-	0.9	0.5	6.8	8.5	8.7	15.5	18.6
TAN, mg KOH/g	3.3	2.6	2.6	1.9	2.0	1.8	1.8	1.7
Bromine No., gBr/100g	14.1	19.3	17.8	22.1	19.3	21.6	23.3	22.6

It was mentioned before the relationship between most of the properties with the conversion (Chapter 5.5), where they tend to increase along with the conversion achieved. For that reason, it becomes a very hard task to evaluate if hydrogenation reactions improved the properties of the products under the evaluated conditions, because different levels of conversion were achieved. Nevertheless, for these experiments, regardless of the increase in conversion, all the properties were slightly improved for the operations at 400 psi, even for the olefins content. This is an interesting result, since the operation at 400 psi improved the residue conversion by 23%, while the properties remained stable and slightly improved. This positive effect of the pressure can be explained as an improvement in the diffusion of the reactants inside the catalyst pores, in order to take advantage of most of the surface area and active sites. Besides, the increase in pressure keeps most of the feedstock in the liquid phase and concentrates the amount of hydrogen contained in the gases, which increases the driving force that favors the hydrogenation reaction. It is also well known for hydrocracking processes that the high partial pressure of hydrogen also improves the catalyst life and suppresses the catalyst fouling rate (Parkash, 2003).

Figure 5.18 is presented as another proof of the improvement in activity and in the possible hydrogenation during the operation of the reactor at 400 psi. As it can be concluded from this chart, at 400 psi the production of carbon dioxide, methane, and paraffins is more pronounced than at 150 psi. The high production of methane and  $\text{CO}_2$  is an indication of the catalytic activity, since the oxygen coming from the water splitting is leaving the reactor as  $\text{CO}_2$ , while methane is being produced from cracking of terminal carbons, but also from the methanation of carbon atoms. As consequence of this hydrogen consumption, the amount of free hydrogen leaving the plant is lower and the content of gas olefins seems to be controlled at about the same values obtained at 150 psi.



**Figure 5.18. Gas analysis for Cat 5 evaluation at 150 and 400 psi**

### 5.3 Upgrading scheme evaluation

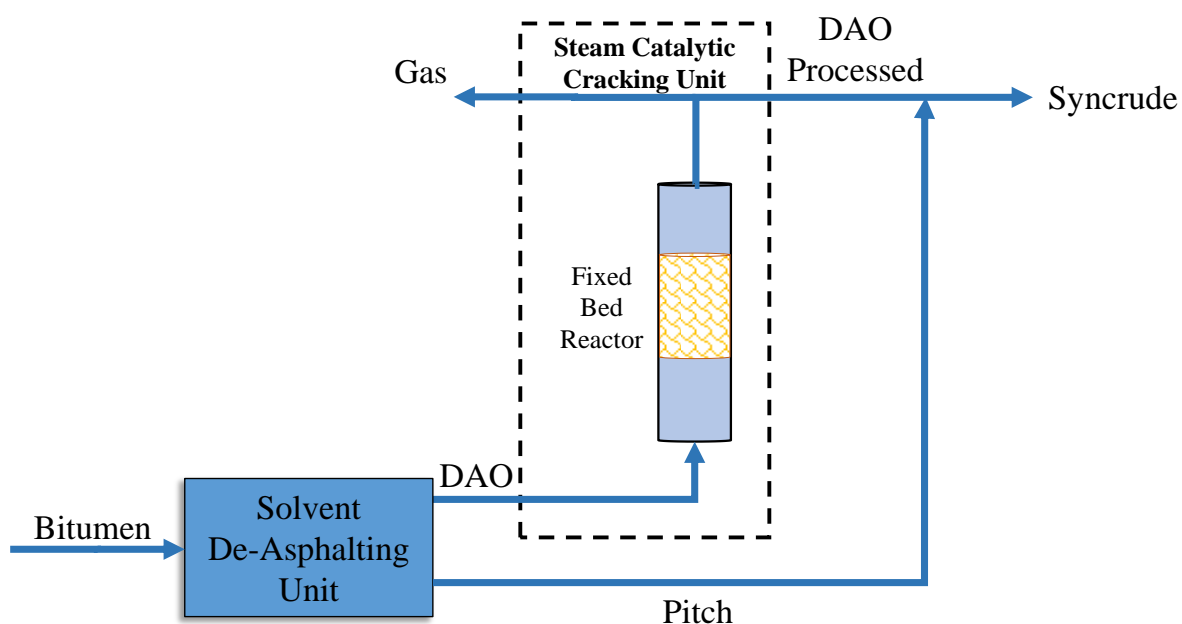
The experimental methodology led to the preparation of a catalyst with active sites for water splitting, acid functions for cracking, but also with a hydrogenating function that can take advantage of the hydrogen produced via water splitting. The study of the variable also favored the use of high pressures to benefit the factors previously discussed. As conclusion, it was possible to obtain about 45% of residue conversion with this catalyst (Cat 5) at 370°C and WHSV of 0.25 h<sup>-1</sup>. Now the question is: What does it mean this conversion of residue and improvement in the oil properties in regards to achieving the initial goals of meeting pipeline specification?

In order to answer this question, let us evaluate the scenario presented in Figure 5.19, where the whole pitch is mixed back with the processed DAO to generate synthetic crude oil (Syncrude) and additionally, gas is also part of the generated products. For this case, Table 5.9 is presented with information about properties for each one of the streams existing in this scheme. As it can be observed, from the original bitumen fed into the plant, 94.8% can be produced as a syncrude with

an important reduced viscosity of 36,936 cP at 20°C (76% reduction), which clearly still does not meet the pipeline specifications, but reduces the consumption of diluent by about 16 %. Moreover, important reductions of 88% and 11% are also obtained for the TAN and sulphur content, respectively. Based on the report prepared by Bacon R. and Tordo S., 2005, for the estimation of price discounts for different crude oils according to their properties, this improvement in oil obtained for the syncrude would generate a gain in discount of the bitumen by 0.02\$/\$Oil Brent in the case of sulphur and 0.1\$/\$Oil Brent in the case of the TAN. In general, with a Brent oil pricing 50\$ per barrel, the upgrading scheme would improve the value of the bitumen by 1.2\$ and 4.9\$ per barrel, for the enhancement obtained in sulphur content and TAN, respectively. It is worth noting that these latter values are not additive, since each one of them was calculated assuming the rest of the properties of the oil remain constant.

On the other hand, if the 26.9% yield that accounts for pitch can be used for the generation of energy, sold for asphalt production or sent to coking, the produced syncrude would be basically DAO processed in the steam catalytic cracking unit. This DAO would not have the 19 API usually required, but the V50 estimated kinematic viscosity will be 350 cSt at 14°C. Thus, at this temperature the fluid could be pumped through pipelines with no problems. Therefore, not much diluent (less than 1 w.% in the mixture) or heat will be needed to pump this oil at the Canadian average temperature of 12 °C, which improves the overall economy of the process. Additionally, the oil has more value, since the TAN and sulphur content are both reduced by 29%.





**Figure 5.19. Upgrading Scheme with only gas and syncrude as products**

**Table 5.9. Properties of the streams in the proposed upgrading scheme**

Property	Bitumen	DAO	DAO processed	Pitch	Syncrude	Gas
Yields, %	-	73.1*	67.9	26.9*	94.8	5.2
API	8.3*	12	14.4	-4.8*	9.0**	-
Viscosity @20°C, cP	152,015	10,000	232	N/A	36,936	-
TAN, mgKOH/g	2.41	3.3	1.7	0	0.3	-
Sulphur, ppm	40,623	35,420	28,916	54,762**	36,256	-
Asphaltenes, %	17.0*	1.7	4.3	57.2*	19.3**	-

\* Values reported by Da Silva, 2014

\*\*Estimated by balances

## **Chapter Six: Summary and Recommended Future Work**

This final chapter aims to present an overview of all the work done with the intention of evaluating the feasibility of processing De-Asphalted Oil (DAO) in a steam catalytic cracking unit, as part of a proposed scheme for the upgrading of Athabasca bitumen. The final conclusion reached at the end of the project are presented as follows:

Five different catalysts were successfully developed with extrudate shape and characterized by different metal contents. These catalysts are: Cat 1 (NiCsBa-Metakaolin), Cat 2 (NiCe-Calcined Hydrotalcite), Cat 3 (NiCe-Aegerine), Cat 4 (NiCe-Faujasite) and Cat 5 (Cat 2+ Mo<sub>2</sub>C). Among their properties, they were characterized by surface areas with the following order Cat 4>Cat 2>Cat 3>Cat 5>Cat 1.

A bench scale plant was designed and constructed to handle very low heavy hydrocarbon flows in the range of 1.8 ml/h and thus, small amounts of catalyst (between 3-10 g). As an advantage, several promising catalysts can be tested in this plant without the need to prepare large amounts of them. The steady operation of the plant could be shown by the minimum pressure drop obtained because of sampling (about 3 psi), the relative low gradient in the reactor temperatures (less than 3°C) and the good average overall mass balance of 101%.

Thermal cracking evaluations were useful to establish a base line to evaluate the catalytic activity of the developed solids along all the experiments. From these runs, the strong effect of temperature variations on the conversion was seen, in comparison with the effect of the residence time. Moreover, the relationship between conversion and properties such as viscosity, micro carbon, micro-deasphalting and API gravity was also established.

- Catalyst Screening

The preliminary evaluation of Cat 1, Cat 2 and Cat 3 showed the fast de-activation of most of the solids in the first 13 hours of operations, except for Cat 2, for which de-activation took place after being operated at 400°C. The gas analysis showed strong evidence for catalytic water splitting, since hydrogen was produced in important quantities, in comparison with the thermal runs. The production of hydrogen and gas hydrocarbons increased with temperature.

- Catalyst Stability

During the long operation at 400 °C, all the catalyst were de-activated in the first 15-20 hours, showing still a capability for hydrogen production afterwards. Cat 2 and Cat 1 showed high activity for water dissociation at the beginning of the experiment, followed by de-activation of 50% and 30% respectively. The production of hydrogen by Cat 3 remained stable during the whole operation. Moreover, analysis of the catalyst after reaction, indicated a strong coke formation on the surface of Cat 2 and the good performance of Cat 3 at avoiding this..

Thermal cracking under the same conditions generated lighter products with lower API and viscosity, but with asphaltene instability. Catalytic products remained stable as obtained from the plant.

Based on product properties, no significant hydrogenation was achieved during these operations.

- Water splitting verification

The mechanism proposed for catalytic steam cracking, where water molecules are dissociated on the surface of the catalyst to generate hydrogen and oxygen radicals, was successfully evaluated with the use of labeled water ( $\text{H}_2^{18}\text{O}$ ) and a quadrupole mass spectrometer. The signals monitored with this equipment were mass to charge ratio ( $m/z$ ) associated to  $^{16}\text{O}=\text{C}=^{16}\text{O}$ ,  $^{18}\text{O}=\text{C}=^{16}\text{O}$ , and  $^{18}\text{O}=\text{C}=^{18}\text{O}$ . The results showed that the active phases loaded into Cat 2 were able to dissociate

water and generate  $^{18}\text{O}=\text{C}=^{16}\text{O}$  in high abundance in comparison with the quantities detected for the thermal runs. Moreover, negligible generation rate for  $\text{CO}^{18}\text{O}^{18}$  was observed. In general, the transfer of labeled oxygen from the water to the carbon atoms was achieved, which shows the water dissociation mechanism.

- Operational and catalyst improvements

Based on the VMG simulation software and taking water as a reference component, the dilution obtained when nitrogen, as carrier, was passed through the reactor was evaluated. It is expected that this dilution also takes place in the case of the produced hydrogen, which would affect the hydrogenating reactions. As a result, the carrier gas was no longer fed into the feed section passing through the reactor, but rather into the hot separator.

It was also concluded that the high temperatures used at the initial stages of the evaluations (380-400°C), were detrimental to the stability of the catalysts, since coking reactions were favored. Therefore, the experiments were shifted toward the use of longer residence time ( $\text{WHSV}=0.25\text{ h}^{-1}$ ), lower temperatures (350-370°C) and using catalysts containing acid sites to keep a high level of residue conversion. Moreover, Cat 5 was developed to fix the lack of hydrogenating function observed in the previous results by the addition of a known hydrogenating solid ( $\text{Mo}_2\text{C}$ ).

Under the new formulated catalyst and operational conditions, the results showed improvement in the catalytic conversion of residue by increasing between 9 and 13 points above the thermal run at 350°C. When Cat 5 was evaluated at 370 °C, this difference increased on average by 15 points in comparison to its respective thermal run.

The evaluation of the parameter pressure using Cat 5, showed that at 400 psi, a higher level of conversion could be achieved for the same catalyst, temperature and space velocity. This improvement because of pressure was mainly observed when temperatures of 370°C were used.

Under these conditions, Cat 5 showed activity during more than 10 hours of operation without evidence of deactivation.

Additionally, relatively stable or slight improvements were observed for the products obtained with Cat 5, despite the extra conversion obtained.

Overall, the best performance of the catalyst was obtained with Cat 5 operating at 400 psi,  $0.25 \text{ h}^{-1}$  and at  $370^\circ\text{C}$ , giving a residue conversion of about 45%.

- Upgrading scheme evaluation

Finally the upgrading scheme was evaluated with the best result obtained using Cat 5 and assuming the whole pitch was completely mixed with the catalytic steam cracking products. As a conclusion, the level of conversion achieved for the DAO was not high enough to decrease the viscosity of the syncrude to such a level that the pipeline specifications could be met. However, a reduction of 16% in the consumption of diluent is achieved in the preparation of the dilbit with this syncrude and a gain in the price discount of the product is also obtained for improvement in TAN and sulphur content.

If the pitch were to be used for other purposes such as for asphalt production, the DAO processed would meet the specifications at temperatures as low as  $14^\circ\text{C}$  without the need of any diluent.

- Recommended Future Work

In general, the work done in this research thesis proved the activity of Cat 4 and Cat 5 toward residue conversion. Hints of hydrogenation were found for the products of Cat 5, but substantial hydrogenation is needed to target higher conversion or better quality products. Therefore, it is recommended to carry out a deep study where molybdenum carbide is incorporated into the preparation of Cat 5 in larger different proportions, while monitoring parameters such as Bromine

Number, asphaltenes and microcarbon, which are usually improved by the avoidance of condensation reactions and olefin generation.

Once a better catalyst, showing good activity for residue conversion and hydrogenation, is developed, long runs of several weeks must be done in order to assess the stability of the catalyst with time. This evaluation is very important for the economy of the process.

In parallel, it is recommended to develop a kinetic model in order to have a good understanding and control over the process.

Finally, the possibility of processing the generated pitch in a parallel catalytic steam cracking unit using a similar kind of catalysts should be evaluated, but incorporating a guard bed to protect them from metal compounds. In this way, additional improvement in viscosity can be achieved, reducing the amount of diluent needed to meet the specifications and eliminating the production of solid wastes.

## References

- Ancheyta, J., Sanchez, S. & Rodriguez, M. A., 2005. Kinetic Modeling of Hydrocracking of Heavy Oil Fractions: A Review. *Catalysis Today*, 109(1-4), pp. 76-92.
- Ancheyta, J., Trejo, F. & Rana, M. S., 2009. *Asphaltenes. Chemical Transformation During Hydroprocessing of Heavy Oils*. 1st ed. Boca Raton: CRC Press. Taylor and Francis Group.
- Andonova, S. et al., 2011. Structure and redox properties of Co promoted Ni/Al<sub>2</sub>O<sub>3</sub> catalysts for oxidative steam reforming of ethanol. *Applied Catalysis B: Environmental*, Volume 105, pp. 346-360.
- Bacon, R. & Tordo, S., 2005. *Crude Oil Price Differentials and Differences in Oil Qualities: A Statistical Analysis*, Washington: ESMAP technical Papers.
- Banerjee, D. K., 2012. *Oil Sands, Heavy Oil & Bitumen. From Recovery to Refinery*. Oklahoma: Penn Well Corporation.
- Bartholomew, C. H. & Farrauto, R. J., 2006. *Fundamentals of Industrial Catalytic Processes*. Second Edition ed. New Jersey: John Wiley & Sons, Inc.
- Basile, F. et al., 2009. Ni-catalysts obtained from silicate intercalated HTlcs active in the catalytic partial oxidation of methane: Influence of the silicate content. *Catalysis Today*, 142(1-2), pp. 78-84.
- Beche, E. et al., 2008. Ce 3d XPS investigation of cerium oxides and mixed cerium oxide (CexTiyOz). *Surfaces and Interface Analysis*, Volume 40, pp. 264-267.
- Cantrell, D. G., Gillie, L. J., Lee, A. F. & Wilson, K., 2005. Structure-Reactivity Correlations in MgAl Hydrotalcite Catalysts for Biodiesel Synthesis. *Applied Catalysis A: General*, 287(2), pp. 183-190.
- Carbognani, L., Gozalez, M. F. & Pereira-Almao, P., 2007. Characterization of Athabasca Vacuum Residue and Its Visbroken Products. Stability and Fast Hydrocarbon Group-Type Distributions. *Energy & Fuels*, pp. 1631-1639.
- Carbognani, L. et al., 2014. Reliable Determination of Water Contents of Bitumen and Vacuum Residua via Coulometric Karl Fischer Titration Using Tetrahydrofuran. *Petroleum Science and Technology*, 32(5), pp. 602-609.
- Carnahan, N., Salager, J.-L. & Anton, R., 2007. Effect of Resins on Stability of Asphaltenes-OTC19002. *Offshore Technology Conference*, pp. 1-9.
- Cavani, F., Trifiro, F. & Vaccari, A., 1991. Hydrotalcite-Type Anionic Clays: Preparation, Properties and Applications. *Catalysis Today*, Volume 11, pp. 173-301.
- Climent, M. et al., 2004. Increasing the Basicity and Catalytic Activity of Hydrotalcites by Different Synthesis Procedures. *Journal of Catalysis*, Volume 225, pp. 316-326.
- Da Costa, P. et al., 2001. Tetralin hydrogenation catalyzed by Mo<sub>2</sub>C/Al<sub>2</sub>O<sub>3</sub> and WC/Al<sub>2</sub>O<sub>3</sub> in the presence of H<sub>2</sub>S. *Catalysis Today*, Volume 65, pp. 195-200.
- Da Silva De Andrade, F. J., 2014. *Kinetic modeling of catalytic in situ upgrading for Athabasca bitumen, deasphalting pitch and vacuum residue*, Calgary: University of Calgary.
- del Bianco, A. et al., 1993. Thermal cracking of petroleum residues. *Fuel*, Volume 72, pp. 75-80.
- Dhandapani, B., Clair, T. S. & Oyama, S., 1998. Simultaneous hydrodesulfurization, hydrodeoxygenation, and hydrogenation with molybdenum carbide. *Applied Catalysis A: General*, Volume 168, pp. 219-228.

- dos Santos Politi, J. R., Viñes, F., Rodriguez, J. A. & Illas, F., 2013. Atomic and electronic structure of molybdenum carbide phases: bulk and low Miller-index surfaces. *Phys. Chem. Chem. Phys.*, Volumen 15, pp. 12617-12625.
- Duprez, D., 1992. Selective Steam Reforming of Aromatic Compounds on Metal Catalysts. *Applied Catalysis A*, Volume 82, pp. 111-157.
- Dyer, A., 2001. Zeolites. En: *Encyclopedia of Materials: Science and Technology*. s.l.:Elsevier Science Ltd., p. 9859–9863.
- Emam, E. A., 2013. Clays as Catalysts in Petroleum Refining Industry. *ARPJ Journal of Science and Technology*, 3(4), pp. 356-375.
- Fahim, M., Al-Sahhaf, T. & Elkilani, A., 2010. *Fundamentals of Petroleum Refining*. First ed. Great Britain: Elsevier.
- Fan, T., Wang, J. & Buckley, J. S., 2002. Evaluating crude Oils by SARA Analysis. *SPE*.
- Fathi, M. & P.-A. P., 2011. Catalytic Aquaprocessing of Arab Light Vacuum Residue via Short Space Times. *Energy & Fuels*, 25(11), pp. 4867-4877.
- Flinn, R., Larson, O. & Beuther, H., 1960. The Mechanism of Catalytic Hydrocracking. *Ind. Eng. Chem.*, 156(52(2)), p. 153.
- Frauwallner, M.-L. et al., 2011. Toluene hydrogenation at low temperature using a molybdenum carbide catalyst. *Applied Catalysis A: General*, Volume 394, pp. 62-70.
- Froment, G., 1992. Kinetic and Reactor Design in the Thermal Cracking for Olefins Production. *Chemical Engineering Science*, 47(9-11), pp. 2163-2177.
- Froment, G. F., 2013. Fundamental kinetic modeling of catalytic hydrocarbon conversion processes. *Rev Chem Eng* 2013, 29(6), pp. 385-412.
- Garbarino, G. et al., 2015. A study of Ni/Al<sub>2</sub>O<sub>3</sub> and Ni–La/Al<sub>2</sub>O<sub>3</sub> catalysts for the steam reforming of ethanol and phenol. *Applied Catalysis B: Environmental*, pp. 21-34.
- Gary, J. H. & Handwerk, G. E., 2001. *Petroleum Refining. Technology and Economics*. Fourth ed. New York: Marcel Dekker.
- Gordon, D., 2013. *The World's Growing Oil Resources: Past Present and Future*, s.l.: Carnegie Endowment for International Peace.
- Green, D. W. & Willhite, G. P., 1998. *Enhanced Oil Recovery*. Richardson, Texas: Society of Petroleum Engineers.
- Greensfelder, B., Voge, H. & Good, G., 1949. Catalytic and Thermal Cracking of Pure Hydrocarbons. *Industrial and Engineering Chemistry*, 41(11), pp. 2573-2584.
- Griffiths, M. & Dyer, S., 2008. *Upgraders Alley. Oil Sands Fever Strike Edmonton*. 1st ed. Drayton Valley, Alberta: The Pembina Institute.
- Hassan, A., Carbognani, L. & Pereira-Almao, P., 2008. Development of an alternative setup for the estimation of microcarbon residue for heavy oil and fractions: Effects derived from air presence. *Fuel*, Volume 87, pp. 3631-3639.
- Hassan, A. et al., 2013. Development of a support for a NiO catalyst for selective adsorption and post-adsorption catalytic steam gasification of thermally converted asphaltenes. *Catalysis Today*, Volume 207, pp. 112-118.
- Henderson, M. A., 2002. The Interaction of Water with Solid Surfaces: Fundamental Aspects Revisited. *Surface Science Reports*, 46(1-8), pp. 1-308.
- Hensen, E. et al., 2010. Formation of acid sites in amorphous silica-alumina. *Journal of Catalysis*, 269(1), pp. 201-218.



- Higuerey, I., Orea, M. & Pereira, P., 2002. Estimation of Visbroken and Selective Catalytic Steam Cracked Product Stability Using IATROSCAN TLC-FID. *Fuel Chemistry Division Preprints*, Volumen 47(2), p. 656.
- Hsu, C. S. & Robinson, P. R., 2006. *Practical Advances in Petroleum Processing*. 1 ed. USA: Springer.
- Huc, A.-Y., 2011. *Heavy Crude Oils - From Geology to Upgrading, an Overview*. Paris: Editions Technip.
- Hu, Y. H. & Ruckenstein, E., 1997. The characterization of a highly effective NiO/MgO solid solution catalyst in the CO<sub>2</sub> reforming of CH<sub>4</sub>. *Catalysis Letters*, Volume 43, pp. 71-77.
- Kaduk, J. A. & Faber, J., 1995. Crystal Structure of Zeolite Y as a Function of Ion Exchange.. *The Rigaku Journal*, 12(2), pp. 14-34.
- Kaewpanha, M. et al., 2015. Hydrogen production by steam reforming of biomass tar over biomass char supported molybdenum carbide catalyst. *International journal of hydrogen energy*, Volume 40, pp. 7974-7982.
- Khasin, A. A. et al., 2006. Structure of the Active Component and Catalytic Properties of Catalysts Prepared by the Reduction of Layered Nickel Aluminosilicates. *Kinetics and Catalysis*, 47(3), pp. 412-422.
- King, R., 2009. Minerals explained 49: Kaolinite. *Geology Today*, 25(2), pp. 75-78.
- Kogel, J. E., Pickering, S. M. & Shelobolina, E., 2002. *Georgia Kaolins : Geology and Utilization*. 1st ed. Colorado: Society for Mining Metallurgy and Exploration.
- Larichev, Y. V. et al., 2007. XPS and TEM Studies on the Role of the Support and Alkali Promoter in Ru/MgO and Ru-Cs<sup>+</sup>/MgO Catalysts for Ammonia Synthesis. *J. Phys. Chem. C*, Volume 111, pp. 9427-9436.
- Lee, Y., Carr, S. W. & Parise, J. B., 1998. Phase Transition upon K<sup>+</sup> Ion Exchange into Na-Low Silica X: Combined NMR and Synchrotron X-ray Powder Diffraction Study. *Chem. Mater.*, Volumen 10, pp. 2561-2570.
- Levy, R. & Boudart, M., 1973. Platinum-Like Behavior of Tungsten Carbide in Surface Catalysis. *Science, New Series*, 181(4099), pp. 547-549.
- Lutz, W., 2014. Zeolite Y: Synthesis, Modification, and Properties—A Case Revisited. *Advances in Materials Science and Engineering-Hindawi Publishing Corporation*.
- Ma, Y. et al., 2014. Low-temperature steam reforming of methanol to produce hydrogen over various metal-doped molybdenum carbide catalysts. *International journal of hydrogen energy*, Volume 39, p. 258.266.
- McKenzie, A. L., Fishel, C. T. & Davis, R. J., 1992. Investigation of the Surface Structure and Basic Properties of Calcined Hydrotalcites. *Journal of Catalysis*, Volume 138, pp. 547-561.
- Minerals, S. R., n.d. *Shree Ram Minerals*. [Online] Available at: <http://shreeramminerals.com/minerals/about-kaolin/> [Accessed 30 January 2015].
- Miranda-Trevino, J. C. & Coles, C. A., 2003. Kaolinite properties, structure and influence of metal retention on pH. *Applied Clay Science*, Volume 23, pp. 133-139.
- Moulder, J., Stickle, W., Sobol, P. & Bomben, K., 1995. *Handbook of X-Ray Photoelectron Spectroscopy*. Eden Prairie, MN: Physical Electronics Inc..
- Muñoz, M., Moreno, S. & Molina, R., 2012. Synthesis of Ce and Pr-promoted Ni and Co catalysts from hydrotalcite type precursors by reconstruction method. *International journal of Hydrogen Energy*, Volume 37, pp. 18827-18842.

- Parkash, S., 2003. *Refining Processes Handbook*. 1 ed. USA: Elsevier.
- Pereira-Almao, P. et al., 1999. *Steam Conversion Process and Catalyst*. United States, Patent No. 5885441.
- Pereira-Almao, P. et al., 2013. *Systems and Methods for Catalytic Steam Cracking of Non-Asphaltene Containing Heavy Hydrocarbons*. US, Patent No. 20130015100 A1.
- Pereira-Almao, P., Vieman, A., Lopez-Linares, F. & Vasquez, A., 2011. *Ultradispersed catalyst compositions and methods of preparation*. US, Patente nº 7897537 B2.
- Pérez Zurita, M. J. et al., 2015. Hydrotalcite type materials as catalyst precursors for the Catalytic Steam Cracking of Toluene. *Fuel*, Volume 154, pp. 71-79.
- Pfeiffer-Vacuum, n.d. *Pfeiffer Vacuum*. [Online] Available at: <http://www.pfeiffer-vacuum.com/en/know-how/mass-spectrometers-and-residual-gas-analysis/introduction-operating-principle/> [Accessed 07 July 2015].
- Pitchford, A. C., 1972. *Upgrading of Crude Oils*. US, Patent No. 3676331 A.
- Praharso, Adesina, A., Trimm, D. & Cant, N., 2004. Kinetic Study of iso-Octane Steam Reforming Over a Nickel-Based Catalyst. *Chemical Engineering Journal*, Volume 99, pp. 131-136.
- Robinson, P. R. & Dolbear, G. E., 2006. Hydrotreating and Hydrocracking: Fundamentals. En: C. S. Hsu & P. R. Robinson, edits. *Practical Advances in Petroleum Processing*. US: Springer, pp. 177-218.
- Rocha, A. S. et al., 2044. Low temperature low pressure benzene hydrogenation on Y zeolite-supported carbided molybdenum. *Catalysis Today*, Volume 98, pp. 281-288.
- Romeo, M. et al., 1993. XPS Study of the Reduction of Cerium Dioxide. *Surface and Interface Analysis*, Volume 20, pp. 508-512.
- Sanchez, S., Rodriguez, M. A. & Ancheyta, J., 2005. Kinetic Model for Moderate Hydrocracking of Heavy Oils. *Ind. Eng. Chem. Res.*, 44(25), pp. 9409-9413.
- Siddique, R., 2008. *Waste Materials and By-Products in Concrete*. 1st ed. Heidelberg: Springer.
- Speight, J., 1999. *The Chemistry and Technology of Petroleum*. 3rd ed. New York: Marcel Dekker.
- Speight, J. G., 2013. *Heavy and Extra-Heavy Oil Upgrading Technologies*. First ed. Massachusetts: Gulf Professional.
- Speight, J. G., 2014. *High Acid Crudes*. MA: Gulf Publishing Company.
- SRI-Instruments, 2014. *SRI Instruments*. [Online] Available at: <http://www.srigc.com/MG3.pdf> [Accessed 2014 01 13].
- Stanislaus, A., Absi-Halabi, M. & Al-Dolama, K., 1989. Effect of Nickel on the Surface Acidity of  $\gamma$ -Alumina and Alumina-Supported Nickel Molybdenum Hydrotreating Catalysts. *Applied Catalysis*, Volume 50, pp. 237-245.
- Tamele, M., 1950. Chemistry of the surface and the activity of alumina-silica cracking catalyst. *Discuss. Faraday Soc.*, Volume 8, pp. 270-279.
- Tang, M., Xu, L. & Fan, M., 2014. Effect of Ce on 5 wt% Ni/ZSM-5 catalysts in the CO<sub>2</sub> reforming of CH<sub>4</sub> reaction. *international journal of hydrogen energy*, Volume 39, pp. 15482-15496.
- Taylor, R. H., Wingbo, C., Christian, G. D. & Ruzicka, J., 1992. Bromine Number Determination by Coulometric Flow-Injection Titration. *Talanta*, 39(7), pp. 789-794.
- Thiel, P. A. & Madey, T. E., 1987. The Interaction of Water With Solid Surfaces: Fundamental Aspects. *Surface Science Reports*, 7(6-8), pp. 211-385.

- U.S. Energy and Information Administration, 2014. *U.S. Energy and Information Administration*. [Online]  
Available at: <http://www.eia.gov/cfapps/ipdbproject/IEDIndex3.cfm?tid=5&pid=57&aid=6>  
[Accessed 16 December 2014].
- U.S. Energy Information Administration, 2014. *International Energy Outlook 2014*, Washington: U.S. Energy Information Administration.
- Uchiyama, M., Kaneko, N. & Ibaraki, 1974. *Catalytic Steam De-alkilation*. United States, Patente n° 3812196.
- Van Den Berg, F. G. A. et al., 2010. *Method of producing a pipelineable blend from a heavy residue of a hydroconversion process*. USA, Patent No. US7799206 B2.
- Villalanti, D. C., Raia, J. C. & Maynard, J. B., 2010. High-temperature Simulated Distillation Applications in Petroleum Characterization. En: *Encyclopedia of Analytical Chemistry*. Chichester: John Wiley & Sons Ltd, p. 6726–6741.
- Vitale, G., 2013. *Iron Silicate Nano-Crystals as Potential Catalysts or Adsorbents for Heavy Hydrocarbons Upgrading*, Calgary: University of Calgary.
- Vitale, G., Frauwallner, M., Scott, C. & Pereira-Almao, P., 2011. Preparation and characterization of low-temperature nano-crystalline cubic molybdenum carbides and insights on their structures. *Applied Catalysis A: General*, Volume 408, pp. 178-186.
- Vitale, G. et al., 2015. Synthesis of nanocrystalline molybdenum carbide materials and their characterization. *Catalysis Today*, Volume 250, pp. 123-133.
- Wang, H. et al., 2009. Effects of olefin on adsorptive desulfurization of gasoline over Ce(IV)Y zeolites. *Fuel Processing Technology*, Volume 90, pp. 835-838.
- Wang, J. et al., 2009. The enhanced adsorption of dibenzothiophene onto cerium/nickel-exchanged zeolite Y. *Journal of Hazardous Materials*, Volume 163, pp. 538-543.
- Ward, J. W., 1993. Hydrocracking processes and catalysts. *Fuel Processing Technology*, Volume 35, pp. 55-85.
- Ward, J. W., 1969. The Nature of Active Sites on Zeolites X. The Acidity and Catalytic Activity of X Zeolites. *Journal of Catalysis*, Volume 14, pp. 365-378.
- Xiao, T.-c. et al., 2000. Preparation of molybdenum carbide-based catalysts for deep HDN. *Acad. Sci. Paris, Série IIc, Chimie / Chemistry*, Volume 3, pp. 451-458.
- Zhang, R., Wang, . H. & Hou, X., 2014. Catalytic reforming of toluene as tar model compound: Effect of Ce and Ce–Mg promoter using Ni/olivine catalyst. *Chemosphere*, Volume 97, pp. 40-46.
- Zhang, Y. et al., 2009. Influence of Rare Earth Promoters on the Performance of Ni/Mg(Al)O Catalysts for Hydrogenation and Steam Reforming of Toluene. *Rare Metals*, 28(6), pp. 582-589.

Appendix A: STANDARD OPERATING PROCEDURE OF CATALYST TESTING UNIT  
(CTU-1)



<b>University of Calgary</b> <b>HEALTH, SAFETY AND ENVIRONMENTAL</b>		
<b>STANDARD OPERATING PROCEDURE</b> <b>FOR: Catalyst Test Unit 1 (CTU-1)</b>	<b>Issued:</b>	<b>Eduardo Garcia</b>
	<b>Revised:</b>	<b>Alejandro Coy</b>
	<b>Reviewed:</b>	
	<b>Pages</b>	

## 1. PURPOSE / BACKGROUND

The Catalyst Testing Unit (CTU-1) was built with the goal of evaluating the performance of different kinds of catalyst in a fixed bed reactor during catalytic steam cracking process of a heavy oil cut. The advantage of this system lies in its small size reactors (3/8" and 1/2"), which allows the user to evaluate a catalyst in relatively small quantities, ranging between 1-10 g. Moreover, the plant can be also used for other processes such as thermal cracking and hydroprocessing. With the current configuration, the plant is able to handle pressures up to 480 psi and a wide variety of temperature up to 500°C for the reactor and 250°C for the feed section.

This procedure is written to comply with all of the U of C HS&E regulatory requirements, and to teach new users, the standard operative protocols of the CTU-1.

## 2. SCOPE

This procedure is intended for all those workers and/or students/interns working in the Upgrading and Refining Lab that will be operating the Catalyst Testing Unit 1 (CTU-1). The procedure covers specific information about starting up of the unit, pressurization, heating up, stabilization period, mass balances procedures, shutting down and learning experiences.

In order to keep track of the information provided in this document, consult the P&ID of the plant and the instruments, thermocouples, valves, manometer and other devices lists shown in the Appendix.

## 3. PREREQUISITES AND SAFETY ISSUES

Specific information related to the feedstock to be processed, catalyst formulation, operational conditions, test length, have to be provided in the experimental plan. Typical machine shop tools are required in case of any repair, change or adjustment in the system.

Successful completion of the University of Calgary generic WHMIS course and H<sub>2</sub>S Alive course are also be required.

Protocol:

- Do not work alone in the laboratory. If required, follow University of Calgary procedures for working alone (<http://www.ucalgary.ca/safety/workingalone>)
- Be aware of the inherent risks associated to, and the nature of, the processes and materials used in the laboratory. This is not limited to the risks and hazards in one own equipment, but extended to include those of every other person in the laboratory.
- Wear appropriate laboratory attire (lab coat, safety glasses, and closed shoes).
- Maintain a neat and organized working environment.

- If leaving an experiment unattended, ensure others are aware and understand the situation including how to deal with an emergency situation. Leave a telephone number at the experiment for contact purposes.
- Dispose of waste in a safe and environmentally friendly manner.

Campus Security:

**Hazard Identification (Hazardous Chemicals or Processes):**

- Hazardous Chemicals
- Products and by-products expected from the system are:
  - Hot heavy oils from the feed section, reactor and heavy product tanks.
  - Toluene in the feed section
  - Nitrogen and/or Hydrogen compressed gas
  - Light liquid hydrocarbons
  - Hydrocarbon gases
  - H<sub>2</sub>S in concentrations lower than 200 ppm

Processes:

Heavy oils flowing under moderate pressure and temperature conditions.

**Hazard Assessment:**

**Products:**

Reaction Gas and the gas exit of the storage tank (T-2) is sweetened in a KOH or NaOH solution at the outlet gases stream.

Personnel must wear personal protective equipment (PPE) all the time when working with the unit.

Use of toluene should be done discretely and only when strictly needed.

**Processes:**

Heat insulation is used in all process lines under high temperature conditions.

Pressure relief device is located in the feed section to protect the system in the case of an overpressure caused by plugging of a process line.

**Engineering/Ventilation Controls:**

The CTU-1 was built inside an enclosure with extraction system able to remove gases produced by the chemicals involved and the gases produced during operation of the system.

**Personal Protective Equipment:**

Personal protective equipment (PPE) required for this SOP includes but is not limited to:

Nitrile gloves, safety glasses and laboratory coats are standard safety equipment for all employees, students and interns in the lab.

Respirators with adequate filters/cartridges when cleaning any oil or emulsion spill from the plant using any type of solvent like toluene, acetone, gasoline, etc.

Quartz gloves are needed for handling high temperature objects.

## 4. PLANT DESCRIPTION

### 4.1. PHYSICAL DESCRIPTION

The unit CTU-1 can be divided in three sections. The first section (Feed section), consist of all the lines and connections involved in the preparation of the reactants at the desired conditions to be sent into the reactor. In the P&ID (see Appendix), it can be seen as all the system to the left of the reactor until the valve V-10. The second section, the reaction sections, involves the reactor, bypass and the valves V-10 and V-11. The final section called sampling section, is the part of the plant where the products are separated into liquid and gases to allow the sampling of them.



The feed section contains three liquid inlets and two gas inlets to the plant. From the three liquid inlets, one is used for pumping oil through a Teledyne isco syringe pump (P-1), another Teledyne isco syringe pump is used for pumping water (P-2) and one extra line is in spare for future reactants. Gases inlets are considered for nitrogen and hydrogen. Nitrogen is used as carrier gas and can be fed into the plant either in the feed section or in the hot separator (S-1). Hydrogen is used for reduction of the metals in the catalyst and can also be used when hydro-conversion operations are needed. Water is heated in the feed section to favor its vaporization and produce steam. This steam is mixed with nitrogen (when fed into the feed section) in M-1 and then with oil. In the last part of the feed section, these three compounds are mixed and heated before entering the reaction zone.

The reaction zone consists basically of a up-flow fixed bed reactor, with temperature measurements in the wall, inside the reactor and at the exit of it, to control the operating conditions. For cleaning and special operations, this section is equipped with a bypass that allows for passing fluids without contaminating the catalytic bed.

The sampling zone is at the same time divided in two parts: Liquid sampling and Gas sampling. The products of the reactor are separated in a 150 ml hot separator (S-1), where gases, water and light hydrocarbons leave the vessel from the top and go to a 75 ml cold separator (S-2). The gases are cooled down in HE-1, which leads to water and light hydrocarbon condensation. The remaining gases leave S-2 and are quantified in a flowmeter (F-1). Before gases leave the plant, they have to go through a pressure controller or back pressure valve, which keep the pressure in the system. After this point, V-34 allows the operator to send the gases for analysis in a GC or to send them for  $\text{H}_2\text{S}$  neutralization in a KOH containing vessel.

The liquids obtained in S-1 are transferred to a 150 ml storage tank (T-1) by aliquots through a two valve system (V-18 and V-19) controlled with the LabVIEW Program. V-18 is constantly open during normal operations. When a sample is needed, V-18 close and V-19 open to fill T-1. After discharging the aliquot of around 3 ml contained in between the two valves, V-18 close and V-19 open again. In this way, it is possible to obtain samples of the liquids products without affecting strongly the pressure in the system. Samples of light hydrocarbons and water from S-2 can be obtained by performing similar operations but with V-15 and V-23. Manually, V-15 must be opened to fill a small volume of tube, and then it must be closed to proceed to open V-23.

#### 4.2. LABVIEW SYSTEM

The CTU-1 is controlled by means of a real time power PC (cRio-9024) from National Instruments, which is in charge of collecting information from the plant such as temperature, pressures and gas flows in order to record them in an excel file in the PC located outside of the extracting enclosure. This system also performs the controlling of the heating tapes, pumps and liquid sampling valves (V-18 and V-19).

The cRio-9024 system starts up by means of a code written in LabVIEW program, whose shortcut can be found in the desktop of the computer under the name CTU-1. Once the CTU-1 program is opened, the following display is obtained.

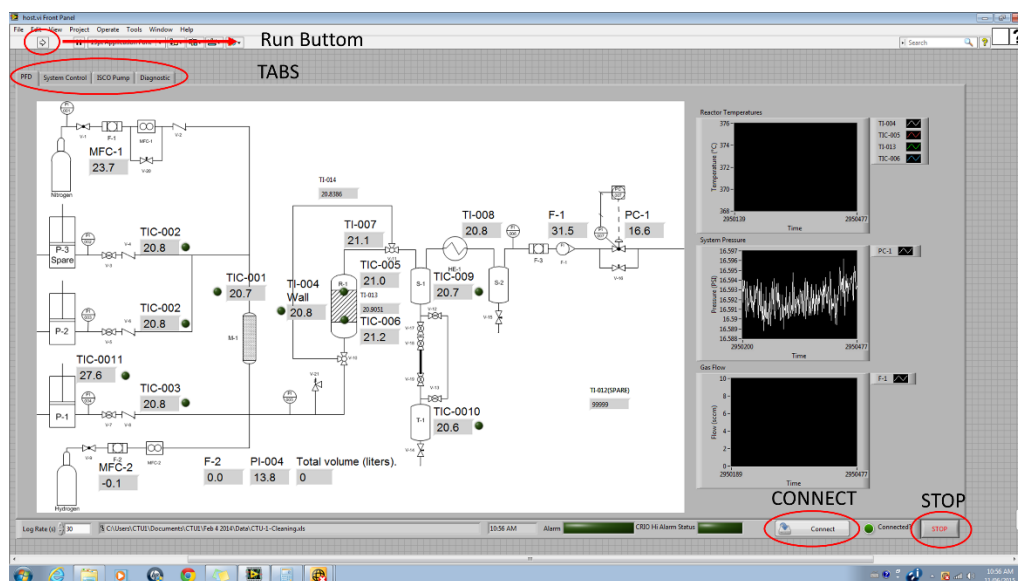


Figure 1. PFD display of the CTU-1 LabVIEW program.

The next step is to click on the run button, which will pop up a window to set the name of the excel file and the place where all the data is going to be saved. Then, it is necessary to click on the connect button to start the interaction with cRio-9024. At any moment desired, the stop button will lead to a completely stop of the program and the activities running by that time.

The whole program consists of four different displays to be selected by means of the tabs buttons in the Figure 1. The PFD tab basically shows the process flow diagram of the plant with basic information to keep track of the process. Specifically, it shows the pressure of the system measured by the pumps and back pressure valve, the temperatures along the plant, the produced gas flow, nitrogen and hydrogen gas flows and the three internal and one external temperature of the reactor.

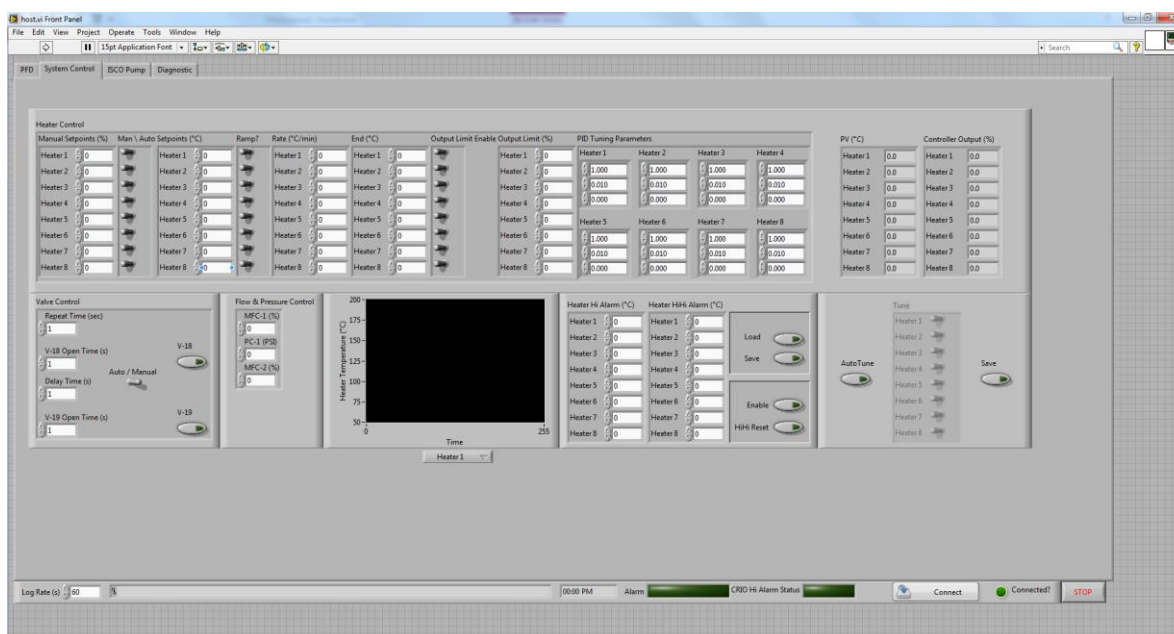


Figure 2. System control display of the ctu-1 LabVIEW program

The second tab, called system control (Figure 2), allows the operator to monitor and control the heating tapes, temperatures, flow delivered by the mass flow controllers, to set the pressure in the pressure controller and to control the liquid sampling valves.

The first row of switches in the Heater Control System gives the possibility to work with a specific percentage of the heating tape (left) or with a desired temperature set point (right). If desired, the temperature set point can be reached by means of a ramp by activating the corresponding switch in the second row of switches. By doing so, it is possible to establish the desired temperature and the rate ( $^{\circ}\text{C}/\text{min}$ ) required to reach it. The third set of switches can be used to activate the output limit to establish a maximum output limit for the heating tapes, usually no more than 75% as per experience. In the PID tuning parameters, the proportional, integral and derivative parameter can be added for each heater. At the far right of that part, the real value of the temperature and the output sent to the heating tapes is shown.

In the valve control section, the operator can choose between either operate the valve manually with the green buttons or configure it to work by itself every certain period of time. In the Flow and Pressure Control, the operator can set the aperture percentage for the MFC-1 and MFC-2; and the pressure for the pressure controller PC-1. By selecting the desired heater, it is possible to keep track of the temperature and the profile through the chart in this section. There is also a Heater Alarm section, in which we can set the HI and HI HI alarms for the heaters. To finish, it is also possible to carry out of the tuning of the heating tapes controllers.

The third display (ISCO Pump) allows the operator to set either the delivery pressure or flowrate. Besides, it also gives information regarding the current pressure, volume remaining in the pumps and flow rate of each pump in the system. The Pump A correspond to the oil pump (P-1) and Pump B to water pump (P-2).

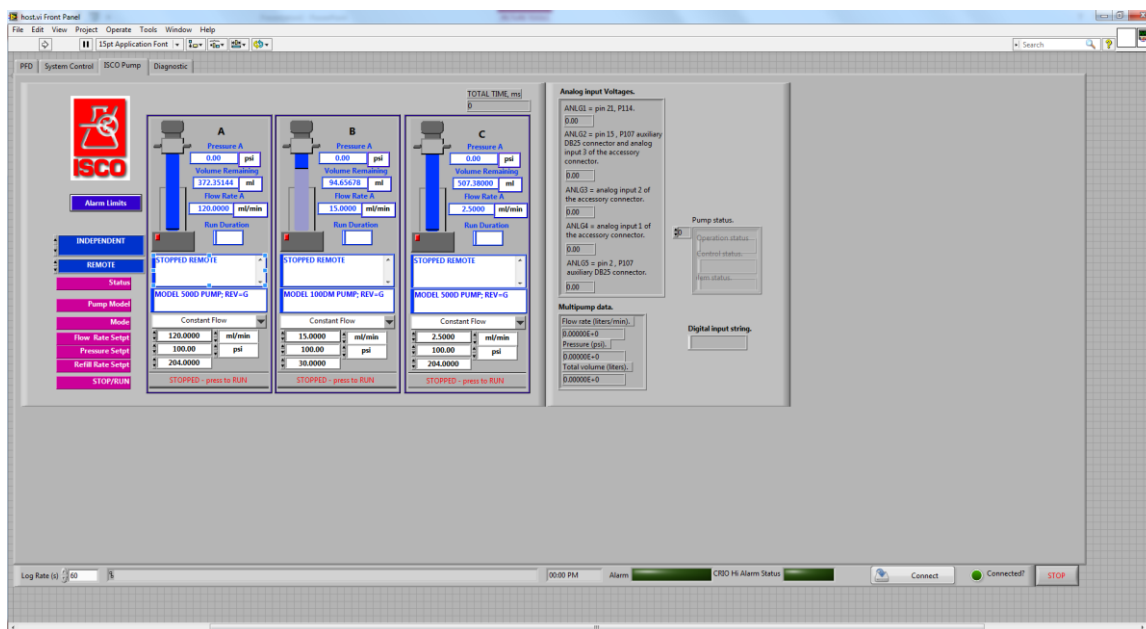


Figure 3. Isco pump display of the CTU-1 LabVIEW program

The last display called Diagnostic (Figure 4) is used to evaluate the right performance of the program regarding temperatures, currents of the instruments and heater output at certain time.

Besides, the calibrations for the instruments can be saved in order to show the measurements in the units required by the user. In case of any error during the running of the program, it will be shown in the System Status.

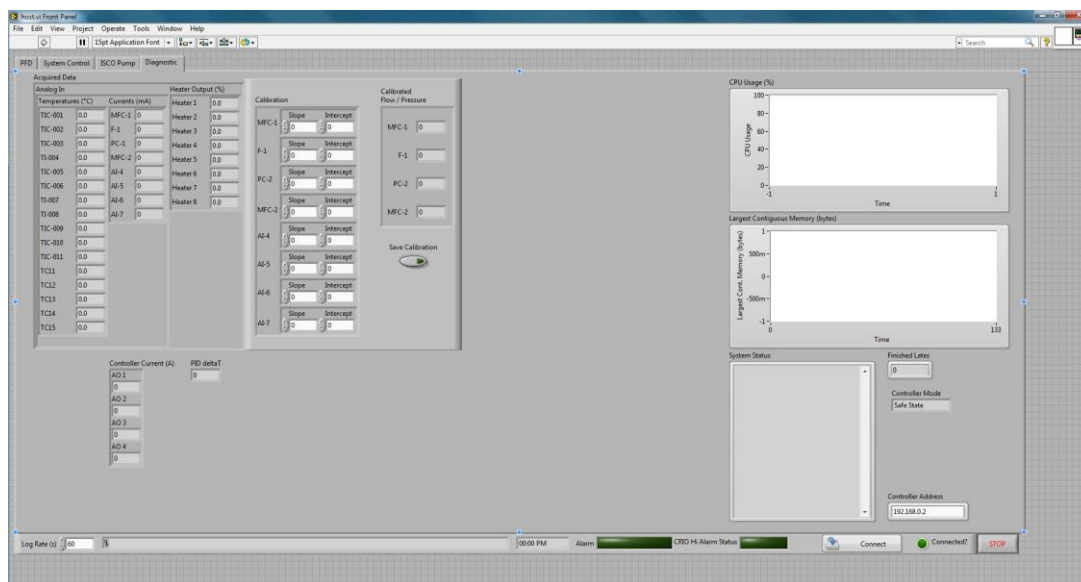


Figure 4. Diagnostic display of the CTU-1 LabVIEW program

## 5. PROCEDURES

### 5.1. PLANT PREPARATION

Verify the plant is not energized by checking the electrical box (Figure 5). At the beginning of each week or after a long period of time without using the plant, the switch must be pointing down and the bulb off, which means that the plant is not energized.

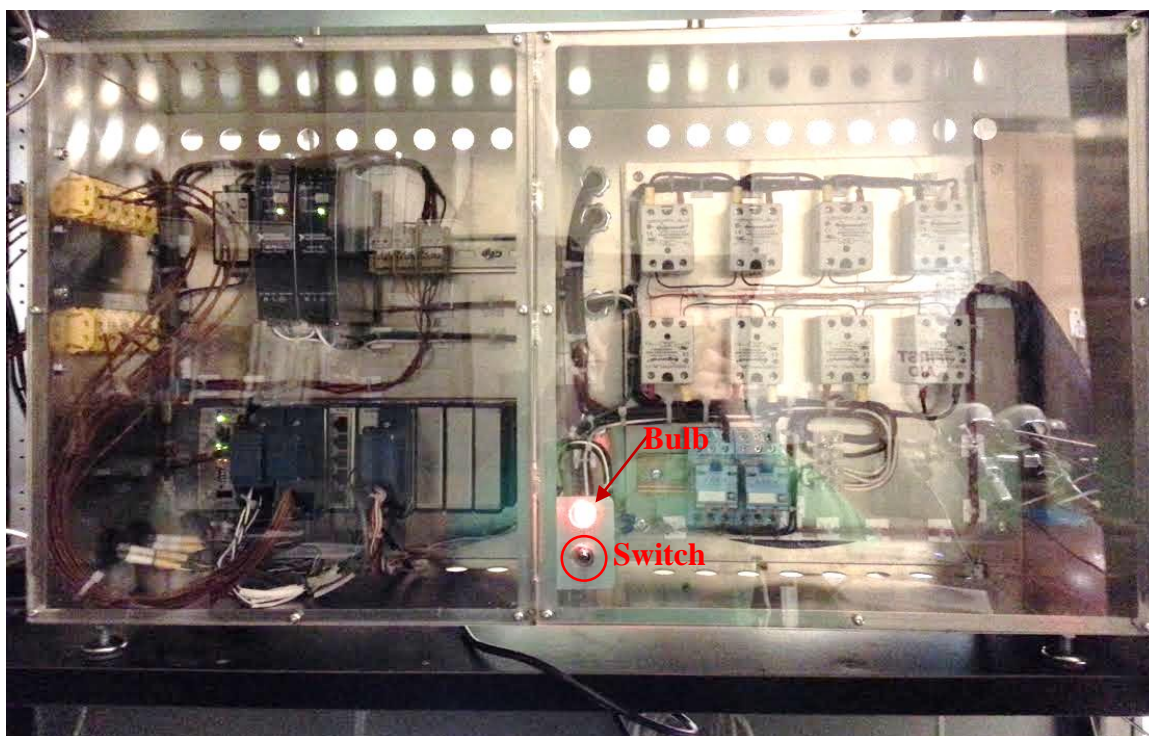


Figure 5. Electrical box.

1. Make sure all the valves in the plant are closed and the manometers indicate 0 psi.
2. Check the pressure of the inlet gases ( $N_2$  and  $H_2$ ). They shouldn't be at values greater than 500 psi.
3. Check Nitrogen cylinder pressure, it shouldn't be below 500 psig.
4. Set the regulator valve at the Nitrogen and Hydrogen cylinder so the supply is 50 psi over the operating pressure and not greater than 500 psig.
5. Verify there is no pressure in the plant by checking the pressure gauges and indicators and the pressure readings of the feed pumps and water pumps. In the case the pressure readings are above 10 psig, open the drain valve on the pressurized section.

### 5.1.1. Reactor Assembling

#### 1. Filling the reactor with the catalyst to be evaluated:

- The reactor must be assembled as in Figure . The top connection is defined as the assembly of SS-400-3, SS-400-6-2 and either SS-600-6-4 or SS-810-R-4. The bottom connection is defined as the piece SS-400-6-2 with SS-810-R-4 or SS-600-6-2.

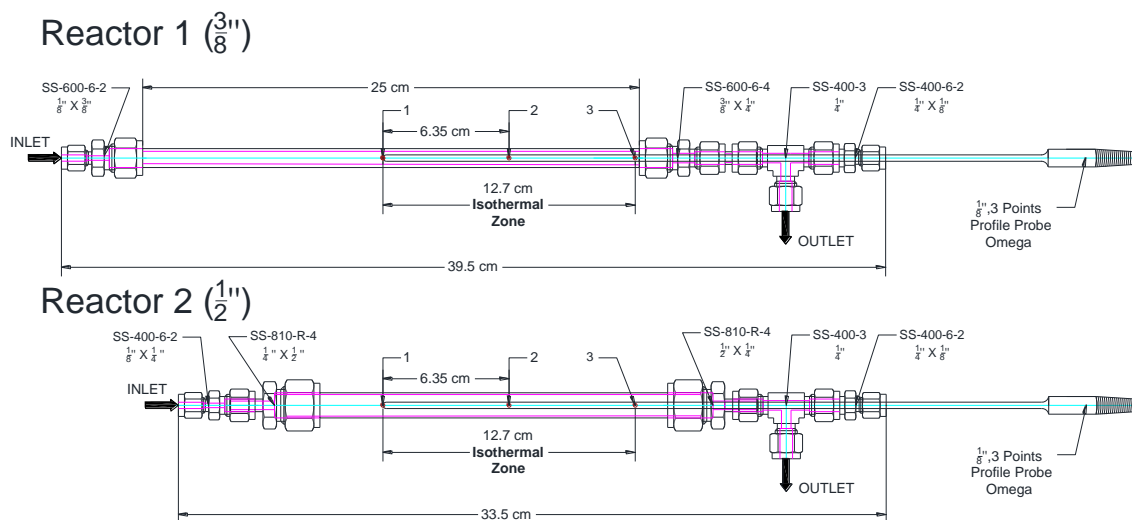


Figure 6. Reactor configuration

-Insert a small amount of glass wool in the top connection of the reactor, through the piece either SS-600-6-4 or SS-810-R-4, respectively.

-Screw the nut of the reactor to the top section of it.

-Turn the reactor upside down (without the bottom connection) and add a washed inert material such as carborundum (SiC) until reaching the isothermal zone.

-Add another small amount of glass wool and proceed to insert the catalyst. It is important to keep in mind the location of the catalyst. Preferably, the catalytic bed shouldn't be longer than the final point of the probe thermocouple.



-Put in more glass wool and continue to insert more carborundum until the reactor is almost full. A small volume must be left for inserting more glass wool.

-Proceed to close the reactor and install it into the plant.

2. Align V-11 to off-mode.
3. Open the valve that feed the system with nitrogen (V-1)
4. Increase the pressure of the system to about 450 psi by opening V-20 (Bypass to the MFC-1).
5. Add a liquid leak detector to each connection of the reactor and its connection with the plant.
6. If bubbles are produced in any connection, proceed to tighten it until the leakage stops.
7. Once the desired pressure is reached, close V-20. Make sure the valves that feed the plant are closed (V-3, V-5, V-7 and V-29).
8. Record the pressure change in the manometer located before entering the reactor (PI-005).
9. In order to operate the plant properly, the pressure drop should be less (preferably zero) than 0.5% of the pressure used to carry out the leak test in a period of one hour.
10. Once the leak test ends up successfully, two heating tapes of 0.5''x 2'' can be located around the reactor. H-005 start wrapping the reactor from the point 2 to the inlet, while H-004 does it from the point 2 to the outlet. Both heating tapes must start from the side of it that is attached to the wire.
11. Allocate the nearby insulation and the jacket.
12. Energize the plant by turning on the switch shown in Figure 5.
13. Turn on the pumps P-1 and P-2.

14. Open LabVIEW Program “CTU-1” located in the desktop of the computer.

#### 5.1.2. Reactor disassembling

1. If the system is energized, check the temperatures of the plant in the LabVIEW Program “CTU-1” and make sure the system had been cooled down.
2. If the electrical box is off, make sure the reactor has been already cooled down.
3. If the manometers are indicating pressure in the system, depressurise the plant as mentioned in Section 5.2.1.
4. Proceed to remove the jacket and the necessary insulation to disassemble the reactor.
5. Loosen the nut in the bottom of the reactor and in the right exit of the Tee settled at the top of it.
6. Remove the reactor from the set up.

#### 5.1.3. Pumps loading

1. Depending on the pump to be filled, close V-3, V-5 or V-7 accordingly.
2. Set V-31 in the filling direction for the water pump or open V-33 and make sure that the drainage (V-32) is close in the case of the oil pump.
3. For P-2, insert the filling tube of the pump into a vessel with the fluid. In the case of P-1, add the oil to the storage tank (T-2) and pressurize the system with nitrogen using V-36.
4. In the case of oil, heat the pump up to 100°C through LabVIEW using Heater 8. The tank can be heated up by means of a rheostat and heating tapes already located in the plant. Wait for a couple of hours to allow all the oil to be heated up. ATTENTION: Always start heating the oil pump with V-33 open to avoid overpressure in the pump, especially if there is already liquids inside it.

5. Proceed to select “Refill” in either the LabVIEW program for pumps or manually in the pumps controller. Preferable, select a low flowrate up to 300 ml/h to avoid the formation of bubbles inside the pump.
6. Once the pumps have been filled up, they must be purged:
  - For P-2, select the run mode for the pump and wait until the liquid comes out. Then, stop the pump and proceed to refill it again. Repeat this step until it pumps liquid right after asking it to. (Attention: make sure V-31 is still in filling mode before running the pump to avoid overpressures)
  - In the case of P-1, it is necessary to close V-33 and open V-32 to proceed to run the pump. As with P-2, stop the pump when the liquid comes out and refill it again by opening V-33 and closing V-32.
7. During the purge process, the pumps can be evaluated to assess if they are well calibrated and sending the right flowrate. In order to do that, just collect and measure the amount of liquid pumped in a specific range of time.
8. Once the pumps are filled and purged, align the valve V-31 to the process line, close V-33 and V-32.
9. To finish, open V-3, V-5 and V-7 accordingly.

## 5.2. PLANT OPERATION

### 5.2.1. Pressurization and depressurization

During the operation of the CTU-1, it is often required to pressurize the plant to reach the operating pressure. In order to do that, it is necessary to check that all the drainage valves are closed. The nitrogen mass flow controller (MFC-1) allows the user to feed the plant with nitrogen until

reaching the desired pressure. However, due to the low volumetric capacity of this instrument, a needle valve controls the bypass line to this instrument and allows the user to increase the pressure manually in a faster way. Once the desired pressure is reached, the MFC-1 bypass valve should be closed. To pressurize the whole plant, it is required to align the two three-way valve before and after the reactor to either “reactor mode” or to the “bypass mode”. The pressure in the system can be controlled by either a backpressure valve or a pressure controller. Each one of those has a set of two valves at the inlet and at the outlet that isolate the one not used. ATTENTION: it is important to bear in mind that the back pressure valve operates up to 490 psi and the pressure controller up to 270 psi. Overpressure can cause serious damage to the equipment, especially to the pressure controller.

The safest way to carry out a depressurization of the system is by opening the back pressure located at the exit of the plant. In order to do that, it is necessary to open both of the valves that isolate the back pressure and then proceed to open it. If the pressure controller (PC-1) is working, it is also possible to depressurize the system by setting a pressure equals to zero psi in the PC-1 in LabVIEW and checking that both of the valves that isolate the PC-1 are open.

In the case that the bypass or the feed zone are isolated from the sampling zone during depressurization, it will be necessary to align the two three-way valves before and after the reactor to either “reactor mode” or “bypass mode”. The bypass can be also depressurized by means of the drainage valve collocated in that section, but it will require collecting the liquid stored in the line.

### 5.2.2. Start-up

During the start-up and stabilization of the plant, some areas require to be heated using the heating tapes. When carrying out this heating, the following temperature increase ramps shall be used:

Table 1. Temperature ramps for heating tapes

<b>Temperature Range [°C]</b>	<b>Ramp [°C / min]</b>
0 - 200	4
200 - 300	3
300 - 400	2
400 - 500	1

### 5.2.3. Reduction of the Catalyst

The reduction of the catalyst can be performed in situ and it is advised to carry it out right before the experiment is performed to avoid oxidation of the metals. If that is not possible, keep flowing nitrogen to the system after reducing. A reduction operation required the following steps:

1. Close V-3, V-5 and V-7.
2. Align V-10 and V-11 to reactor mode.
3. If using back pressure, make sure that it is completely open. If using pressure controller, set 0 psi for the instrument in the LabVIEW program.
4. Open hydrogen stream, valve V-9 and V-29.
5. Set the hydrogen flow in the MFC-2 in 30%, which is equivalent to 60 ml/min
6. As indicated in Table 1, increase the temperature of the reactor at the proper rate with H-04 and H-05 until the reduction temperature.
7. Once the temperature has been reached, leave the system at those conditions for at least six hours.
8. Modify the set point for H-04 and H-05 to cool down the reactor.
9. Set hydrogen flow to zero.

10. Close V-29, V-9 and the hydrogen cylinder.
11. Set a flow rate to the MFC-1 of 50% (15 ml/min) and let the nitrogen flush the hydrogen out of the plant.

#### 5.2.4. Reaction

Once the catalyst has been reduced, the following step must be accomplished in order to successfully perform the operation of the unit:

1. Make sure V-10 and V-11 are in reactor mode.
2. Leave back pressure or pressure controller fully open.
3. By opening V-17, V-18, V-19, V-14, and V-22 drain the hot separator; and by opening V-15 and V-23, drain the cold separator.
4. Close all the valve involved in step 3 except for V-17 and V-18.
5. Set a nitrogen flow for MFC-1 of 13.5% (4.1 ml/min) and record the value measured by the flowmeter (F-1) after stabilization of it (check on the charts for gas flow in the LabVIEW program.)
6. With the ramps range for each temperature shown in the Table 2, reach the following set point for the heating tapes:

Table 2. Initial heating tapes set points.

Heating Tape	Temperature (°C)
H-01	210-250
H-02	210-250
H-03	210-250
H-04 (Top)	Reaction temperature

H-05 (Bottom)	Reaction temperature
H-06	208-250
H-07	115
H-08	100

7. Pressure setting: With pressure controller, set the pressure at the operating pressure. With back pressure close the valve around 4 turns and half to adjust it in about 150 psi. Then, use MFC-1 bypass valve (V-20) and the back pressure to increase the pressure in the system until the desired pressure.
8. Once the set points for the heating tapes are reached, open the water inlet (V-5) and make sure the three ways valve of the water pump is aligned toward the plant.
9. Set a flowrate of 24 ml/h in the water pump (P-2) and wait for about 15 minutes to fill the dead volume in the plant.
10. Set the flowrate in 1 ml/h and pre-treat the catalyst for at least 3 hours with steam.
11. Then, set the flowrate for the water pump according to the one required by the experiment.
12. Open the oil inlet valve (V-7) and make sure V-32 and V-33 is closed.
13. Then, set 24 ml/h for the oil pump (P-1) for about 15 min.
14. Change set point for P-1 according to the one required by the experiment.
15. Drain the hot separator and cold separator one more time.
16. At this point, the automatic operating of the double valve system (V-18 and V-19) must be adjusted to favor the proper transfer of the sample to the storage tank. The values in Table allow to automatically drain the aliquot into the storage tank (T-1) for almost 5 min.

Therefore, if sampling is required e.g. every 90 min (5400 s), the value of X should be 5100 s.

Table 3. V-18 and V-19 automatic timing

Parameter	Time, s
Repeat Time	5
V-18 open time	x
Delay Time	5
V-19 Open time	290

17. When all the conditions (temperatures, pressure and flow) reach the desire set point, the stabilization period is started. Wait the time established in the experimental plan (as a rule of thumb, the time required will be the minimum time to pass 3.5 times WHSV).
1. During the stabilization period, change V-34 from Vent mode to GC mode, in order to send the gases to the GC.
2. Make sure that the GC is on and working properly. Check the valve in RTU-1, as shown in the Figure 6, is on CTU-1 mode to send gases to the GC located in either in RTU-1 or RTU-2.



Figure 7. Valve located in RTU-1 to send gases to GC.



3. There are two three ways valve located each one in RTU-1 and RTU-2. Make sure that if it is desired to use the GC in RTU-2, the valve in RTU-1 should be in RTU-2 mode and the valve in RTU-2 should be in RTU-2 mode. In the case that the GC to be used is the one located in RTU-1, the valve in RTU-2 should say RTU-2 and the valve in RTU-1 should say RTU-1.
4. Once the valves for the gases are settled in the right position, measure the gas flow from F-1 and from the flow meter attached to the GC. Then, run the GC.

The length of each mass balance is determined by the flowrate used for water and oil and the amount of sample required for analysis. At the end of the mass balance, the heavy products should rest in T-2 for about 30 min to allow the oil to reach the end of the tank and obtain better mass balances. The sampling of lights is done right when the mass balance closes by operating V-15 and V-22 like the way V-18 and V-19 do.

### 5.3. SHUTDOWN

In order to shut the plant down during or at the end of an experiment, follow the next steps:

1. Set the oil pump (P-1) to 0 ml/h, close valve V-7 and open V-33
2. Leave water pump running for around 30 minutes to clean the system out.
3. After 30 min, set all the heating tapes to 0°C to cool down the system.
4. When all thermocouples indicate temperatures lower than 100 °C, proceed to depressurize the system.
5. Set the water pump (P-2) to 0 ml/h.
6. Let the nitrogen to flow the system for at least 30 min at 50%.
7. Drain completely the hot separator (S-1), storage tank (T-1) and cold separator (S-2).

8. After draining, close the two valves at the exit of the T-1 and S-1.
9. Set the MFC-1 to 0 ml/h.
10. Make sure everything was recorded in the computer.
11. Stop the LabVIEW program and turn the electrical box off.
12. Let the system to cool down.
13. Once it is cold, disassemble the reactor as explained in 4.1.3 (reactor disassembling)

#### 5.4. EMERGENCY SHUTDOWN

If any emergency situation is presented that is required to shut down the unit immediately, follow the procedure below:

1. Decrease the whole plant temperature to room temperature (Turn heating tapes off).
2. Turn off the feed pump, water pump, and Hydrogen flow controller.
3. Depressurize the system.
4. If it is a high risk emergency, turn off the switch of the electrical enclosure located close to the computer. It will de-energize all heating tapes and flow controllers. Switch off both syringe pump.
5. Another way to de-energize the unit is disconnecting the plugs from the electrical enclosure and the pumps.

#### 6. Roles & Responsibilities

##### **Key Personnel**

##### **Main operator and responsible of the system:**

Luis Alejandro Coy - Eduardo García

**Alternate operators:** N/A

## 7. Training

It is recommended that a person to operate the CTU-1 be educated or pursuing studies in the area of chemical or petroleum engineering and/or chemistry.

Any new operator of the RTU-1 has to follow an operational training conducted by either the main operator or alternate operator. The operational training would be no shorter than three whole experimental runs which include previous preparation of the unit, starting up, stability condition, mass balances and shutting down of the plant.

As per the pre-requisites of entering the lab, The University of Calgary Generic WHIMS course must be successfully completes.

## 8. Monitoring Requirements

Not applicable

## 9. Record Management

Each SOP shall be reviewed within 12 months of the date of issuance or date of last, review to ensure the SOP is up-to-date.

This first SOP for the CTU-1 unit has been submitted on February 14, 2014

## 10. References

## 11. Definitions

Not applicable

## 12. Emergency:

**Contact 911**

**University Emergency:****Immediately supervisor: Luis Alejandro Coy****Principal Investigator: Dr. Pedro Pereira-Almao**

## 13. University Notification

Indicate if there are any concerns that EH&S should be made aware of prior to the start of a particularly hazardous protocol, such as a disruption to a water source, loss of power, loss of gas detection systems etc.

\*Indicates elements which may be required for particularly hazardous substances or processes.

**Signed:** \_\_\_\_\_ **Date:** \_\_\_\_\_

**Principal Investigator/Manager Signature**

## 14. Appendix

Table 4. List of equipment

<b>TAG</b>	<b>Description</b>
HE-1	Heat Exchanger after Reactor
M-1	Mixer in Feed Zone
P-1	Oil Pump
P-2	Water Pump
P-3	Spare Pump (Currently not available)
R-1	Reactor
S-1	Hot Separator
S-2	Cold Separator

T1	Sampling Tank
T2	Oil Storage Tank
-	Nitrogen Cylinder
-	Hydrogen Cylinder

Table 5. List of valves

<b>Tag</b>	<b>Type</b>	<b>Description</b>
V-01	Ball	Nitrogen Inlet to the System
V-02	Check	Nitrogen Line
V-03	Ball	Spare Inlet for Different Feed
V-04	Check	Spare Inlet for Different Feed
V-05	Ball	Water Inlet
V-06	Check	Water Inlet
V-07	Ball	Oil Inlet
V-08	Check	Oil Inlet
V-09	Ball	Hydrogen inlet to the system
V-10	Ball (three way)	Bypass/Reactor Inlet
V-11	Ball (three way)	Bypass/Reactor Outlet
V-12	Ball	Bang Bang Bypass Inlet

V-13	Ball	Bang Bang Bypass Outlet
V-14	Needle	Storage Tank (T-1) Outlet
V-15	Needle	Cold Separator (S-2) Outlet
V-16	Back Pressure	Back Pressure
V-17	Ball	Bang Bang Enable
V-18	Ball/ Electrical Actuator	Bang Bang System Inlet
V-19	Ball/ Electrical Actuator	Bang Bang System Outlet
V-20	Needle	Bypass to the MFC1/ Pressurization valve
V-21	Spring/Relief	Relief valve
V-22	Ball	T-1 Safe Drainage
V-23	Ball	S-1 Safe Drainage
V-24	Ball	Back Pressure isolator
V-25	Ball	Back Pressure isolator
V-26	Ball	Pressure Controller isolator
V-27	Ball	Pressure Controller isolator
V-28	Ball	Bypass Drainage
V-29	Ball	Hydrogen Line Isolator
V-30	Check	Hydrogen Line

V-31	Ball/Three way	Filling or Pumping Path for P-2
V-32	Needle	Drainage for P-1
V-33	Ball	Filling of P-1
V-34	Ball/Three Way	To Send Gases to Either Gas Chromatographer or to Vent
V-35	Check	Protection Against Oil Back Flow
V-36	Needle	Pressurization of T-2
V-37	Needle	T-2 depressurization.
V-38	Ball/Three Way	Used to Send Nitrogen to Either the Reactor or Hot Separator.
V-39	Check	Nitrogen Line
V-40	Needle	Used for Better Cleaning of T-1

Table 6. List of instruments

<b>Tag</b>	<b>Description</b>
MFC-1	Mass Flow Controller for Nitrogen
PC-1	Pressure Controller
MFC-2	Mass Flow Controller for Hydrogen
F-1	Flow Meter

Table 7. List of Thermocouples

<b>TAG</b>	<b>Description</b>	<b>Function</b>
TIC-001	Nitrogen and Mixer	Controller
TIC-002	Steam Line	Controller
TIC-003	Oil Line	Controller
TI-004	Reactor-External	Indicator
TIC-005	Reactor-Internal (Point 3)	Controller
TIC-006	Bypass (Point 1)	Controller
TI-007	Exit Reactor	Indicator
TI-008	Exit Heat Exchanger	Indicator
TIC-009	Hot Separator (S-1)	Controller
TIC-010	Storage Tank (T-1)	Controller
TIC-011	Oil Pump (P1)	Controller
TI-012	Connection in spare	Indicator
TI-013	Reactor Internal (Point 2)	Indicator



Table 8. List of Pressure indicators

<b>Tag</b>	<b>Description</b>
PI-01	Manometer in Nitrogen Line
PI-02	Internal in P-3. Not Currently Available.
PI-03	Internal in Water Pump (P-2).
PI-04	Internal in Oil Pump (P-1).
PI-05	Manometer Before Reactor
PI-06	Manometer after Cold Separator (S-2)
PIC-07	Internal in Pressure Controller
PI-08	Manometer in Hydrogen Line
PI-09	Pressure in Oil Storage Tank (T-2)

Table 9. List of heating Tapes

<b>Tag</b>	<b>Description</b>	<b>Associated Thermocouple</b>
H-001	Nitrogen and Mixer	TIC-001
H-002	Steam Line	TIC-002
H-003	Oil Line	TIC-003
H-004	Reactor (Internal)	TIC-005

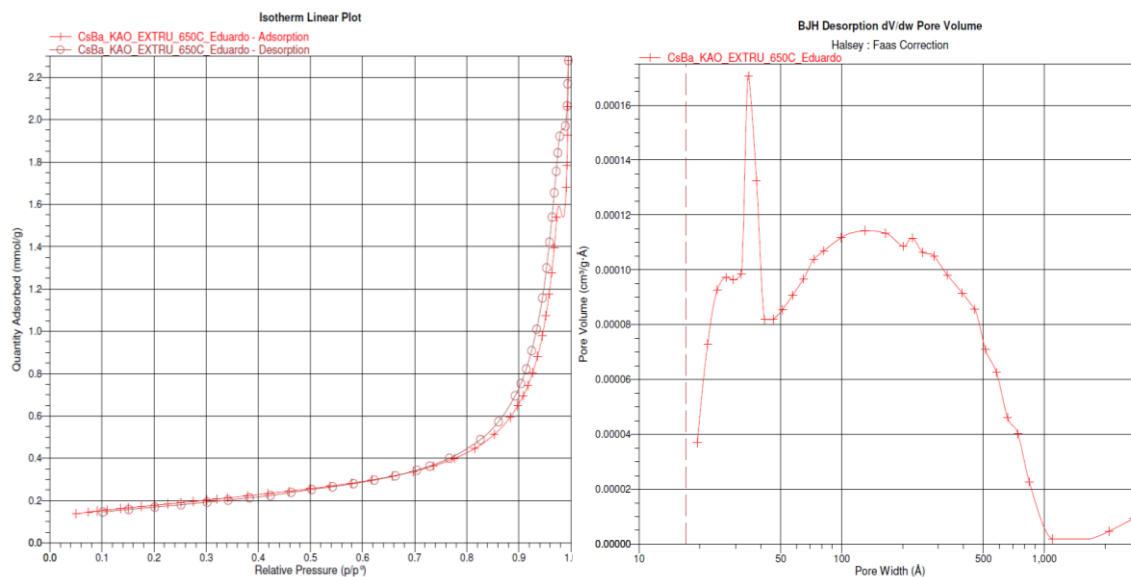
H-005	Reactor (Internal)	TIC-006
H-006	Hot Separator (S1)	TIC-009
H-007	Tank (T1)	TIC-010
H-008	Oil Pump(P-1)	TIC-011

\*Proper connection must be done to align the heating tape with the corresponding thermocouple.

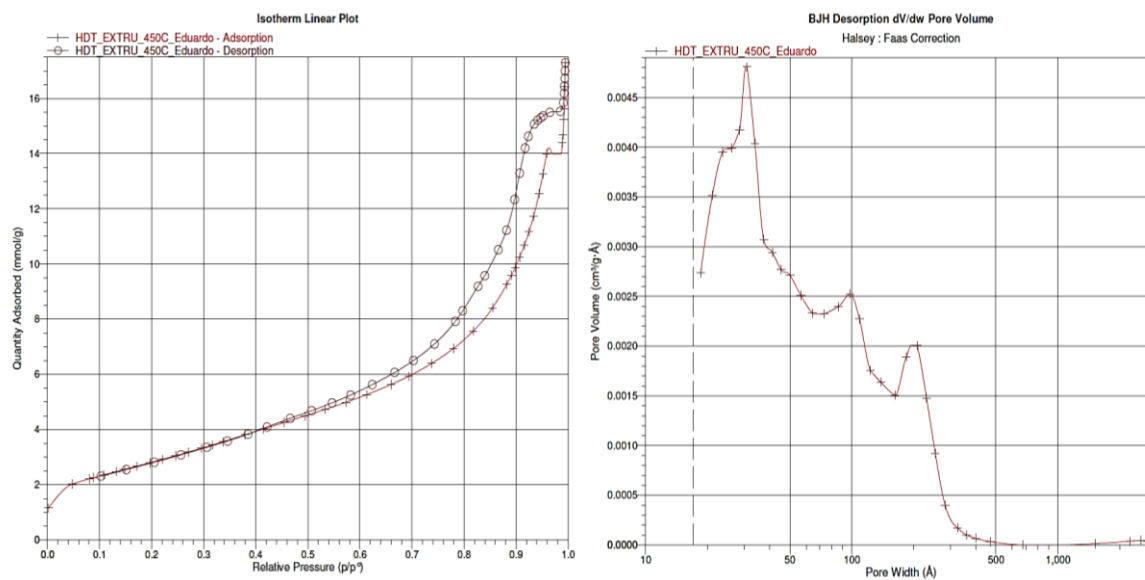


## Appendix B: Catalyst Characterization Data

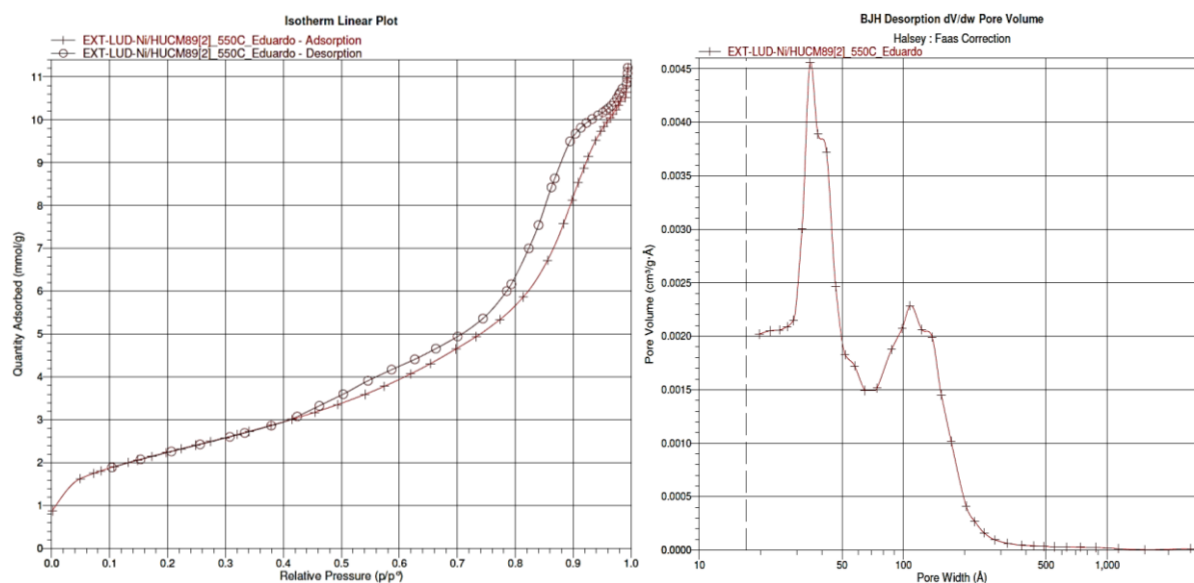
This appendix contains information about the characterization of the catalysts.



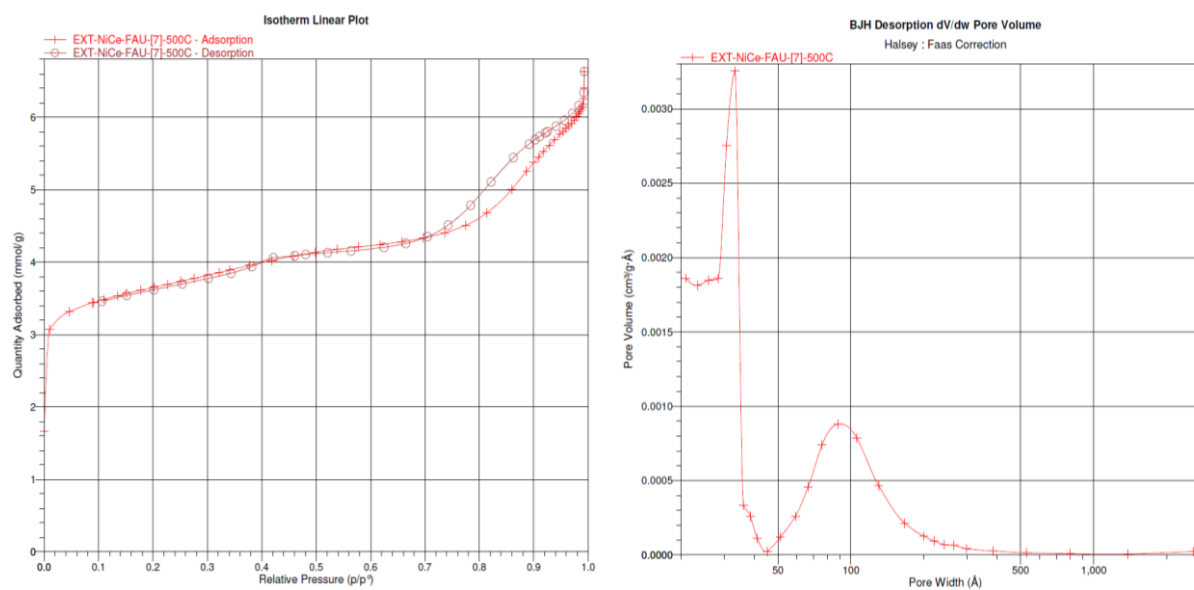
**Figure B.1. Isotherm and pore distribution charts for Cat 1**



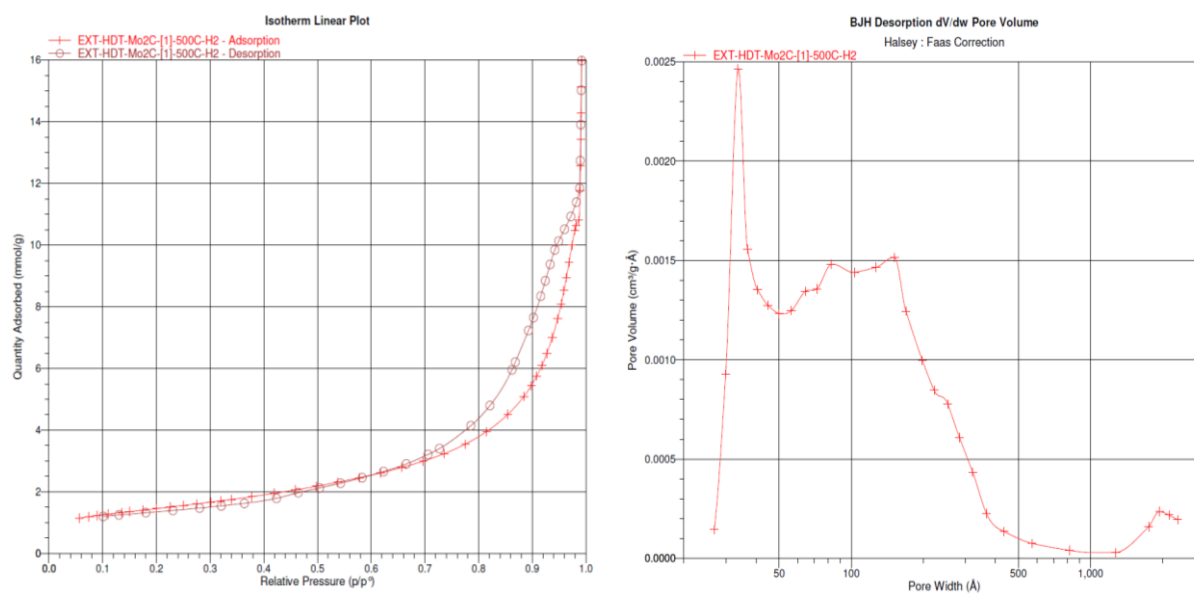
**Figure B.2. Isotherm and pore distribution charts for Cat 1**



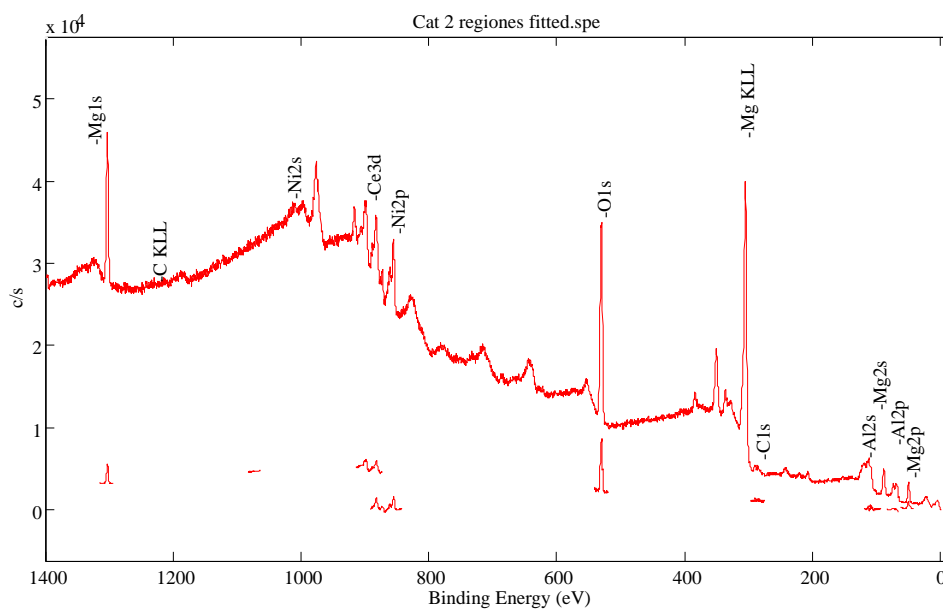
**Figure B.3. Isotherm and pore distribution charts for Cat 3**



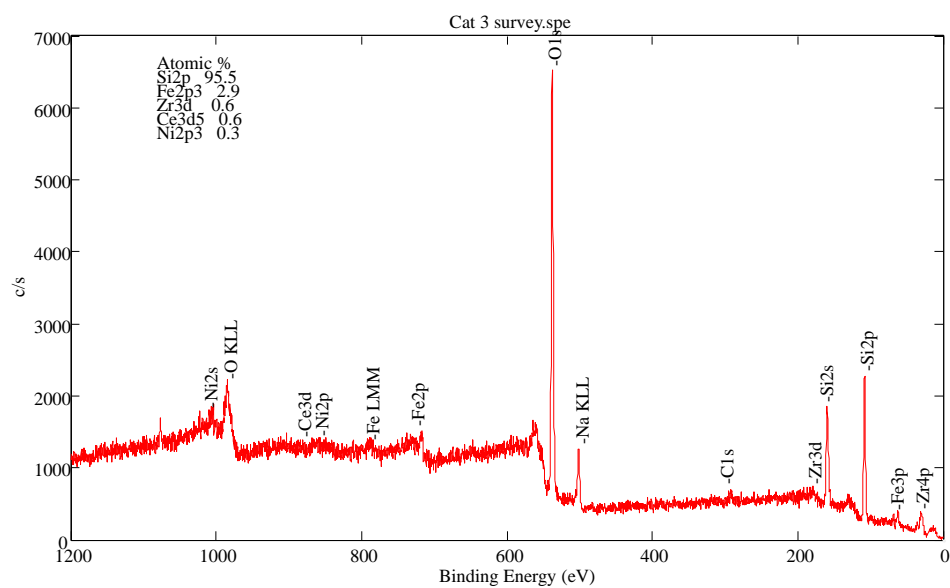
**Figure B.4. Isotherm and pore distribution charts for Cat 4**



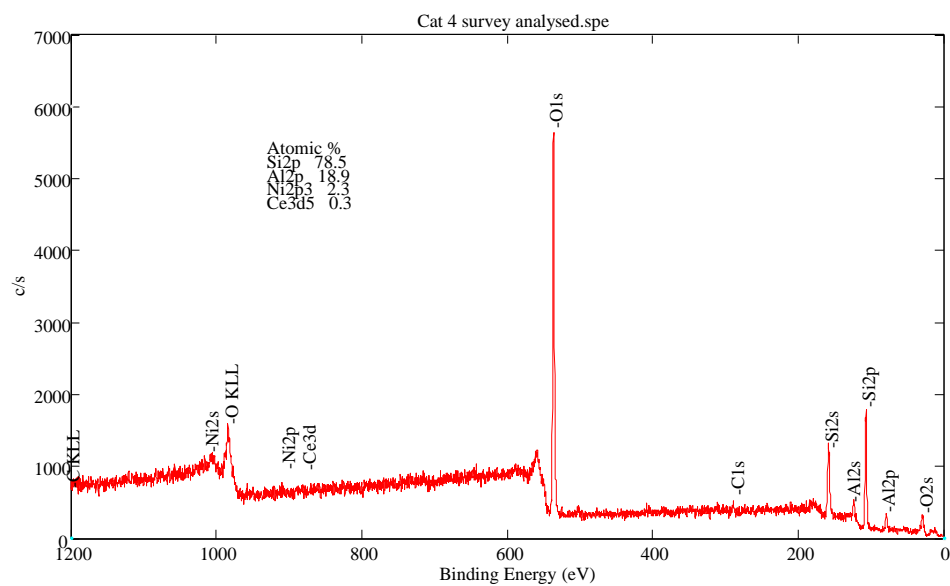
**Figure B.5. Isotherm and pore distribution charts for Cat 5**



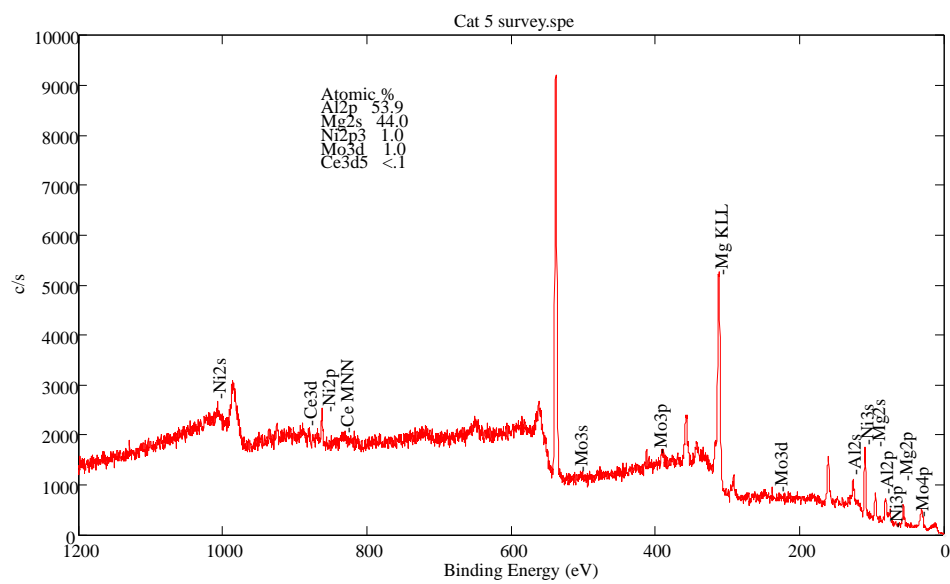
**Figure B.6. Survey scan for Cat 2**



**Figure B.7. Survey scan for Cat 3**



**Figure B.8. Survey scan for Cat 4**



**Figure B.9. Survey scan for Cat 5**